SARS-CoV-2 and The Immune Response; The Establishment of a SARS-CoV-2 Neutralization Assay and Subsequent Immune Utilization

By

Delania Gormley

A dissertation submitted in fulfillment of the requirements for the degree of Master of Science in Medicine (Immunology and Infectious Diseases)

Division of Biomedical Sciences
Memorial University of Newfoundland

October 2023

St. John’s, Newfoundland

Abstract

SARS-CoV-2 (severe acute respiratory syndrome coronavirus 2) has become increasingly important since the onset of the coronavirus disease 2019 (COVID-19) pandemic. In less than a year, there were numerous vaccination guidelines. After the vaccination program, the scientific field raced to answer questions regarding the immune response at the cellular and molecular levels. We aimed to bridge innate and adaptive immune responses to uncover the pathophysiological factors that mediate immune pathogenicity. The introductory part of the project was focused on the adaptive immune response to measure how antibodies and sera affect spike-mediated viral infection. To monitor disease outcomes and determine vaccine efficacy, we evaluated the neutralizing antibody potency using an HIV-1 pseudovirus in a cohort of SARS-CoV-2 infection and/or vaccinated individuals. We hypothesized that high neutralization titer would positively correlate to immune protection and decreased disease severity. The SARS-CoV-2 pseudovirus system and neutralization assay are established and future work could gain neutralization data. These results highlight a valuable complement to ELISA-based methods and the importance of studying spike-mediated viral infection on the immune response. The accompanying part of this research concentrated on the innate immune responses to SARS-CoV-2 ORF3a viral infection. In this regard, it was apparent early on that COVID-19 involved extensive inflammation and immune dysregulation. Therefore, we decided to evaluate the key regulatory factors and mediators involved in inflammasome formation/activation and programmed cell death by an inflammasome array. We hypothesized that the SARS-CoV-2 ORF3a protein would induce pyroptosis through the upregulation of the NLRP3 inflammasome and its components. We found that the *CCL5, MEFV, NLRC5, NLRP3*,

MOK, and *TNF* genes were all statistically significantly upregulated. These genes have implications in both apoptosis and pyroptosis, and both cell death pathways could be activated simultaneously in response to the SARS-CoV-2 ORF3a protein. These results highlight a future application for therapeutic development for SARS-CoV-2 and other inflammatory diseases.

General Summary

In this research, we examined various aspects of the pathophysiological factors mediating immune pathogenicity in innate and adaptive immune responses. We assessed the adaptive immune response by measuring how antibodies and sera affect spike-mediated viral infection. To analyze the adaptive immune response, we successfully generated a SARS-CoV-2 spike pseudovirus, verified its function, and established a neutralization assay. In relation to the innate immune response, we examined the inflammatory response dysregulation resulting from SARS-CoV-2 ORF3a viral infection. We identified that the *CCL5, MEFV, NLRC5, NLRP3, MOK*, and *TNF* genes were all statistically significantly upregulated. The upregulation of these genes suggests that in response to the SARS-CoV-2 ORF3a protein, both apoptosis and pyroptosis cell death pathways could be activated simultaneously.

Acknowledgments

First and foremost, I would like to extend my gratitude to my supervisor Dr. Rodney Russell, who continued to push me to improve continuously. This research would not have been possible without his vision, and his guidance helped propel me through the various challenges experienced.

Secondly, I would like to thank Cassandra Gardner, the Research Assistant of the Russell laboratory, for the skills and techniques she taught me that allowed me to conduct this research. Cass was instrumental in answering all my questions and helping me figure out experimental setups.

I also thank Dr. Michael Grant, Dr. Kayla Holder, Danielle Ings, and Dr. Craig Moore. Dr. Grant was the Principal Applicant on the research grant that funded this work, and Dr. Holder was a Co-applicant on the proposal. Dr. Holder and Danielle were vital in collecting and processing serum and plasma samples. Lastly, Dr. Craig Moore was kind enough to let us use his Cytation plate reader for all the luciferase/neutralization data.

The research conducted throughout this thesis was funded by the COVID-19 Immunity Task Force, the Canadian Institutes of Health Research (CIHR), the School of Graduate Studies (SGS) and Research and Graduate Studies (RGS) at Memorial University. The funding for the equipment used throughout the objectives was from the Canada Foundation for Innovation (CFI) and the Department of Industry, Energy, and Technology (IET) from the Government of Newfoundland and Labrador.

COVID-19 Impact Statement

This research, unfortunately, was affected by the COVID-19 pandemic. When I started in January of 2021, I faced the second pandemic lockdown and density restrictions when re-opening. As a result, I was delayed in my training and the initial start of my experiments until the summer. In addition, the pandemic was going on throughout this project; therefore, experiments may have been conducted slower due to regulations, shipping delays, and shortages. Consequently, some of the research objectives could not be explored by me due to time constraints. However, I was able to establish the system and employ multiple methods to validate, titer, and neutralize the pseudovirus.

Table of Contents

List of Figures

List of Abbreviations

AA- Amino acid

ACD- Acid-citrate dextrose

ACE2- Angiotensin Converting Enzyme 2

AIM2- Absent in Melanoma 2

ARDS- acute respiratory distress syndrome

ASC- Apoptosis-associated speck-like protein

B cells- B lymphocytes

Bcl2- B cell lymphoma 2

BSA- Bovine serum albumin

BSL2- Biohazard Safety Level 2

BSL3- Biohazard Safety Level 3

CARD- Caspase activation and recruitment domain

CCL5- C-C chemokine ligand 5

CFI- Canada Foundation for Innovation

CIHR- Canadian Institute of Health Research

CMV- Cytomegalovirus

COVID-19- Coronavirus disease 2019

C_t- Cycle threshold

DAMPs- Damage-associated molecular patterns

DAPI- 4',6-diamidino-2-phenylindole

DMEM- Dulbecco's modified minimal essential medium

DNA- Deoxyribonucleic acid

E- Envelope

EF1a- Elongation factor 1a

ELISAs- Enzyme-linked Immunosorbent Assay

ER- Endoplasmic reticulum

ERGIC- endoplasmic-reticulum Golgi intermediate compartment

FBS- Fetal bovine serum

Gag- Group-specific antigen

GAPDH- Glyceraldehyde 3-phosphate dehydrogenase

GSDMD- Gasdermin D

HE- Hemagglutinin esterase

HIV- Human immunodeficiency virus

ICTV- International Committee on Taxonomy of Viruses

IET- Industry, Energy, and Technology

IFN- Interferon

Ig- Immunoglobulin

IL- Interleukin

IRES- Internal ribosomal entry site

IRF1-interferon regulatory factor 1

Kb- kilobases

LB- Luria Bertani/ Lysogeny Broth

LDH- Lactate dehydrogenase

LPS- Lipopolysaccharide

LTR- Long terminal repeat

M- Membrane

mAb- Monoclonal antibody

MAPK- Mitogen-activated protein kinase

MERS-CoV- Middle Eastern Respiratory Syndrome Coronavirus

MLV- Murine leukemia virus

MOK- MAPK/MAK/MPK overlapping protein kinase

mRNA- messenger RNA

N- Nucleocapsid

nAbs- Neutralizing Antibodies

Nef- Negative Factor

NF-κB- Nuclear factor kappa B

NLR- Nod-like receptors

NLRC5- Nod-like receptor family CARD domain containing 5

NLRP3- Nucleotide oligomerization domain, leucine-rich repeat, pyrin-domain containing protein 3

Nsp- Non-structural proteins

ORF- Open Reading Frame

PAMPs- Pathogen- associated molecular patterns

PBS- Phosphate buffered saline

PEG- polyethylene glycol

PFA- Paraformaldehyde

PLB- Passive lysis buffer

Pol- DNA polymerase

pp- protein phosphatase

PRR- Pattern recognition receptors

psBbi- BB-sleeping beauty transposon system

Psv- Pseudovirus

PYD- Pyrin domain

RBD- receptor binding domain

RdRp- RNA-dependent RNA polymerase

Rev- Regulator of expression of virion proteins

RGS- Research and Graduate Studies

RLU- Relative light units

RNA- Ribonucleic acid

ROS- Reactive oxygen species

RPMI- Roswell Park memorial institute

RT- Real-time

RT-qPCR- Real-time quantitative reverse transcription polymerase chain reaction

S- Spike

SARS-CoV- Severe Acute Respiratory Syndrome Coronavirus

SARS-CoV-2-Severe Acute Respiratory Syndrome Coronavirus 2

SGS- School of Graduate Studies

SST- Serum-separating tube

T cells- T lymphocytes

Tat- Trans-activator of transcription

TCID_{50}-50% tissue culture infectious dose

TLR- Toll-like receptors

TMPRSS2- Transmembrane protease serine 2

TNFα- Tumor necrosis factor alpha

TRAF3- TNFR-associated factor 3

Vif- Viral Infectivity Factor

Vpr- Viral Protein R

Vpu- Viral Protein U

VSV- Vesicular Stomatitis Virus

WHO- World Health Organization

ZsGreen- *Zoanthus sp*. green fluorescent protein

2019-nCoV- Novel Coronavirus

Δ21- C-terminal 21 AA deletion

Introduction

1. Introduction
    1.1 Overview

In March 2020, the World health organization (WHO) designated the SARS-CoV-2 (severe acute respiratory syndrome coronavirus 2) a global pandemic. The SARS-CoV-2 currently circulating worldwide is the etiological agent of the coronavirus disease 2019 (COVID-19). There have been over 600 million infections reported worldwide, with over 6 million known deaths (WHO, 2023). Due to the pandemic nature of the virus, there was a collective global effort to determine the impact that SARS-CoV-2 would have. In less than a year, there were mitigation measures and numerous versions of vaccination strategies (Piret & Boivin, 2020). As a population, we needed to decrease the risk of overwhelming health services. After the vaccination program, researchers raced to answer questions regarding the immune response at the cellular and molecular levels. The scientific field sought to know if the vaccines worked, if they would continue to work after mutations in the virus, and the duration of protection conferred. Various research groups, including ours, used multiple mechanisms to gain insights into the complex mechanisms that underlie the host immune response to SARS-CoV-2 to cease the pandemic.

1.1.1 History of Coronaviruses

In the 1930s, the first coronavirus was isolated from a case of infectious bronchitis (Fields et al., 2007), which was later, through the advancement of technology and the introduction of the electron microscope, designated as *coronavirus*. The designation of the family *Coronaviridae* resulted from the distinct petal projections or crown-like bulbous distal ends that protruded

from the surface (Fields et al., 2007; Kahn & McIntosh, 2005). Since then, numerous coronaviruses have been detected in a wide range of animals and humans, which have been shown to have similar genome organization and replication strategies (Fields et al., 2007). The family of coronaviruses can further be distinguished by four genera: *alpha-coronavirus*, *beta-coronavirus*, *gamma-coronavirus*, and *delta-coronavirus* (Saleemi et al., 2020). In humans, the coronavirus family primarily infects the respiratory and gastrointestinal tracts causing mild symptoms. However, three coronaviruses have caused more consequential and fatal diseases in humans. The first emerged in the early 2000s (2002-2004). It was denoted SARS-CoV (severe acute respiratory coronavirus), the second MERS-CoV (middle eastern respiratory syndrome coronavirus) emerged in 2012, and the last, in 2019, was SARS-CoV-2 (Kahn & McIntosh, 2005; Perlman, 2020). The novel SARS-CoV outbreak generated renewed interest in efforts to understand coronaviruses, the disease they cause, and treatment and prevention strategies (Fields et al., 2007). This previous research was an undoubtable asset in management and rapid understanding of the SARS-CoV-2 global pandemic.

1.1.2 SARS-CoV-2

1.1.2.1 Background

The SARS-CoV-2 that has caused the current epidemic is a single-stranded, positive-sense ribonucleic acid (RNA) virus belonging to the *Coronaviridae* family and the *beta-coronavirus* genus (Saleemi et al., 2020). It was first identified in late 2019 from individuals in Wuhan, China, who presented with respiratory illness. At the time, scientists gave it the provisional name of the 2019 novel coronavirus (2019-nCoV). After sequencing the viral genome and identifying close sequence homology (~79%) to SARS-CoV, the International Committee on Taxonomy of

Viruses (ICTV) denoted the virus SARS-CoV-2 (Abdelrahman et al., 2020; Yap et al., 2020a). It is believed that SARS-CoV-2 resulted from a spillover event during which the virus had zoonotic origins and possibly an undetermined intermediate species facilitated the transfer to the human population (Piret & Boivin, 2020). This evidence comes from the close sequence homology, 96.2%, to the bat coronavirus (Bat CoV RaTG13) (Abdelrahman et al., 2020; Grifoni et al., 2020). Research is still being conducted to determine which intermediate species was involved. The SARS-CoV-2 has a high pathogenicity and infectivity, resulting in a biosafety hazard level 3 (BSL3) classification. The requirement for a BSL3 has impeded research into SARS-CoV-2 for numerous laboratories and prevented further understanding of pathology and therapeutic design.

1.1.2.2 Disease Symptoms

Infection with SARS-CoV-2 can lead to COVID-19 disease, which can be associated with various clinical manifestations. The WHO defines symptoms as asymptomatic, mild, moderate, severe, and critical in the illness field spectrum (Schultze & Aschenbrenner, 2021; WHO, 2022). Infected individuals can present with fever, coughs, shortness of breath, and fatigue. In more severe morbidity, immune dysregulation leads to a hyperinflammatory response causing pneumonia, organ damage, and acute respiratory distress syndrome (ARDS). Infection with SARS-CoV-2 can also lead to mortality. Due to extensive variability in symptoms on the individual level, and the heterogenous nature of disease severity, researchers have been trying to uncover the various mechanisms and immune response factors that could be protective or detrimental. By identifying common characteristics, we could better understand immune pathology.

1.1.2.3 Viral Genome

The genome of SARS-CoV-2 is approximately 30 kilobases (kb) long, making it one of the largest RNA viruses (Fields et al., 2007; J. Zhang et al., 2022). Within the virion genome, there are four structural genes encoding the spike (S), envelope (E), membrane (M) and nucleocapsid (N) glycoproteins. The virion core is enclosed by a lipoprotein E, formed during the virus budding from the intracellular membranes making a critical part of the virus particle assembly (Fields et al., 2007). The envelope also contains the M glycoprotein, which has roles in determining the budding virus site, and interactions with the viral N, S, and E glycoproteins, and viral particle formation (Fields et al., 2007; Huang et al., 2020). The N glycoprotein houses the RNA genome that associates with the N phosphoprotein to form a long, flexible, helical nucleocapsid. Lastly, the S glycoprotein protrudes on the virion surface and mediates virion entry by binding to specific cellular receptors. The S glycoprotein is of research interest as it is the target of neutralizing antibody responses and elicits cell-mediated immunity (Fields et al., 2007). The SARS-CoV-2 genome also encodes 16 non-structural proteins (nsp1-16) and several accessory proteins termed open reading frame (ORF)- 3a, 3b, 6, 7a, 7b, 8a, 8b, 9b and 10 (Hartenian et al., 2020; Redondo et al., 2021; W. Yan et al., 2022; J. Zhang et al., 2022). The SARS-CoV-2 viral genome can be observed in Figure 1. The accessory proteins are crucial in pathogenicity by modulating virus-host interactions and the host immune response. By understanding the interplay and function of the proteins, we can further understand the pathogenesis to identify biomarkers for therapeutics and disease severity.

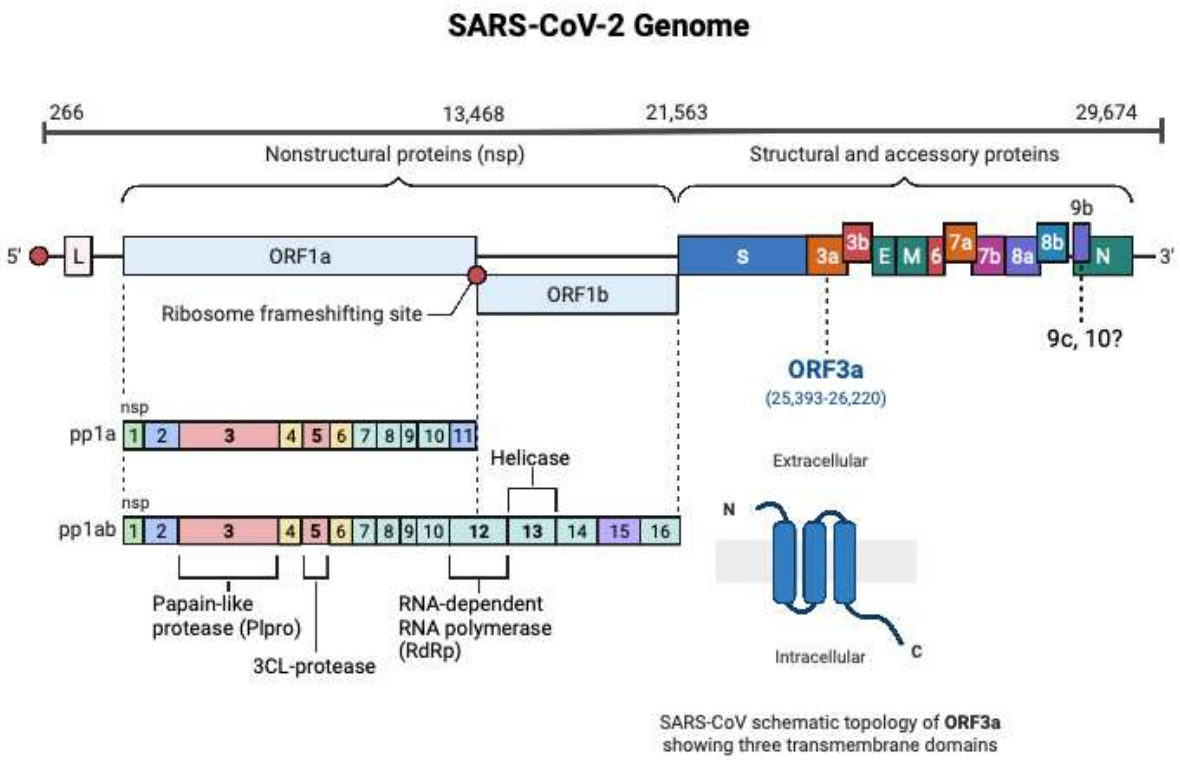

Figure 1: SARS-CoV-2 Genome Organization. The SARS-CoV-2 RNA genome encodes non-structural (nsp) proteins and structural and accessory proteins. ORF1a and ORF1b encode the nsp. Briefly, cap-dependent translation begins at ORF1a producing protein phosphatase 1a (pp1a), which encompasses nsp1-11. Additionally, ORF1a also makes pp1ab which encodes nsp 12-16. The recognition of the stop codon by the ribosome at ORF1a determines the production of either polypeptide. The structural and accessory proteins are synthesized by translating their respective subgenomic mRNAs. Lastly, the proposed structure of ORF3a protein was included for further understanding in our latter project. Created using biorender.com template adapted from Glaunsinger laboratory and Hugues Abriel (Hartenian et al., 2020; J. Zhang et al., 2022).

1.1.2.4 Pathology Through Spike

The coronaviruses rely on their S glycoproteins on the surface of the virus envelope for mediating viral entry. Thus, the trimeric transmembrane glycoprotein is responsible for SARS-CoV-2 tropism (Ni et al., 2020). The S protein has three structural domains: a transmembrane domain; a short carboxyl-terminal cytoplasmic domain; and a large external domain (Huang et al., 2020). The S protein is further divided into two subdomains, S1 (houses the receptor binding domain (RBD)) and S2 (Fields et al., 2007; Huang et al., 2020). The S1 subdomain contains the sequences responsible for binding to specific receptors on the surface of susceptible cells (Fields et al., 2007). In the context of SARS-CoV-2, this receptor is angiotensin-converting enzyme 2 (ACE2) (Ni et al., 2020). Previous research has shown that mutations in the S1 sequence are associated with altered antigenicity and pathogenicity of the virus (Fields et al., 2007). The S2 subdomain mediates fusion and viral entry in conjunction with the transmembrane protease serine 2 (TMPRSS2). The SARS-CoV-2 entry route can be cleaved by different proteases depending on the cell surface pathway. In Figure 2, the replication cycle is shown where there is sufficient TMPRSS2 and thus, S2 cleavage occurs at the cell surface depicting the endosomal entry route. If the target cell has insufficient TMPRSS2, then the ACE2-virus complex is internalized via clathrin-mediated endocytosis and cleavage is performed by cathepsins (Hartenian et al., 2020; Lebeau et al., 2020). Within the human body, the ACE2 protein is expressed in various human organs and tissues, such as the lungs, heart, kidney, and intestines (Fields et al., 2007; Saleemi et al., 2020). The wide dispersion of ACE2 is the highest within the gastrointestinal tract (Ni et al., 2020). Most studies on the S protein suggest that it is multifunctional and plays a central role in the biology and pathogenesis of coronavirus

infections (Fields et al., 2007). In addition, its interaction with the ACE2 receptor has been used to study pathophysiological questions and the ability of antibodies to neutralize virus infectivity.

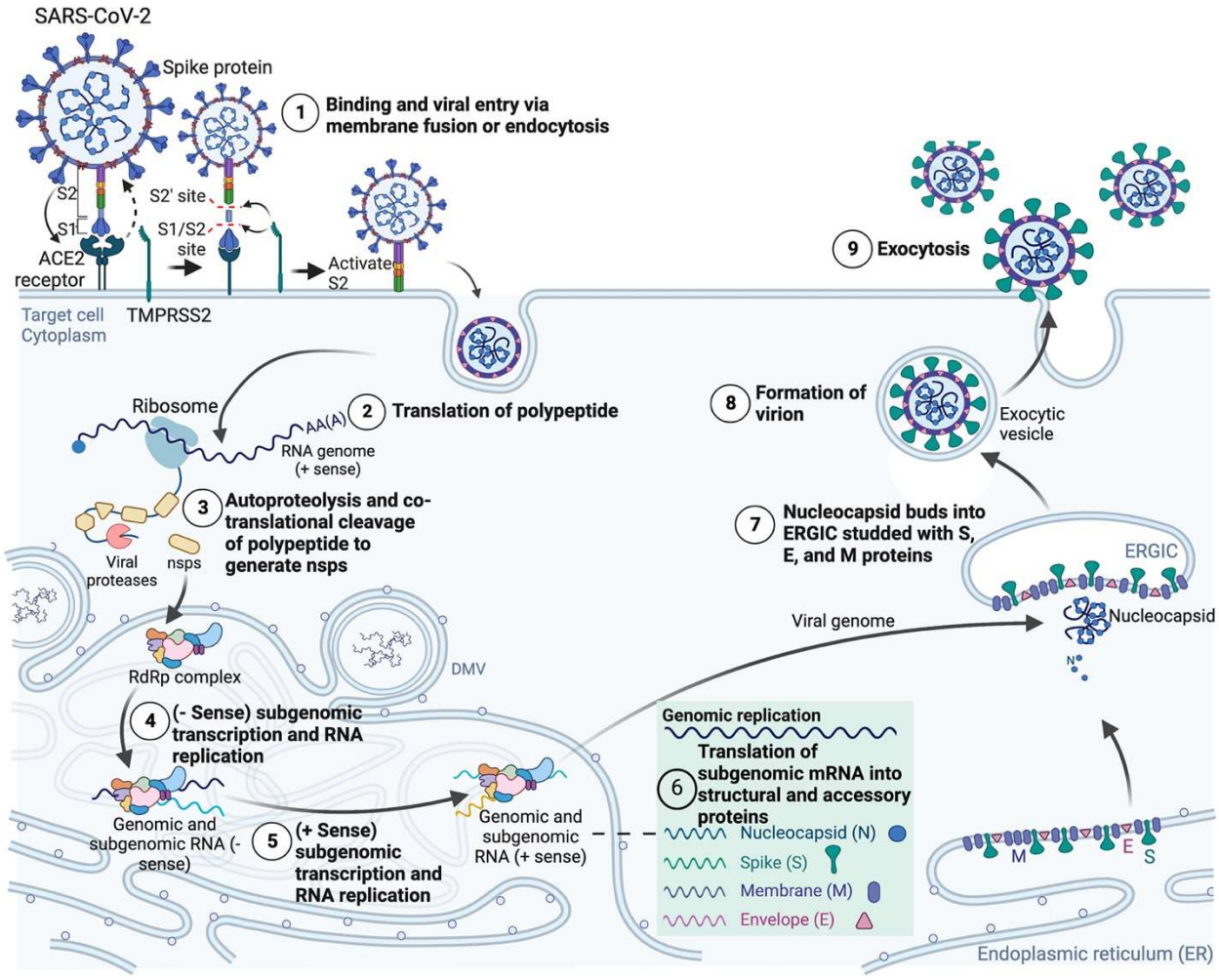

Figure 2: SARS-CoV-2 Viral Entry and Replication. For access, the SARS-CoV-2 S glycoprotein engages with the susceptible host receptor ACE2. The binding elicits the cleavage of S1/S2 by TMPRSS2 protease. The S2 domain is then activated and drives the fusion of the viral and host membranes (1). The RNA genome is then deposited into the cytoplasm, and the genome is translated by the host translation machinery (2). Next, polyproteins are co-translationally cleaved by a protease to generate nsp and components of the RNA-dependent RNA polymerase (RdRp) complex (3). The RdRp generates negative-sense subgenomic and genome-length RNAs (4) that are used as templates for synthesizing progeny genomes and subgenomic messenger RNA (mRNAs) (5). The structural and accessory proteins are translated from the subgenomic mRNAs (6). The genomic RNA is bound by nucleocapsid with structural proteins S, E, and M and buds into the endoplasmic-reticulum-Golgi intermediate compartment (ERGIC) (7). The virion is then formed and exported by exocytosis (8 and 9). Created using biorender.com template adapted from Glaunsinger laboratory and Dr. Benjamin Goldman-Israelow (Hartenian et al., 2020; Lebeau et al., 2020).

1.1.3 Immune response

1.1.3.1 Overview

The immune system has evolved to protect multicellular organisms from an array of pathogens and toxins that disrupt homeostasis. Two distinct aspects are central to the immune response: the innate and the adaptive responses (Owen, 2013). Both branches eliminate foreign stimuli through humoral and cell-mediated responses (Owen, 2013). The innate immune response is the first line of defence to create a quick non-specific reaction (Schultze & Aschenbrenner, 2021). Immune cells like neutrophils, macrophages, and monocytes recognize molecular patterns and bind to mark infected cells for death. The adaptive immune response is more specific and therefore takes longer to mount a response. B lymphocytes (B cells), and T lymphocytes (T cells) somatically rearrange to assemble antigen-binding molecules against specific antigens (Owen, 2013). These immune cells can be long-lived and persist in an immune repertoire in case of re-infection (Crawford et al., 2021; Fields et al., 2007). By studying the immune response through both branches, one can gain insights into the complex mechanism that underlines the host's immune response to a foreign stimulus. The pathophysiological mechanisms observed, and the soluble mediators revealed could be used to develop diagnostic markers.

1.1.3.2 Adaptive immune response

1.1.3.2.1 Antibodies

A significant component of the adaptive humoral immune response that combats pathogens or foreign macromolecules is antibodies. B cells produce antibodies through affinity maturation, somatic hypermutation and differentiation (Owen, 2013). The antibodies produced have a paratope interacting with the antigen's epitope (Owen, 2013). The antibody binds to the

antigen by spatial complementarity, and the affinity of binding can be strong or weak. In the case of weak binding, there is potential for cross-reaction with different antigens. Once the antibodies are produced, they are transported throughout the body. The antibodies produced can have various functions. Some antibodies utilize agglutination to clump virus-infected cells targeting them for phagocytosis (Owen, 2013). Other antibodies can activate complement and lead to lysis or signal other immune cells to destroy the virus (Owen, 2013). Lastly, neutralizing antibodies bind to the virion rendering its attack ineffective (Owen, 2013). The variations in the heavy chains determine antibody class and function. The most common immunoglobulin (Ig) is IgG, which is in large quantities in the blood and tissues (Owen, 2013). IgG antibodies are often used as a correlate of protection in immunological assays (Owen, 2013). IgM is the first response produced by the maturation of B cells and is the antigen receptor on the B cell surface (Owen, 2013)- binding of IgM cause the microorganisms to agglutinate (Owen, 2013). The primary antibody found in bodily secretions is IgA, although it is found in deficient concentrations in the serum (Owen, 2013). IgM, IgG, and IgA antibody fractions mediate neutralizing antibody activities (Owen, 2013). By characterizing the humoral immune response against SARS-CoV-2, a critical parameter to determine protection against the virus will be uncovered.

1.1.3.2.2 Neutralizing Antibodies

The SARS-CoV-2 pandemic has shown researchers that it is necessary to understand the quality, quantity, and duration of antibody protection during the different clinical stages of COVID-19 in both convalescent plasma and from vaccination. One way to determine virus infectivity is to measure the neutralizing antibodies (nAbs) level. Neutralizing antibodies bind to

a pathogen to prevent infection by blocking the interaction between receptors and antigens (Crawford et al., 2021). In addition, nAbs can prevent virus conformational changes, decreasing the pathogenicity. As a result, the virus will then be unable to infect healthy cells and be unable to replicate, thereby reducing infection (Owen, 2013). Once the virus is bound by nAbs, it can be degraded by white blood cells and eliminated from the body. Since nAbs can be generated by natural infection or vaccinations and have been used previously as a correlate of protection, they are of research interest (Garcia-Beltran, Lam, Astudillo, et al., 2021). On a clinical level, nAbs have also been used to prevent or treat disease by passive transfer. However, the current bottleneck around nAbs is the methodology used to measure their presence and robustness.

1.1.4 Methods to Characterize Neutralization

1.1.4.1 ELISA

Throughout the development of technology, there are now many well-characterized high throughput assays to measure the level of antibodies to determine the immunological response (Crawford et al., 2020). One serological assay used is enzyme-linked immunosorbent assay (ELISA). In general, ELISAs are used to quantify a specific antigen present in a sample through the production of color development in which the optical density is proportional to the quantity of antigen in the sample (Shah & Maghsoudlou, 2016). The downside of ELISAs is that they generally measure the total antibody binding levels to SARS-CoV-2 or some of its vital constituent proteins (Amanat et al., 2020; Crawford et al., 2020; S. Khan et al., 2020; Okba et al., 2020), but do not necessarily reflect the level of neutralization antibodies present (Almahboub et al., 2020; Pi-Estopiñan et al., 2022). In addition, depending on the type of ELISA used, an assay could have low sensitivity or risk of cross-reactivity associated with the

secondary antibodies (Shah & Maghsoudlou, 2016). Thus, adding other confirmatory functional bioassays would be beneficial to confirm the results. For the purpose of this project, we focused on neutralizing antibodies since the grant obtained from the COVID-19 Immunity Task Force was in conjunction with Dr. Michael Grant's laboratory, and they were responsible for analyzing total antibody responses via ELISAs.

1.1.4.2 Neutralization Assay

Neutralization assays measure the specific ability of nAbs to block viral infection by binding to the viral antigens. The utilization of this assay tends to be more difficult due to being cumbersome and expensive. The most biologically relevant method would be to utilize replication-competent virus culture systems (Crawford et al., 2020; Fields et al., 2007). However, as previously mentioned, the accessibility of live virus assay is limited because SARS-CoV-2 is a BSL3 agent and requires specialized facilities that are unfortunately not yet available at Memorial University. Many laboratories have used a pseudovirus (psv) neutralization assay to overcome this hurdle. Previous research has shown that coronaviruses lacking the hemagglutinin esterase (HE) protein only have one neutralizing antibody target: the spike protein (Crawford et al., 2020; Fields et al., 2007). Thus, since SARS-CoV-2 lacks HE, we can measure the neutralization of virus infectivity by measuring nAbs against spike protein, while also alleviating biosafety limitations (M. Chen & Zhang, 2021; Fields et al., 2007). In addition, pseudovirus neutralization assays have been shown to correlate significantly to replication-competent viruses in evaluating antibody responses (Shen et al., 2021). Furthermore, in the serum, pseudoviruses are not easily inactivated by complement, leading to unambiguous

results (Inglis et al., 2008). Neutralization assays also correlate well with protection from infection and are sometimes considered the standard against which other serologic assays should be measured (Fields et al., 2007). Thus, it has become an increasingly popular virological tool.

1.1.5 Pseudovirus

1.1.5.1 Overview

Pseudoviruses were first developed in the 1960s when scientists studied vesicular stomatitis virus (VSV) (Fields et al., 2007; Kahn & McIntosh, 2005). In the 1980s, human immunodeficiency virus (HIV)-based platforms largely replaced the VSV platform as the most common model for developing pseudo and chimeric viruses as the HIV platform was more efficient (Fields et al., 2007; Kahn & McIntosh, 2005; Saleemi et al., 2020). In the HIV system, once the virus is integrated the positive-strand RNA genome can instantly begin translation; in VSV, the genome must be transcribed first (Saleemi et al., 2020). Pseudoviruses are a useful virological tool as they are versatile, replication-incompetent, and can be utilized in BSL2 laboratories (Fields et al., 2007; Nie et al., 2020). Since SARS-CoV-2 is a classified BSL3, using pseudoviruses meant that more laboratories could aid in studying neutralizing antibodies against the virus. In general, pseudoviruses are recombinant viruses with their backbone and surface proteins derived from different viruses. The produced pseudoviruses can infect susceptible host cells but can only replicate for a single round (Nie et al., 2020). The pseudoviruses contain a reporter gene, such as luciferase, that allows quantification of infectivity. In research, pseudoviruses are used to study cellular tropism, receptor recognition, and drug discovery as well as to develop and evaluate antibodies and vaccines under less stringent biosafety conditions (Fields et al., 2007).

With SARS-CoV-2 research, groups have utilized VSV, HIV-1, and murine leukemia virus (MLV) pseudovirus systems, but within this thesis, the focus will be on the HIV-1 lentiviral system (Crawford et al., 2020; Legros et al., 2021).

1.1.5.2 Retrovirus

Using an HIV-1 lentiviral system means we are using a retroviral backbone. HIV-1 is classified in the *retroviridae* family and *lentivirus* genus. Retroviruses get their classification by utilizing reverse (retro) transcription. This process uses reverse transcriptase to produce deoxyribonucleic acid (DNA) from its RNA genome for the basis of viral replication. Previously, the central dogma was that genetic information could only cascade in one direction, where DNA translates into RNA, the intermediate, and then to the functional proteins (Gallo, 1986). Once the DNA is produced, a copy is inserted into the host cell's genome by an integrase enzyme, thus changing that cell's genome. The retroviral DNA is referred to as provirus, and the cell treats it as its genome to produce new copies of the virus. There are three primary groups of retroviruses: oncogenic (oncoretroviruses), lentiviruses (slow retroviruses), and spumaviruses (foamy viruses) (Gallo, 1986; Miller, 1990). Lentiviruses are a widely used research tool to introduce a gene product *in vitro* or to overexpress specific genes stably.

1.1.5.3 Generation of Pseudovirus

At the beginning of the pandemic, a collaborative effort from the Balazs and Bloom laboratories published a paper listing the protocol and reagents required to generate pseudotyped lentiviral particles for neutralization assays (Crawford et al., 2020). Our laboratory used this paper and others (M. Chen & Zhang, 2021; Moore et al., 2004; Nie et al., 2020) as a template for generating our pseudovirus and developing the neutralization assay. At the time,

such detailed information was not widely available to the scientific community. The pseudovirus system utilized in this research employs an HIV-1 lentiviral packaging system. The HIV-1 lentiviral backbone has been used as one of the gold standards for generating pseudovirus due to the large delivery of genetic information integration in both dividing and non-dividing cells (M. Chen & Zhang, 2021; Merten et al., 2016). To reduce the risk of recombination in lentiviral packaging systems, the essential genes are separated into different plasmids, and the viral accessory genes are deleted (Merten et al., 2016). The four accessory genes of viral infectivity factor (vif), viral protein R (vpr), viral protein U (vpu), and negative factor (nef) were eliminated. Lentiviral vectors with wild type 5' long terminal repeats (LTR) need a trans-activator of transcription (Tat) for activation (Merten et al., 2016). The LTRs, packaging signal psi, and the transgene of interest are cloned to generate a lentiviral vector (Merten et al., 2016). In addition, there is a need for helper, packaging, and envelope plasmids. Another vital component is the packaging cell line, where the pseudoviruses get assembled. For this research, cell lines HEK293T (human embryonic kidney cells) and A549 (human lung adenocarcinoma) expressed the SARS-CoV-2 ACE2 receptor. By studying viral entry, we can answer questions regarding viral pathogenicity.

1.2 Experiment Rationale

The introductory part of this project was focused on the adaptive immune response to SARS-CoV-2 infection and/or vaccination. Our laboratory has also been interested in understanding the various aspects of the innate immune responses to viral infections. In this regard, COVID-19 involved extensive immune dysregulation and a hyperinflammatory response.

Therefore, we also decided to examine inflammation in relation to SARS-CoV-2 infection. The knowledge gained can improve the ability to prevent and manage various diseases.

1.2.1 Innate Immune Response

1.2.1.1 Overview

As previously mentioned, the immune response is a complex mosaic of networks essential for multicellular organisms to maintain homeostasis. A critical component of the innate response is the ability to discriminate pathogens from naturally occurring features. The innate immune response can be activated by recognizing various diverse stimuli, such as pathogen-associated molecular patterns (PAMPs). Some common PAMPs recognized by germ-line innate immune receptors (such as toll-like receptor (TLR) or nod-like receptors (NLR)) are peptidoglycan, lipopolysaccharide (LPS), and foreign nucleic acids (Franchi et al., 2009). The binding of molecules induces the activation of host signalling pathways, leading to the activation of innate and adaptive responses (Franchi et al., 2009). The innate response includes the induction of the inflammatory response such as the production of cytokines/chemokines, which can elicit cell death.

Previous research from multiple groups has highlighted the inflammatory response's correlation with the diverse clinical outcomes of COVID-19 (Yap et al., 2020b). In a subset of individuals, SARS-CoV-2 viral infection leads to a mismanaged antiviral response through immune dysregulation and a hyperinflammatory response. The mechanistic and pathological factors mediating this disease progression remain unclear. Therefore, we can help with one of the greatest enigmas surrounding the pandemic by studying immune components that may activate or inhibit the innate response. To do this, we aimed to develop an expression panel to

uncover markers for immune dysregulation. This panel was streamlined based on an inflammasome array kit. The information gained could be vital in overcoming excessive inflammatory activity by finding targets of cellular inflammation while still leaving the antiviral pathways intact (Yap et al., 2020b). Thus, the implications of this research could be used in future applications for therapeutics.

1.2.1.2 Cell Death

Cell death is a vital component of the innate antiviral response by being a critical physiological event to help regulate biological processes. Cell death is a multifactorial process that is driven by distinct molecular pathways. Although, depending on the cellular context, the different cell death pathways might share common regulatory factors and can be triggered by the same stimuli. In addition, there is novel evidence that many cell death pathways can co-occur and act upon bystander cells (Wallace et al., 2022). There are many types of cell death, including but not limited to apoptosis, necroptosis, and pyroptosis. Most forms of cell death are highly regulated programmed death, but in some cases, cell death can be accidental. This thesis will focus on apoptosis (non-lytic pathway) and pyroptosis (lytic highly inflammatory pathway).

1.2.1.3 Apoptosis

One distinct form of programmed cell death is apoptosis. Apoptosis is a highly regulated, non-lytic, controlled process that morphologically results in cell shrinkage, apoptotic body formation, and destruction by phagocytes (Ren et al., 2020). Apoptosis, on a molecular level, can be activated by two pathways. The first is the extrinsic pathway, which is initiated by death-receptor-mediated binding. In the extrinsic pathway, ligands bind to the plasma membrane

receptor leading to the activation of initiator caspase-8 (Tang et al., 2019; Ward et al., 2008). Depending on the cellular tropism, the cascade can continue the extrinsic pathway by activating the effector caspase-3, or caspase-8 can directly amplify cell death through the intrinsic pathway. The second is the intrinsic pathway that is directed by the mitochondria. In this apoptotic pathway, pro- and anti-apoptotic B-cell lymphoma 2 (Bcl-2) family proteins monitor the intrafamily proteins interactions on the mitochondrial surface (Tang et al., 2019; Ward et al., 2008). In this cascade, cytochrome c is released, activating the apoptosome complex, caspase-9 and the effector caspases (Tang et al., 2019; Ward et al., 2008). Once either pathway is initiated, the events are irreversible. The protease enzymes listed above have been used widely as biomarkers for apoptosis to determine the molecular events occurring and to distinguish cell death pathways.

1.2.1.4 Pyroptosis

Another form of programmed cell death is pyroptosis. Pyroptosis is morphologically characterized by gasdermin-D (GSDMD)-mediated formation of pores in the membrane leading to cell lysis. Pyroptosis is a highly inflammatory type of cell death activated by inflammasomes. The inflammasomes can be either canonical or non-canonical (Riera Romo, 2021). After activating the inflammasome, caspase-1 processes pro-interleukin 1 beta (IL-1β) and pro-interleukin-18 (IL-18) into their functional cytokine forms and proteolytically cleaves the pore-forming protein GSDMD (Riera Romo, 2021). The cleavage of GSDMD results in amino-terminal and carboxy-terminal fragments. The GSDMD amino-terminal fragment binds to acidic lipids, oligomerizes, and inserts itself into an organelle membrane to form sizable pores (Ding et al., 2016; X. Liu et al., 2016; Shi et al., 2015; Vora et al., 2021). These pores are large enough to

release and secrete IL-1β and IL-18 directly and enable the influx of Na^+ and water molecules. The influx results in cell swelling and subsequent membrane rupture while also releasing larger alarmins such as lactate dehydrogenase (LDH) tetramer (Vora et al., 2021). The protease enzymes, proteins, and cytokines listed above have been used as biomarkers for the activation of pyroptosis. However, the regimen of inflammasome activation followed by pyroptotic cell death can differ depending on cell type and stimulus.

1.2.1.5 Inflammasomes

The generation of inflammasomes is a fundamental innate immune mechanism that promotes the antiviral response through the induction of the inflammatory pathways and the programmed cell death pyroptosis (Guo et al., 2015). Excessive inflammation can lead to inflammatory diseases, while insufficient inflammation can lead to persistent infections (Guo et al., 2015). Inflammasomes are multiprotein cytosolic complexes and can assemble after encountering various stimuli, such as pathogen-associated and stress-associated cellular insults. Pattern-recognition receptors (PRRs) are several germline-encoded families that are essential components in the inflammasome complex. These families can be distinguished based on their structure and biomarkers, but all have similar transduction cascades. This thesis will focus on the nucleotide-binding domain, leucine-rich repeat-containing proteins NLRs and absent in melanoma 2 (AIM2)-like receptors. PAMPs, danger-associated molecular patterns (DAMPs), or cytosolic DNA (for AIM2) trigger downstream signalling cascades. The resulting cascade leads to the production of type-1 interferons and proinflammatory cytokines (Guo et al., 2015). Inflammasomes are of clinical interest as they have been implicated in various autoinflammatory and autoimmune diseases and have potential therapeutic applications.

1.2.1.6 NLRP3

NLRP3 (Nucleotide oligomerization domain, leucine-rich repeat, pyrin-domain containing protein 3) is an intracellular sensor that detects an array of microbial motifs, environmental irritants, and endogenous danger signals resulting in the formation of the NLRP3 inflammasome (Swanson et al., 2019; Ting et al., 2008). Within the NLR family, the NLRP3 inflammasome is suggested to be the most broadly activated inflammasome sensor in the innate immune response (Swanson et al., 2019). The NLRP3 inflammasome has three main components: the NLRP3 sensor, the adaptor apoptosis-associated speck-like protein (ASC) containing caspase activation and recruitment domains (CARD), and the effector caspase-1 (Swanson et al., 2019). Germline-encoded host sensors PRR sense an upregulation in PAMPs or DAMPs which triggers the immune response. Upon activation PAMPs or DAMPs recruit ASC-containing CARD (Fields et al., 2007; Ren et al., 2020). Then caspase-1 is recruited and activated, and the subsequent cascade leads to pyroptosis. The activation of the NLRP3 inflammasome by SARS-CoV-2 can be observed in Figure 3. By studying the molecular and biochemical bases of NLRP3 activation in SARS-CoV-2, we could identify new targets leading to potential therapeutics. The targets uncovered could also be utilized in other inflammatory disease treatments.

1.2.1.7 AIM2

The AIM2 innate immune sensor is more specifically activated than the NLRP3 sensor. AIM2 detects the presence of DNA molecules that have been altered, mislocalized, or damaged. In most cases, the DNA is seen in the cytosol upon the loss of envelope integrity or from the accumulation of foreign DNA (Lugrin & Martinon, 2018). AIM2 oligomerizes and recruits ASC via the pyrin domain (PYD) and its interactions upon activation. Caspase-1 is also recruited by CARD

interactions, leading to a parallel immune cascade, as in the case of NLRP3. The initiation of the cascade is known as the priming phase, and for AIM2, this phase is mediated by type-1 interferon (IFN) induction (Vora et al., 2021). A pre-print showed that when monocytes were infected with SARS-CoV-2 by CD16/CD64, both NLRP3 and AIM2 inflammasomes were activated simultaneously (Junqueira et al., 2021). The phenomenon that multiple inflammasome sensors can be activated simultaneously has been observed but has yet to be completely understood (Man et al., 2014). AIM2 involvement in SARS-CoV-2 pathology is unexpected given that it is a double-stranded DNA sensor and SARS-CoV-2 is an RNA virus. However, AIM2 has been shown to participate in other RNA viruses, such as influenza (Wallace & Russell, 2022; H. Zhang et al., 2017). For the most part, inflammasome activation and pyroptosis have critical events central to COVID-19 pathogenesis.

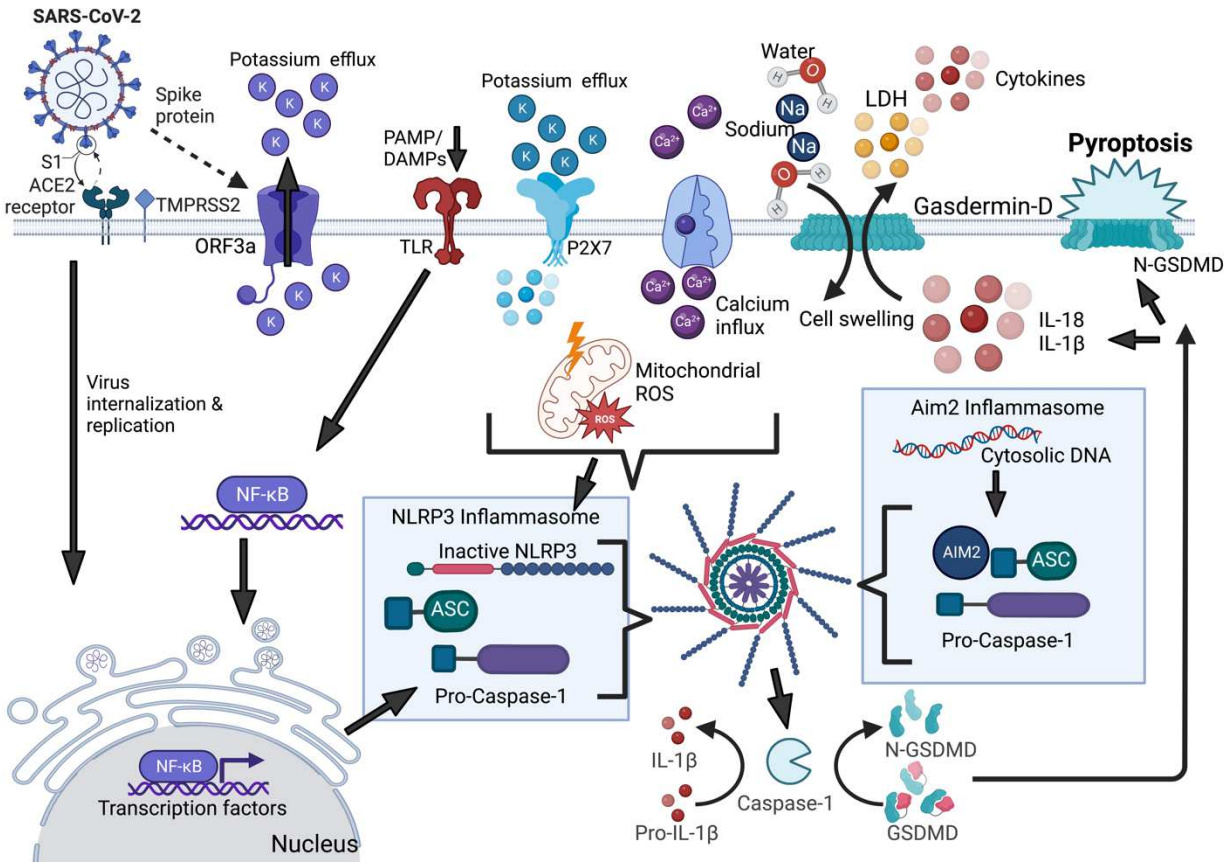

Figure 3: Activation of the NLRP3 and AIM2 Inflammasome by SARS-CoV-2. The first activation comes from cytokines or PAMPs, leading to transcriptional upregulation of canonical and non-canonical NLRP3 inflammasome components. Numerous PAMPs or DAMPs, such as k^+ efflux, Ca^+ flux, mitochondrial reactive oxygen species (ROS), and lysosomal disruption, provide the second activation. These signals all recruit inflammasome components and form the inflammasome. The formed inflammasome activates caspase-1, which oligomerization leads to the cleavage of pro- IL-1β and pro-IL-18. GSDMD is cleaved by caspase-1 and is inserted into the membrane, forming pores and inducing pyroptosis (Swanson et al., 2019; Xu et al., 2022). For the AIM2 inflammasome, cytosolic DNA is detected and recruits the AIM2 inflammasome components, which activate caspase-1 leading to similar cleavage of IL-1β, IL-18, and GSDMD as seen with the NLRP3 inflammasome. In this diagram, ORF3a was included due to its viroporin activity inducing k^+ efflux at the plasma membrane. This could lead to an imbalance in ionic concentration leading to ROS and eventually triggering the NLRP3 inflammasome. It has also been suggested that ORF3a could promote assembly through TRAF3-mediated ubiquitination of ASC (Yap et al., 2020b). Created using biorender.com adapted from (W. Yan et al., 2022; Yap et al., 2020b).

1.2.1.8 SARS-CoV-2 ORF3a Protein

The SARS-CoV-2 ORF3a protein is the largest accessory protein that resides between the S and E glycoproteins. The ORF3a gene is found only in *Sarbecovirus* subgenus but may be distantly related to ORF5 in MERS-CoV (Yap et al., 2020b). Previous research into SARS-CoV showed that at least three proteins could activate the NLRP3 inflammasome: the E protein, ORF3a and ORF8b (Ren et al., 2020; Xu et al., 2022; J. Zhang et al., 2022). This research showed that ORF3a and E protein work simultaneously through facilitating $k^+$and Ca^{2+}transport, respectively. NLRP3 is sensitive to cytosolic Ca^{2+}but is also inhibited by high k^+concentrations. Therefore, the E protein-mediated Ca^{2+}entry while ORF3a mediated k^+efflux. The disruption in ionic balance promotes mitochondrial damage through ROS, which coactivates NLRP3 (Xu et al., 2022; J. Zhang et al., 2022). This is possible as both ORF3a and E are suggested to act as viroporins. The ORF3a protein can also stimulate NF-κB signalling, driving the transcription of pro-IL-1β, pro-IL-18, and IL-8 to prime NLRP3 at a functional level (Yap et al., 2020a). In addition, SARS-CoV ORF3a could also promote TNFR-associated factor 3 (TRAF3) mediated ubiquitination of ASC, thus promoting the NLRP3 inflammasome (Yap et al., 2020b). Given that SARS-CoV-2 and SARS-CoV share approximately 79% overall genetic similarity and the ORF3a protein shares 72% amino acid identity between the two viruses, it was hypothesized that there might be a conservation of function (J. Zhang et al., 2022). However, most of this research is currently being conducted on how many ORF3a gene products are generated and how their production is regulated.

Current research thus far into SARS-CoV-2 ORF3a has implicated that it acts as a viroporin facilitating ion transport across the cell membrane (Xu et al., 2022). Another group has

suggested that the SARS-CoV-2 ORF3a protein induces and activates the NLRP3 inflammasome in antibody-opsonized monocytic or macrophage cells (I.-Y. Chen et al., 2019; Vora et al., 2021). Another proposed mechanism of activation involves the direct interaction with viral proteins. In the case of ORF3a, it can interact with the inflammasome adaptor ASC, resulting in its polyubiquitination and speck formation (I.-Y. Chen et al., 2019). In a recent pre-print, Xu et al., reported that SARS-CoV-2 ORF3a overexpression induced k+ efflux, NLRP3 activation and IL-1β release in lung epithelial cell line A549 (Xu et al., 2022). Beyond these mechanisms, it is conceivable that SARS-CoV-2 activates inflammasomes by novel processes not known to occur in SARS-CoV (Vora et al., 2021). Therefore, the SARS-CoV-2 ORF3a function remains poorly understood, and more work still needs to be done to understand the feedback mechanisms that suppress or activate inflammasomes.

The implications of the previous research show that ORF3a could be vital in ensuring viral release but also could be coincident with inflammasome activation. Overall, ORF3a-mediated contribution to the induction of inflammation is currently relatively unexplored. Due to the multifunctional capacity of ORF3a, we aim to characterize the critical genes involved in ORF3a-mediated pathogenesis by using a direct infection-induced system that might lead to inflammasome formation and downstream cell death signalling responses to determine cytopathogenic effects.

The research in this thesis aimed to measure the level of nAbs contained in the blood of a patient cohort infected with SARS-CoV-2, received a vaccination, or had an infection with subsequent immunization. As previously mentioned, this was done to answer questions about the magnitude and durability of the immune response. The second objective of this thesis was

to use the SARS-CoV-2 ORF3a protein to examine the activation of inflammasome-related genes and pyroptosis and to isolate and develop an expression panel to potentially identify predictive biomarkers for immune responses to COVID-19 vaccination and severity of disease following infection with SARS-CoV-2.

1.3 Experimental Objectives

The research objectives of this thesis are:

1. To observe both innate and adaptive branches of the immune response.
    a. For the adaptive branch:
        i. To generate SARS-CoV-2 spike-expressing pseudovirus.
        ii. To verify SARS-CoV-2 spike and HIV-1 Gag protein expression through Western blots.
        iii. To titer our pseudovirus.
        iv. To establish/develop a neutralization assay.
        v. To quantify how nAbs and sera affect spike-mediated infection across a cohort of infected and/or vaccinated individuals.
    b. For the innate branch:
        i. To determine whether SARS-CoV-2 ORF3a protein can activate pyroptotic programmed cell death.
        ii. To identify key regulatory and mediatory factors of ORF3a-meditated pathogenesis through an inflammasome array.

iii. To use RT-qPCR (Real-time quantitative reverse transcription polymerase chain reaction) to develop a panel to verify gene expression, activation, and upregulation of inflammasome-related genes.

Materials and Methods

2. Material and Methods

2.1 Cell Lines

The cell lines used and maintained throughout this thesis were Huh-7.5, HEK239T, A549, HCT-8, HEK293T-ACE2, and A549-ACE2.

The Huh-7.5 cells (human hepatocyte-derived cellular carcinoma) are an epithelial-like immortal cell line. This cell line was a gift from the Charles M. Rice laboratory from the Virology and Infectious Disease Center at Rockefeller University (Blight et al., 2002). However, it can be acquired from Apath (Apath, LLC). Huh-7.5 cells were propagated in Dulbecco's Modified Eagle medium (DMEM) (Cat: 11995073, ThermoFisher Scientific) supplemented with 10% heat-inactivated fetal bovine serum (FBS) (Cat: 10438034, ThermoFisher Scientific) and 1% penicillin/streptomycin (Cat: P4333-100ML, Millipore-Sigma).

The HEK293T cells (human embryonic kidney cells) are an epithelial-like cell line transfected with the SV40 T-antigen (Cedarlane, ATCC). It has been widely used due to its high transfection efficiency. HEK293T cells were propagated in DMEM supplemented with 10% heat-inactivated FBS, 1% penicillin/streptomycin and 5 mL of L-Glutamine (Cat: 25030081, ThermoFisher Scientific).

The A549 cells (human lung adenocarcinoma) are alveolar basal epithelial cells (Cat: CCL-185, Cedarlane ATCC). A549 cells were propagated in F-12K medium (Cat: 21127022, ThermoFisher Scientific) supplemented with 10% heat-inactivated FBS and 1% penicillin/streptomycin.

The HCT-8 cells (human colon adenocarcinoma) are another epithelial-like cell type (Cat: CCL-244, Cedarlane ATCC). HCT-8 cells were propagated in Roswell Park Memorial Institute (RPMI) 1640 medium (Cat: A1049101, ThermoFisher Scientific) that has been pre-supplemented with L-Glutamine and additionally supplemented with 10% heat-inactivated FBS and 1% penicillin/streptomycin.

The HEK293T-ACE2 (human embryonic kidney cells expressing human angiotensin-converting enzyme 2 (ACE2)) (Cat: NR-52511, BEI resources) were created by transducing HEK293T cells with a lentiviral vector expressing ACE2. This was done under the control of the human elongation factor 1a (EF1a) promoter (Cat: NR-52512, BEI resources). This work was previously done, and cells expressing ACE2 were isolated and expanded by flow cytometry as there was no antibiotic selection marker in the vector by BEI resources before acquisition (BEI resources). HEK293T-ACE2 cells were propagated in the same medium as the HEK293T cell line.

The A549-ACE2 cell line (human lung carcinoma cell expressing ACE2) (Cat: NR-53821, BEI resources) was created using an EF1a promoter for stable insertion of ACE2. This was done using the sleeping beauty transposon system (pSBbi-BB) (Cat: 60521, Addgene). Transfected cells were selected by the blasticidin resistance gene. This work was done previously before the cells were acquired. Cells expressing ACE2 were isolated and expanded by flow cytometry as there was no antibiotic selection marker in the vector by BEI resources. A549-ACE2 cells propagated in the same medium as the A549 cell line.

2.2 Cell Culture

All cell lines were passaged every 3-4 days. The complete medium for each cell line was warmed in a 37℃ water bath for at least 15 minutes before use. Aliquots of 0.25% trypsin EDTA

1x (10 mL) (Cat: 25200072, ThermoFisher Scientific) were also warmed in the water bath. Briefly, the culture fluids were removed and discarded, and 1.5 mL of trypsin (for a 10 cm plate) was added. This trypsin rinse was removed and discarded. Then 3.5 mL of trypsin was added, and plates were moved to a 37℃ 5% CO_2 atmosphere for ~6 minutes (depending on the cell line). After this brief incubation, the cells should be detached from the plate. To collect the cells and inactivate the trypsin, 5 mL of the respective complete medium was added to the trypsin/cell suspension. The suspension was then collected and transferred into a 15 mL polypropylene tube. The plate was then rinsed with another 5 mL of complete medium to collect any remaining cells and was added to the same 15 mL tube. The cell suspension was then centrifuged at 400 x *g* for 5 minutes. After centrifugation, the supernatant was decanted, and the cell pellet was resuspended with the desired medium concentration. Cell culture dishes were then labelled and supplemented with complete media and diluted cell suspension to make a total volume of 10 mL. The amount added to each depended on the confluency needed for experiments—plates were placed in a 37℃ 5% CO_2 atmosphere until the following propagation or experimental continuation. Unless otherwise stated, all cell/ virus culture experiments were performed at a 37℃ 5% CO_2 atmosphere.

2.3 Study Population

Whole blood was collected as part of a prospective longitudinal cohort of individuals to determine SARS-CoV-2 infection and vaccine-induced immunity. The research conducted in this study was approved and carried out following recommendations from the Newfoundland and Labrador Health Research Ethics Authority and the Canadian Tri-Council Policy Statement: Ethical Conduct for Research Involving Humans, respectively. All participants (n=395) in the

study were recruited through word of mouth, news outlets, and poster placements. Written informed consent was collected following the Declaration of Helsinki, and a questionnaire was administered at study enrollment. Samples were collected at three-month intervals. This research involved individuals with previously confirmed SARS-CoV-2 infection (from RT-qPCR) or who received a vaccine regimen to study immunity. Participants receiving any medical treatments or having any underlying immune comorbidities were excluded as it was thought their treatment could interfere with their immune response.

It should be noted that whole blood sample processing was done by our collaborative laboratory (Dr. Grant). A detailed protocol for isolation can be found in the following publications (Holder et al., 2022; Ings et al., 2022).

2.4 Plasmids

All plasmids used in the pseudovirus system were obtained from BEI resources. The identical plasmids and their sequences can be found in the supplementary file S1 at (Crawford et al., 2020). The plasmids used in our experiments were pHAGE-CMV-Luc2-IRES-ZsGreen-W (Cat: NR-52516, BEI resources) lentiviral backbone plasmid that uses a cytomegalovirus (CMV) promotor to express luciferase followed by an internal ribosomal entry site (IRES) and Zoanthus sp. green fluorescent protein (ZsGreen). The lentiviral backbone plasmid contains two reporters, luciferase and ZsGreen, that allows the utilization of both luminescent and fluorescent assays. The following plasmids were also used and were all expressed under a CMV promoter: an HDM-Hgpm2 (Cat: NR-52517, BEI resources) lentiviral helper plasmid expressing HIV Gag-Pol, an HDM-tat1b (Cat: NR-52518, BEI resources) lentiviral helper plasmid expressing HIV Tat, and a PRC-CMV-Rev1 b (Cat: NR-52519) lentiviral helper plasmid expressing HIV Rev.

For the SARS-CoV-2 spike plasmids we used either a pHDM containing the SARS-related coronavirus 2, Wuhan-Hu-1 Spike glycoprotein (Cat: NR-52514) or a pHDM SARS-related coronavirus 2, Wuhan-Hu-1 Spike glycoprotein with C-terminal 21 amino acid (AA) deletion ($\Delta 21$) (Cat: NR-53742). All these plasmids are available in a lentiviral kit through BEI resource under the catalogue number NR-53816. All the plasmids in this system contain the beta-lactamase gene to provide ampicillin resistance in *E. coli*.

In addition, for our latter experimental projects, we used a SARS-CoV-2 ORF3a plasmid named pcDNA3.1(+)-N-HA (Addgene). The sequence for this plasmid can be made available upon request. The plasmid was transformed in the same way as the other plasmids.

2.5 Maxi Preparation of Plasmids

All plasmids must be transformed, extracted, and purified before conducting experiments. Luria-Bertani (lysogeny broth-LB) broth (Cat: BP1427-500, ThermoFisher Scientific), agar plates of LB agar (Cat: BP1425-500, ThermoFisher Scientific), and ampicillin (Cat: 11593027, ThermoFisher Scientific) solutions were prepared in advance as per the Qiagen Maxiprep kit (Cat: 12163, Qiagen) protocol.

The plasmids were transformed in DH5α according to the Qiagen Maxiprep kit (Cat: 12163, Qiagen) protocol. Briefly, 2 μL of either the desired plasmid, positive control plasmid, or no DNA negative control were added to the DH5α aliquot. The samples then underwent a brief heat-shock (45 sec) to form holes in the bacterial cell membrane, which aids in the ability of the bacteria to take up the DNA. The tubes were then agitated at 225 rpm in a 37℃ atmosphere for 1 hr after the addition of S.O.C. medium. This step mediates the bacteria to express the ampicillin resistance genes. Bacteria were spread by the streaking method to form single-cell

colonies. The Qiagen Maxiprep kit was also used to purify our DNA based on the manufacturer's protocol. This kit used ethanol precipitation to purify the nucleic acids. For detailed methodology, please refer to the Qiagen-supplied protocol.

2.6 Generation of Pseudovirus Through a Transfection

HEK293T cells were seeded at 6x10^6 cells per 10cm plate to obtain a 50-70% cell confluency the following day. At 16-24 hours post-seeding, the cells were transfected with the plasmids required for pseudovirus production. The transfection reagent Lipofectamine 3000 (Cat: L3000008, ThermoFisher Scientific) delivered the plasmids in a lipid nanoparticle complex. One experiment used 30 μL of L3000 and 40 μL of P3000. The experimental conditions used were SARS2psv (backbone, rev, tat, gag/pol, and spike plasmids), No Spike (all plasmids except for spike), and an un-transfected control. Please refer to section 2.4 for details about the plasmids. The following plasmid mix was used: 6 μg of HIV-1 lentiviral backbone, 1.32 μg of each plasmid Rev, Tat, and Gag/Pol, and 2.04 μg of the SARS-CoV-2 Spike. A DNA master mix was prepared for each sample and was incubated at room temperature for 15 minutes. While incubating, plates were rinsed twice with 2 mL of opti-MEM. Culture plates were then supplemented with 1 mL (for (transfected) plasmid plates) or 3 mL (for un-transfected) of opti-MEM. The DNA mixture was then added to its corresponding plate and incubated overnight. At 18-24 hours post-transfection, plates were rinsed (twice with 2 mL medium) and supplemented with a new complete medium (8 mL). The transfected culture plates were then incubated for another ~48 hours. At 60 hours post-transfection, the pseudovirus was harvested by collecting the supernatant (centrifuged at 400 x *g* for 5 minutes) and then stored at -80°C.

In later experiments, there was a modification made to the previous protocol. The $\Delta 21$ spike plasmid replaced the original Wuhan-Hu-1 strain spike plasmid (please refer to section 2.4 for more information on the plasmids). The same protocol and DNA amounts were used with the $\Delta 21$ spike plasmid. Our laboratory switched to the $\Delta 21$ spike plasmid as other research groups (Crawford et al., 2021; Nie et al., 2020) showed that truncating the last 21 AA removed the endoplasmic reticulum (ER) retention signal from the spike. This meant that the spike protein could move out of the ER and Golgi more easily to join the structural proteins assembling at the plasma membrane (Crawford et al., 2020). As a result, this modification enhanced our pseudovirus titer.

A transfection was also conducted for the SARS-CoV-2 ORF3a experiments. The same general protocol described above was used except for the following changes. The experimental conditions were SARS-CoV-2 ORF3a, a MOCK control (exposed to all transfection reagents except for plasmids), and an un-transfected control. The amount of SARS-CoV-2 ORF3a DNA added was 24 μg. Please refer to section 2.4 for details about the plasmid. Lastly, for harvesting of the cells, Qiazol lysis reagent was added to prepare the cell lysates and the cells were homogenized with a syringe before storage at -80℃.

2.7 Fluorescent Microscopy

A549, HCT-8, and HEK293T-ACE2 cell lines were utilized for these experiments. Please refer to section 2.1, Cell Lines, for more information on the cell types. For these experiments, 1x10^5 and 3x10^5 cells per well were used for Huh-7.5/A549 and HEK293T-ACE2, respectively. Two well chamber slides were utilized (Cat: 125656, ThermoFisher Scientific) and loaded for a final chamber volume of 2 mL. The chamber slides were incubated overnight. At 24 hours post-

seeding culture medium was carefully aspirated off the chamber wells and discarded. Then 1 mL of the experimental condition psv/medium was added to the corresponding well. The experimental conditions used were SARS2psv, No Spike, transfection control (un-transfected cells), and an infection control (un-infected and un-transfected). Chamber slides were rocked every hour for 3 hours. The original pHDM containing the SARS-CoV-2, Wuhan-Hu-1 Spike glycoprotein (Cat: NR-52514) plasmid was used for these experiments. After 3 hours, the infection medium was removed, discarded, and 2 mL of new complete medium was added. Chamber slides were then incubated for 3 days. After incubation, cells were fixed using acetone and stained with a Vectashield Vibrance mounting medium containing 4',6-diamidino-2-phenylindole (DAPI) (Cat: VECTH180010, BioLynx). This stain is used to stain the nuclei blue.

2.8 Western Blotting

For Western blot analysis, cells were seeded at a density of 6x10^6 in 10-cm culture dishes. The next day, cells were transfected per the protocol in section 2.6. After three days, supernatant and cell lysates were collected. Cell lysates were collected in RIPA++ cell lysis buffer and stored until use. The protein was then extracted from the cell lysates by centrifugation. Next, the Bradford assay was used to quantify protein concentrations using the Bio-Rad protein assay dye reagent (Cat:5000006, BioRad). Briefly, a BSA standard curve was used to determine the protein concentrations of our samples from a spectrophotometer. Cell lysates and supernatants were then run on 7.5% and 15% separating gels with a 4.5% stacking gel. A total volume of 20 μL of each sample was loaded into the gel. To detect the spike protein, the following antibodies were used: anti-SARS-CoV-2 Spike Protein S1 rabbit monoclonal (mAb) antibody (Cat: MA5-36250, Invitrogen) at a 1:1000 dilution, an HRP-conjugated mouse anti-

rabbit antibody (Cat: sc-2357, Santa Cruz) at a 1:2000 dilution, an anti-GAPDH (6C5, mouse monoclonal) antibody (Cat: sc-32233, Santa Cruz) at a 1:1000 dilution, and an HRP-conjugated anti-mouse antibody (Cat: sc-516102, Santa Cruz) at a 1:2000 dilution. The following antibodies were used to detect Gag: anti-HIV-1 p24 Gag mouse monoclonal antibody (Cat: ab9071, Abcam) at a 1:1000 dilution, an HRP-conjugated anti-mouse antibody (Cat: sc-516102, Santa Cruz) at a 1:2000 dilution, and an anti-GAPDH (6C5, mouse monoclonal) antibody (Cat: sc-32233, Santa Cruz) at a 1:1000 dilution. The BLUElf protein ladder was also loaded in each gel (Cat: PM008-0500K, FroggaBio). The Clarity Western Blot ELC Substrate (Cat:1705060, BioRad) was used to detect the proteins bound to the membrane. All membranes were read on the ChemiDoc BioRad imaging system.

2.9 Titering of Pseudovirus

There were two methods utilized to measure the titer of the pseudovirus generated. The first method utilizes a firefly luciferase reporter as the functional enzyme is created immediately upon pseudovirus genome transcription. The luciferase assay was plausible as we had the luciferase-IRES-ZsGreen backbone and not the ZsGreen backbone. We used 96-well white opaque plates (Cat: 136101, ThermoFisher) for all luminescent assays as they reflect light to maximize the signal output. These plates were pre-coated with poly-L-lysine, which aids in improving cell adherence and preventing cell disruption. Briefly, HEK293T-ACE2 cells were seeded at 1.25x10^4 cells per well and placed in the incubator overnight. The following day the complete medium was carefully removed and discarded, and a serial dilution of SARS2psv to be titered was added, resulting in a final well volume of 150 μL. Experimentally, the serial dilution started at an undiluted (150 μL) amount and then went down by 15 μL, supplementing to 150

μL with complete medium. Polybrene (Cat: TR-1003-G, MilliporeSigma) was added to each well at a 5 μg/mL concentration to facilitate lentiviral infection by minimizing the charge-repulsion (Crawford et al., 2020). At 60-72 hours post-infection, cells were prepared by removing all medium and adding 30 μL of 1x passive lysis buffer (PLB) (Cat: E1941, Promega) for 15 minutes in the dark. Lastly, 30 μL of One-Glo EX luciferase assay reagent (Cat: E8110, Promega) was added, and the plate was covered and transported for reading on the Cytation 5 plate reader (Cytation 5 Imager, BioTek). The relative light units (RLUs) were plotted against the virus dilution. For future experiments, the standardized amount of SARS2psv used was determined by having a sufficient (>1000 fold) signal above the virus-only background and a linear relationship between the virus added and RLUs (Crawford et al., 2020).

Flow cytometry was used as the second method as flow utilizes lasers as the excitation source of fluorophore-labeled cell samples. The cell samples absorb the light and then is emitted in a band of wavelengths that can be read by detectors. Thus, this method can also detect the fluorescent signal produced by the luciferase-ZsGreen backbone. Please refer to the flow cytometry section 2.10 for a detailed protocol.

2.10 Flow Cytometry

Flow cytometry was used for multiple research objectives. Therefore, a general flow protocol will be outlined below. All flow cytometry experiments utilized this general protocol unless otherwise indicated. Please refer to the specific sub-sections for more detailed information. At ~72 hours post-transfection or infection, cells were harvested using trypsin and collected into tubes. Cells were centrifuged at 400 x *g* for 5 minutes, and the supernatant was discarded. The cell pellet was resuspended in 1000 μL 1x phosphate-buffered saline (PBS) and transferred to

1.5 mL microcentrifuge tubes. The cells were then centrifuged at 300 x *g* for 5 minutes. The supernatant was discarded, 1000 μL of paraformaldehyde (PFA) was used to re-suspend, and cells were centrifuged again (300 x *g* for 5 minutes). The cells were washed twice with 3% bovine serum albumin (BSA) in 1x PBS (1000 μL first wash, 500 μL second) with centrifuging between washing steps. The supernatant was discarded, and the cells were resuspended in 500 μL 1% BSA in PBS and transferred into filtered capped flow cytometry tubes. The cell samples were then transported to the CytoFlex (Beckman Coulter CytoFlex Cytometer MELSS, Health Science Centre). Flow cytometry data were analyzed using the Kaluza software (version 2.1.1, Beckman Coulter). The overall cell populations were gated on forward vs side scatter plots, and gates were generated from the negative un-infected/un-transfected cell controls. Gating on the negative controls eliminates background fluorescence. Once gates were developed, the same gates were applied to all experimental conditions for analysis.

Flow cytometry was used to verify the neutralization assays functional capacity through a monoclonal antibody or patient samples. HEK293T-ACE2 cells were seeded at a density of $7.5x10^4$ in a 24-well plate and placed in a 37℃ 5% CO_2 atmosphere overnight. An anti-SARS-CoV-2 spike RBD neutralizing human IgG antibody (Cat: SAD-S35, Cedarlane) was used for the experiment at the following dilutions 1:1000, 1:500, and 1:100 (may vary depending on experimental optimization). The patient samples used in these experiments were either vaccinated, RT-qPCR confirmed SARS-CoV-2 infected, or a mixture of both. In addition, samples used for these experiments showed high total antibody responses through our collaborative laboratory and their ELISAs. The following serum antibody-positive and antibody-negative dilutions were used 1:1000, 1:500, 1:250, 1:100, and 1:50.

2.10.1 Titering Pseudovirus by Flow Cytometry

HEK293T-ACE2 cells were seeded in a 6-well plate at a density of 3x10^5 cells per well and placed in the incubator overnight. For the experimental conditions, cells were inoculated with undiluted SARS2psv, a 1:3, 1:9, or a 1:27 SARS2psv dilution. There was also a No Spike and un-infected control. This experiment used the pseudovirus transfection from the C-terminal Δ21 spike plasmid. The titers of psv were calculated using the Poisson formula. The titer per mL was represented as: -ln(1-p/100) x (number of cells per well/ volume of virus per well in mL), where P is the ZsGreen positive cell percentage. It should be noted and was explained in the literature that when the percentage of cells that are ZsGreen positive is low, the formula is equal to (% ZsGreen positive/100) x (number of cells per well/ volume of virus per well in mL). Furthermore, Crawford et al. suggest titers are only accurate if the percentage of ZsGreen positive cells is relativity low. They suggest that % positive should be between 1-10% (Crawford et al., 2020).

2.10.2 Verification of ACE2 expression by Flow Cytometry

To verify ACE2 expression, HEK293T-ACE2 and A549-ACE2 were plated at 5x10^6 and 3x10^6 cells per 10 cm cell culture dish. Cells were stained with anti-human ACE2 polyclonal goat IgG primary antibody at 2 μg/mL (Cat: AF933, R&D Systems) followed by donkey anti-goat IgG (H+L) highly cross-adsorbed (Alexa Fluor 647) secondary antibody (Cat: A32849, ThermoFisher Scientific) at a 1:1000 dilution. Cells were incubated at 4℃ for 30 minutes in the dark for each staining step. Cells were washed twice with 3% BSA in 1x PBS following each staining step. Cells were resuspended in 500 μL 1% BSA in PBS and transferred into flow cytometry tubes.

2.10.3 Determination of Caspase-1 Activation by Flow Cytometry

HEK293T cells were seeded at a density of 5x10^5 cells per well in a 6-well plate and placed in the incubator overnight. The following day, cells were transfected with either SARS-CoV-2 ORF3a, SARS-CoV-2 E protein, or MOCK control. Cells were placed in the incubator overnight, and the following day plates were rinsed twice with the complete medium and then supplemented with the new medium. For positive control, a day before staining cells was treated with LPS (Cat: L5024-10MG, Millipore-Sigma) at 5 μg/mL for 3 hours, followed by the addition of Nigericin (InvivoGen) used at 167.5 μM and incubated overnight. At three days post-infection, cells were collected using the same methods in the cell culture section 2.1 up to 1200 rpm for 5 minutes of centrifugation. The heat shock controls were then isolated, resuspended in complete media, placed in a 65℃ water bath for 5 minutes and centrifuged at 400 x *g* for 5 minutes. The supernatant was discarded, and cell pellets were resuspended in 200 μL of 30x caspase-1 probe reconstituted in complete medium (FAM-FLICA caspase-1 inhibitor kit (cat: 98, ImmunoChemistry Technologies)) and incubated for 45 minutes at 37℃. Following incubation, an additional 400 μL of complete medium was added, and the cells were incubated for an additional hour. Cells were centrifuged at 2000 x *g* for 5 minutes, and the supernatant was discarded. Cell pellets were resuspended in 300 µL of apoptosis wash buffer, and cells were fixed by adding 60 µL of fixative from the caspase-1 probe kit (ImmunoChemistry Technologies, product number 98). The cells were then incubated at room temperature in the dark for 20 min. Following incubation, cells were centrifuged as above, and the supernatant was discarded. Cells were resuspended in 500 µL PBS and stored at 4°C until analysis. Cells were run on a CytoFLEX flow cytometer (Beckman Coulter), and FAM-FLICA fluorescence was detected

using the 525/40 detector on the 488 nm laser. For a more in-depth protocol, please refer to (Wallace et al., 2022), as our laboratory previously established this protocol.

2.11 Neutralization Assay

Serum or plasma was heat inactivated at 56℃ for an hour or 30 minutes to inactivate complement. The "negative" serum sample was collected prior to the pandemic from our collaborative laboratory and utilized upon receiving consent. Briefly, HEK293T-ACE2 cells were seeded at 1.25x10^4 cells per well in 96-well opaque white plates pre-coated with poly-L-lysine. Plates were placed at a 37℃ 5% CO_2 atmosphere overnight. Approximately 1 hour before infection, the serum sample to be tested were serially diluted and pre-incubated with a standardized quantity of infectious pseudovirus in a separate, 96-well plate. For the dilutions, an initial 1:20 dilution was made and did serial 3- or 10-fold dilutions. In parallel, a similar virus inoculum that had not been incubated with serum was used for a control. The separate serum/psv/medium plate was then incubated for an hour. The pre-seeded cell plate was then collected, and all medium was carefully removed. Then 150-190 µL (depending on the experiment) of the serum/psv/medium dilutions was added to the corresponding wells in the cell plate. Polybrene was added to each well to a final 5 µg/mL concentration. The plate was placed in a 37℃ 5% CO_2 atmosphere for 60-72 hours. After the three-day incubation, the luciferase assays were done as described in section 2.9 above. For a positive assay control, a 1:100 dilution of the luciferase-IRES-ZsGreen plasmid transfection harvest was used.

2.12 Inflammasome Array

An amount of 6x10^6 HEK293T cells were plated in 10 cm culture dishes for the inflammasome array assays. For a detailed protocol on the transfection, please refer to section

2.6 (generation of pseudovirus through a transfection). At 3 days post-transfection, cells were harvested in 700 µL of Qiazol lysis reagent, and lysates were transferred to a 1.5 mL tube. Lysates were then passed through a 20 gauge/0.9mm syringe 10-20 times to homogenize the cells. A Qiagen miRNeasy mini kit (Cat: 217004) was used to purify the total RNA. The protocol was followed per the Qiagen miRNeasy mini kit handbook. RNA concentration and purity were measured using the Nanodrop spectrophotometer. Next, the Qiagen RT^2 First Strand Kit (Cat: 33041) was used to reverse-transcribe mRNA into cDNA and eliminate genomic DNA in our RNA samples. For the genomic DNA elimination mix, we used 0.5 µg of RNA and the reverse transcription mix was made for two reactions. Next, we used the Qiagen RT^2 profiler PCR array format C (Cat: 330231, PAHS-097ZC-6) and Qiagen RT^2 SYBR Green master mix (Cat: 330524) as per the manufacturer's protocol. The threshold was set at 0.05, and the C_t values were exported to Excel. Data analysis was conducted at Qiagen's Geneglobe Data Analysis Centre web resource.

2.13 RT-qPCR

The RNA used in the RT-qPCR experiments was isolated and purified using the Qiagen miRNeasy mini kit (Cat: 217004). The PrimeTime Gene Expression 2x Master Mix (Cat: 1055772, Integrated DNA Technologies) was used to check the samples for DNA contamination. After confirmation of no DNA contamination in our RNA samples, we prepared a 1:9 dilution of the purified RNA in an elution buffer. A master mix of primer pools targeting genes of interest was also prepared (2 µL of each sequence (forward and reverse), 5 µL of SYBR green dye at 100x, and 116 µL of RNA-free water). The RT-qPCR was performed on a 20 µL reaction mixture containing 10 µL of RNA dilution/water control, 5 µL of the primer pool, and 5 µL of TaqMan

Fast Virus 1-Step Master Mix (Cat: 4444432, ThermoFisher Scientific). The thermal cycling parameters were initiation at 50℃ for 5 minutes, denaturing at 95℃ for 20 seconds and 45 cycles of 95℃ for 3 seconds, and annealing at 60℃ for 30 seconds. In addition, a melt curve was performed to assess the dissociation characteristics of our primers during heating. The data were normalized to Glyceraldehyde 3-phosphate dehydrogenase (GAPDH) and exported to excel, where we could calculate the delta C_t values. GAPDH is a housekeeping gene due to being stably and constitutively expressed at high levels in most cell types (Barber et al., 2005). To detect differential gene(s) expression between two subsets, researchers need a control for experimental variations in the amount of RNA and batch-to-batch variations in the PCR reagents. Housekeeping genes are used to normalize the target gene expression data. The primers were synthesized by Thermofisher Scientific and are shown in the table below.

Table 1: Primer Sequences used for real-time PCR in this thesis.

Primer	Sequence
NLRP3 F	5’-TCTGCTCATCACCACGAGAC -3’
NLRP3 R	5’-CTTGGGCCTCATCAGAGAAG-3’
MOK F	5’-GCTTTCGGGAGTGGTCAG-3’
MOK R	5’-TTCTTGCTCGCAGGGATG-3’
TNFa F	5’-TCCTCAGCCTCTTCTCCTTCCT-3’
TNFa R	5’-ACTCCAAAGTGCAGCAGACAGA-3’
Caspase-1 F	5’-CGCAGATGCCCACCACT-3’
Caspase-1 R	5’-TGCCCACAGACATTCATACAG-3’
Caspase-8 F	5’-AATGTTGGAGGAAAGCAATC-3’
Caspase-8 R	5’-CATAGTCGTTGATTATCTTCAGC-3’
CCL5 F	5’-TACCATGAAGGTCTCCGC-3’
CCL5 R	5’-GACAAAGACGACTGCTGG-3’
NLRC5 F	5’-AGTGGCTCTTCCGCTTGGACAT-3’
NLRC5 R	5’-CGGAACCCTAAGAACTTGGCTG-3’
Aim2 F	5’-TAGCGCCTCACGTGTGTTAG-3’
Aim2 R	5’-TTGAAGCGTGTTGATCTTCG-3’
IL-1b F	5’-TCAGCCAATCTTCATTGCTC-3’
IL-1b R	5’-GCCATCAGCTTCAAAGAACA-3’
IL-18 F	5’-GATAGCCAGCCTAGAGGTATGG-3’
IL-18 R	5’-CCTTGATGTTATCAGGAGGATTCA-3’
NFkB F	5’-GCAGCACTACTTCTTGACCACC-3’
NFkB R	5’-TCTGCTCCTGAGCATTGACGTC-3’
IFN B1 F	5’-GGCAGTATTCAAGCCTCCCAT-3’
IFN B1 R	5’-TCTCCTGTTGTGCTTCTCCAC-3’
IRF1 F	5’-GAGGAGGTGAAAGACCAGAGCA-3’
IRF1 R	5’-TAGCATCTCGGCTGGACTTCGA-3’
GAPDH F	5’- GGTGGTCTCCTCTGACTTCAACA -3’
GAPDH R	5’- TGAGGGCAATGCCAGCC-3’

Results

3. Results
    3.1 Generation of Pseudovirus

A five-plasmid packaging system was used to generate pseudoviruses with SARS-CoV-2 spike protein. The first plasmid encodes the HIV-1 lentiviral backbone with a Luciferase-IRES-ZsGreen reporter protein (Crawford et al., 2020). The second plasmid encodes the SARS-CoV-2 S protein driven by a CMV promoter (Crawford et al., 2020). The original Wuhan-Hu-1 spike sequence protein was used for the first few experiments. The last three plasmids expressed the minimal set of lentiviral proteins required to package and assemble the viral particles: Gag/pol (group-specific antigen/ DNA polymerase), Rev (regulator of expression of virion proteins), and Tat (trans-activator of transcription) (Crawford et al., 2020). The HEK293T-transfected cells produce the pseudovirus, as shown in Figure 4(A). The HEK293T cell line was chosen due to its high transfection efficiency. After harvesting the pseudovirus, these particles were used to infect permissive cell lines expressing ACE2, the SARS-CoV-2 receptor protein, as shown in Figure 4(B). The SARS-CoV-2 S infected cells will fluoresce green due to the expression of ZsGreen.

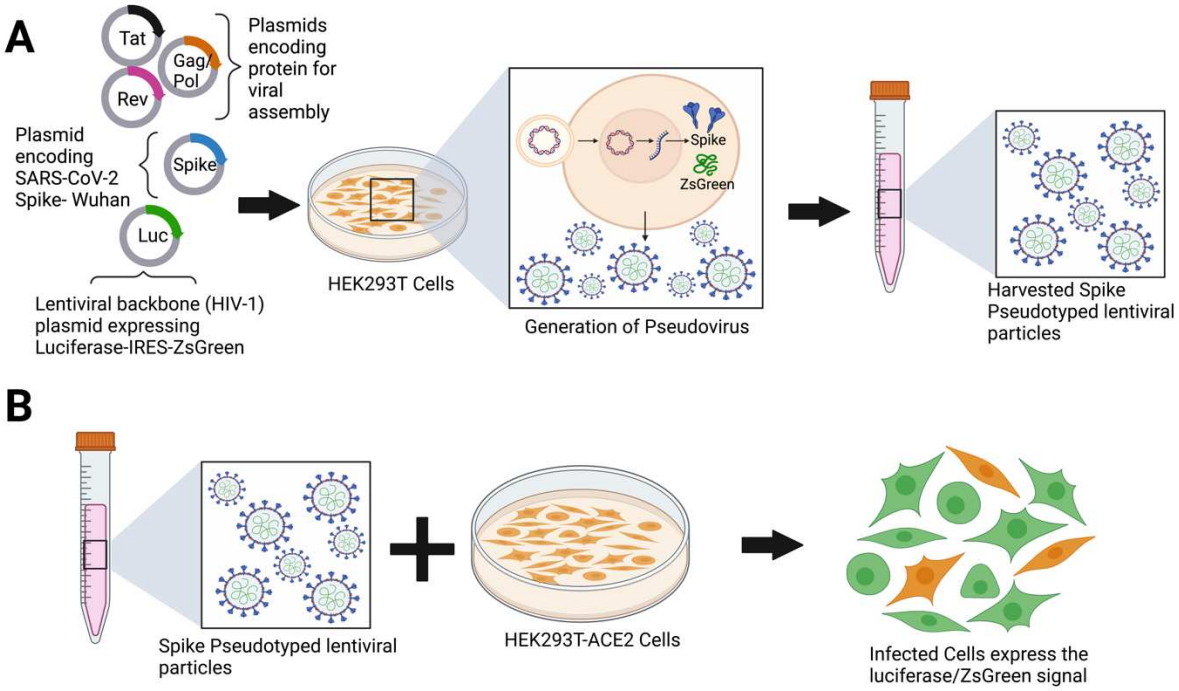

Figure 4: Generation of SARS-CoV-2 Pseudovirus. (A) HEK293T cells were transfected with a plasmid containing the HIV-1 lentiviral backbone expressing the luciferase-IRES-ZsGreen reporter protein, a plasmid expressing spike (from the Wuhan-Hu-1 strain), and the plasmids expressing the other HIV-1 proteins needed for virion formation (Gag/pol, Tat, Rev). Transfected cells produce the pseudovirus particles with the spike on their surface and the fluorescent marker as their genome. These particles were then harvested for use in experiments. (B) The harvested pseudovirus was then used to infect permissive cell lines that express the ACE2 receptor (HEK293T-ACE2). Infected cells can be distinguished from non-infected cells as they express the luciferase-ZsGreen signal. Created with biorender.com; adapted from (Crawford et al., 2020).

3.1.1 Analysis of Pseudovirus Infection Efficiency in Various Cell Lines.

To monitor pseudovirus infection efficiency and to identify the cell line with the highest susceptibility to the spike-pseudotyped particles, we performed fluorescence microscopy to detect infected cells expressing luciferase-IRES-ZsGreen. A549, HCT-8, and HEK293T-ACE2 cell lines were used for these experiments. It should be noted that cell lines H1793 (female human lung adenocarcinoma cell), Huh-7.5, and HEK293T cells were also examined. The pseudovirus stock was generated using the original Wuhan-Hu-1 spike sequence plasmid. For this experiment, the following pseudovirus stocks were used: SARS2psv (HIV-1 backbone, Rev, Tat, Gag/pol, and spike plasmids), No spike (HIV-1 backbone and all machinery plasmids (Rev, Tat, and Gag/pol)), and a transfection control (supernatant from the cells that were exposed to all transfection reagents but no plasmids). The infection control was also included (cells not infected with any previously generated pseudovirus stocks). As seen in Figure 5(A), the only cell line to show susceptibility to SARS2psv infection by luciferase/ZsGreen expression was A549. Although, it was quickly determined that there was noticeable fluorescence in all wells (even the controls). It was believed that the non-specific fluorescence resulted from ROS or cellular stress (Hsieh et al., 2015; M. I. Khan et al., 2012; Nova et al., 2020). Based on these results, we wondered if the A549 cell line might generate better titers of SARS2psv and, therefore, performed an A549 transfection (instead of HEK293T) to produce pseudovirus. An infection of the previously generated SARS2psv-A549 was then done in HCT-8 and HEK293T-ACE2 cell lines. Figure 5(B) shows that the infection efficiency obtained was not improved. The results in Figure 5 were unexpected as we obtained low infection capacity with permissive cell lines. Since the HIV-1 lentiviral backbone with the luciferase-ZsGreen reporter was used, the reduced

magnitude in signal might have been due to ZsGreen being driven by an IRES rather than the primary promotor (Crawford et al., 2020).

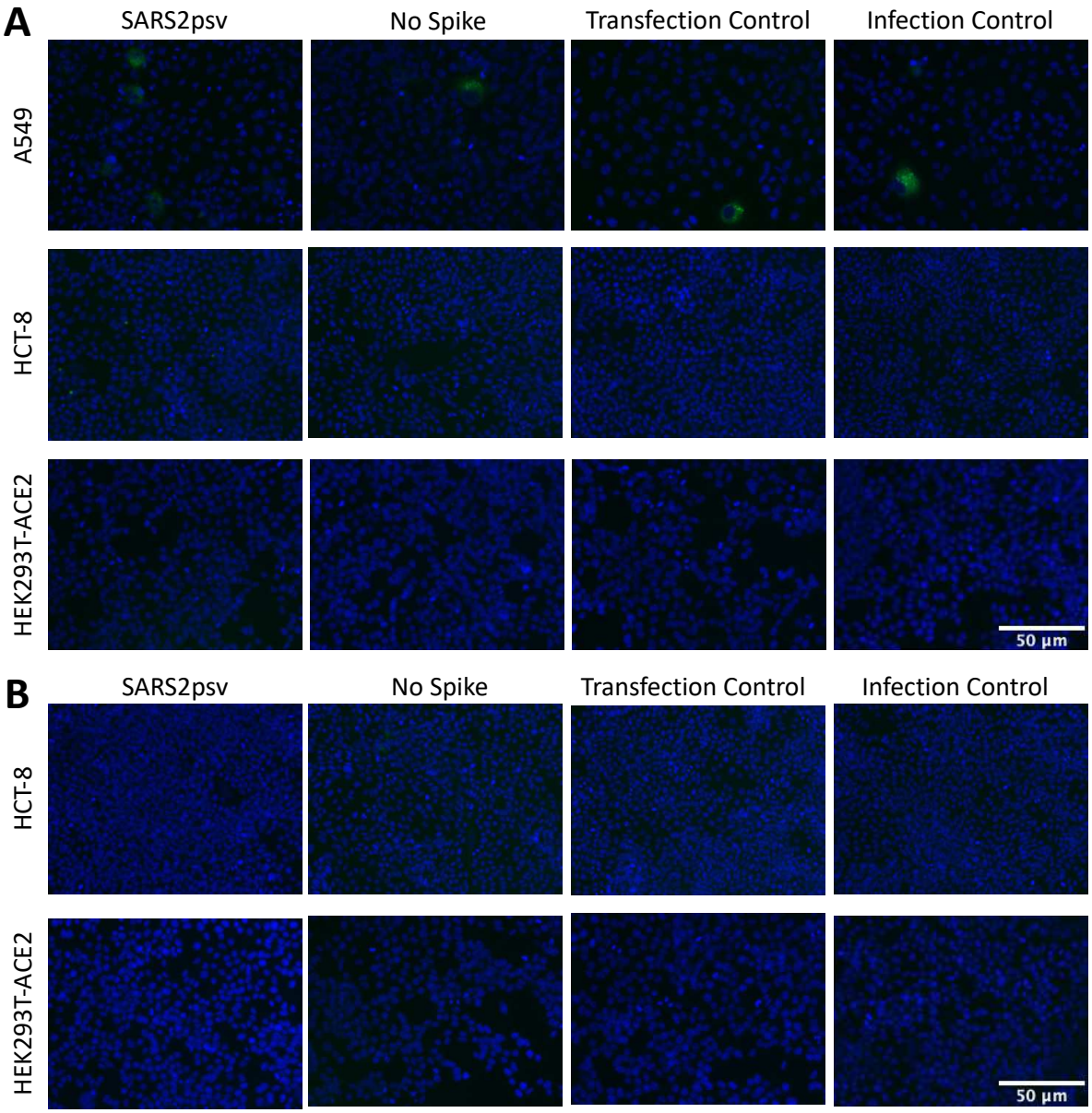

Figure 5: Analysis of Pseudovirus Infection Efficiency in Various Cell Lines. Microscope images showing Luciferase-IRES-ZsGreen expression (green) in cell lines at 72 hours post-infection. The following pseudovirus stocks were used: SARS2psv (HIV-1 backbone, Rev, Tat, Gag/pol, and spike plasmids), No spike (HIV-1 backbone and all machinery plasmids (Rev, Tat, and Gag/pol)), and a transfection control (supernatant from the cells that were exposed to all transfection reagents but no plasmids). An infection control was also used in which the cells were not infected with any previously generated psv stocks. The nuclei were stained with DAPI (blue). All image acquisition was taken at a 20x magnification. (A) A549, HCT-8, and HEK293T-ACE2 cell lines infected with HEK293T generated psv stocks. Scale bar, 50 μm(B) HCT-8 and HEK293T-ACE2 cell lines infected with A549 generated psv stocks. Scale bar, 50 μm. Images were collected with both the DAPI and GFP/FITC filters. Representative images of results with HEK293T-ACE2 and HCT-8 having an n=2 and A549 n=3.

3.1.2 Determination of SARS-CoV-2 Spike Pseudovirus Infection Capacity.

To determine the generated SARS-CoV-2 spike pseudovirus infection capacity, we utilized a luciferase assay. For these experiments, the HEK293T-ACE2 permissive cell line was used. The pseudovirus stock was generated using the original Wuhan-Hu-1 spike sequence plasmid. The following experimental conditions were used: SARS2psv (supernatant from HIV-1 backbone, Rev, Tat, Gag/pol, and spike plasmids), No spike (supernatant from HIV-1 backbone and all machinery plasmids), reporter control (supernatant from the HIV-1 backbone only), transfection control (supernatant from the cells that were exposed to all transfection reagents but no plasmids), cell control (HEK293T cell line infected with SARS2psv), cell medium control (cell medium only), and SARS2psv control (SARS2psv with no cells). These experimental conditions were implemented in all other experiments unless otherwise stated. For these experiments, a 1:3 dilution of psv was utilized per the suggestion of multiple research publications (Crawford et al., 2020; Legros et al., 2021; Nie et al., 2020). The potential enhancement of infection due to adding polybrene was also evaluated. A schematic representation of the luciferase assay methodology can be observed in Figure 6(A). The addition of polybrene significantly increased the infection efficiency of the SARS-CoV-2 psv, which can be observed in Figure 6(B). Unfortunately, we were unable to confirm this result (Figure 6(C)). The decreased RLU observed in Figure 6(C) was expected as there typically is a 2-3-fold variation in multiple step assays due to different cell passages and cell growth rates. However, in both Figures 6(B & C), we obtained low background or “signal-to-noise” ratios in the control wells versus infected wells. The lack of reproducibility could have been due to variability in the amounts of psv produced among different transfections. From this point

forward, all transfection supernatants were pooled. Lastly, it was concluded that the original Wuhan-Hu-1 spike sequence plasmid was not going to achieve the titers needed for robust neutralization experiments.

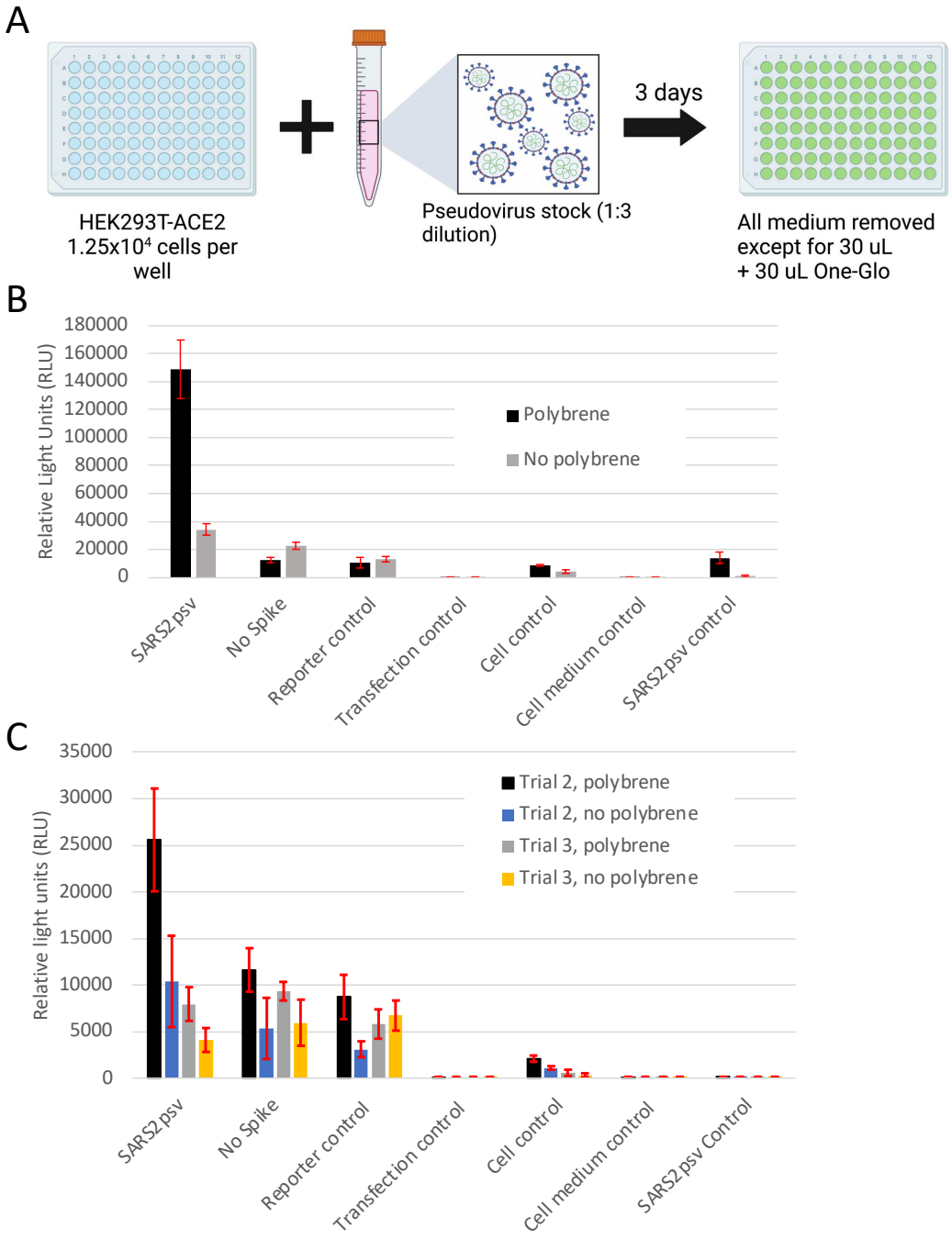

Figure 6: Infection Capacity of the Spike Pseudovirus. (A) HEK293T-ACE2 cells were infected with a 1:3 pseudovirus dilution and left for 72 hours. The pseudovirus stock used in this experiment was prepared by transfection of HEK293T cells with the spike plasmid containing the original Wuhan-Hu-1 spike sequence. Cells were incubated either with polybrene (5 μg/mL) or without polybrene (B) HEK293T-ACE2 cells infected with supernatant from SARS2psv, No spike, Reporter control, or transfection control. In addition, we included a cell control, cell medium control, and SARS2psv control. (C) Biological replicates of (B). Each bar shows the average of triplicate values, with error bars indicating the standard error.

3.1.3 Modification to the Pseudovirus System.

Multiple research groups discovered and published that a cytoplasmic tail truncation that removed the last 21 amino acids (AA) (Δ21) from the spike sequence contained in the original Wuhan-Hu-1 spike plasmid improved the efficiency of pseudovirus production (Crawford et al., 2021; Garcia-Beltran, Lam, Astudillo, et al., 2021; Garcia-Beltran, Lam, St. Denis, et al., 2021a). This Δ21 spike plasmid soon replaced the original Wuhan-Hu-1 plasmid in the BEI repository. Thus, a few months after our laboratory generated our pseudovirus and established the luciferase assay, we pivoted to this plasmid. The rationale for switching to this plasmid was due to other groups reporting that removing the ER retention signal would improve the plasma-membrane expression of the spike (Crawford et al., 2020, 2021; Garcia-Beltran, Lam, St. Denis, et al., 2021b) and by deleting the cytoplasmic tail, it would improve pseudotyping efficiency without affecting neutralization sensitivity (Crawford et al., 2021). The generation of our new Δ21 spike pseudovirus can be observed in Figure 7(A). All experiments carried out from this point forward used the Δ21 spike plasmid.

3.1.4 Confirmation of Viral Protein Expression in Cells Transfected with the SARS-CoV-2 Pseudovirus.

We utilized Western blot analysis to examine protein expression to verify that our generated pseudoviruses had functional capacity. To confirm spike protein expression, we used an anti-SARS-CoV-2 spike S1 antibody. We tested cell lysates and supernatant from SARS2psv, No Spike, reporter control (HIV-1 backbone only), and transfection control. In Figure 7(B), spike protein was expressed in the transfected cell lysates with SARS2psv (HIV-1 backbone, Rev, Tat, Gag/pol, and spike plasmids) (lane 2). Based on the product data sheet for our spike antibody, bands were expected and observed at ~180 kDa (unprocessed spike) and cleaved S1 at ~90 kDa.

No bands were observed in the harvested supernatant, but this was not surprising as visualization of viral proteins by Western blot usually requires concentration of virus by columns, ultracentrifugation, or PEG (polyethylene glycol) precipitation. To demonstrate Gag protein expression, we used an anti-HIV-1-p24 Gag antibody. In Figure 7(C), Gag protein was expressed in cell lysates of SARS2psv (lane 2) and No spike (HIV-1 backbone and all machinery plasmids (lane 3)). Based on the Gag antibody product sheet, bands were expected and observed at ~24 kDa. The full-length Gag at ~55 kDa and its processing intermediates can also be observed in Figure 7(C). Glyceraldehyde 3-phosphate dehydrogenase (GAPDH) was used as a loading control, and bands can be observed at ~36 kDa in the bottom panels of Figure 7(B & C). These results show that our pseudovirus components were being expressed (transcribed and translated), and pseudoviruses were being produced in the cell lysates. Since there was no protein expression in the supernatant, probably due to the lack of concentration, it may be possible that the proteins are expressed, but the pseudovirus is not being assembled, released, or the spike is not incorporated. Although, when observing the infection capacity data in Figure 6, you can see that the spike pseudovirus is meditating entry and infection.

3.1.4.1 Verification of ACE2 Expression in the Permissive Cell Lines.

Since we were achieving lower than expected levels of pseudovirus infection, we questioned whether the ACE2 over-expressing cell lines we received from BEI resources were indeed expressing high levels of ACE2. It was possible that our stocks of cells had lost expression of the transgene. Consequently, checking for ACE2 expression levels was done towards the end of experiments because we were still obtaining unexpected results. Nevertheless, ACE2 expression was verified with an anti-human ACE2 polyclonal goat IgG

primary antibody and donkey anti-goat IgG (H+L) highly cross-adsorbed (Alexa Fluor 647) secondary antibody. The percent of positive cells that expressed ACE2 can be seen in Figure 7(D). The percent positivity for the HEK293T-ACE2 cell line was ~95% in cell passages 6 and 19, and for the A549-ACE2 target cell line, the percent positivity was ~40%. The parental cell lines showed ACE2 percent positivity of less than 1%. These results indicate that our target cell lines readily express ACE2 in various passages and that unexpected results were not due to low ACE2 expression.

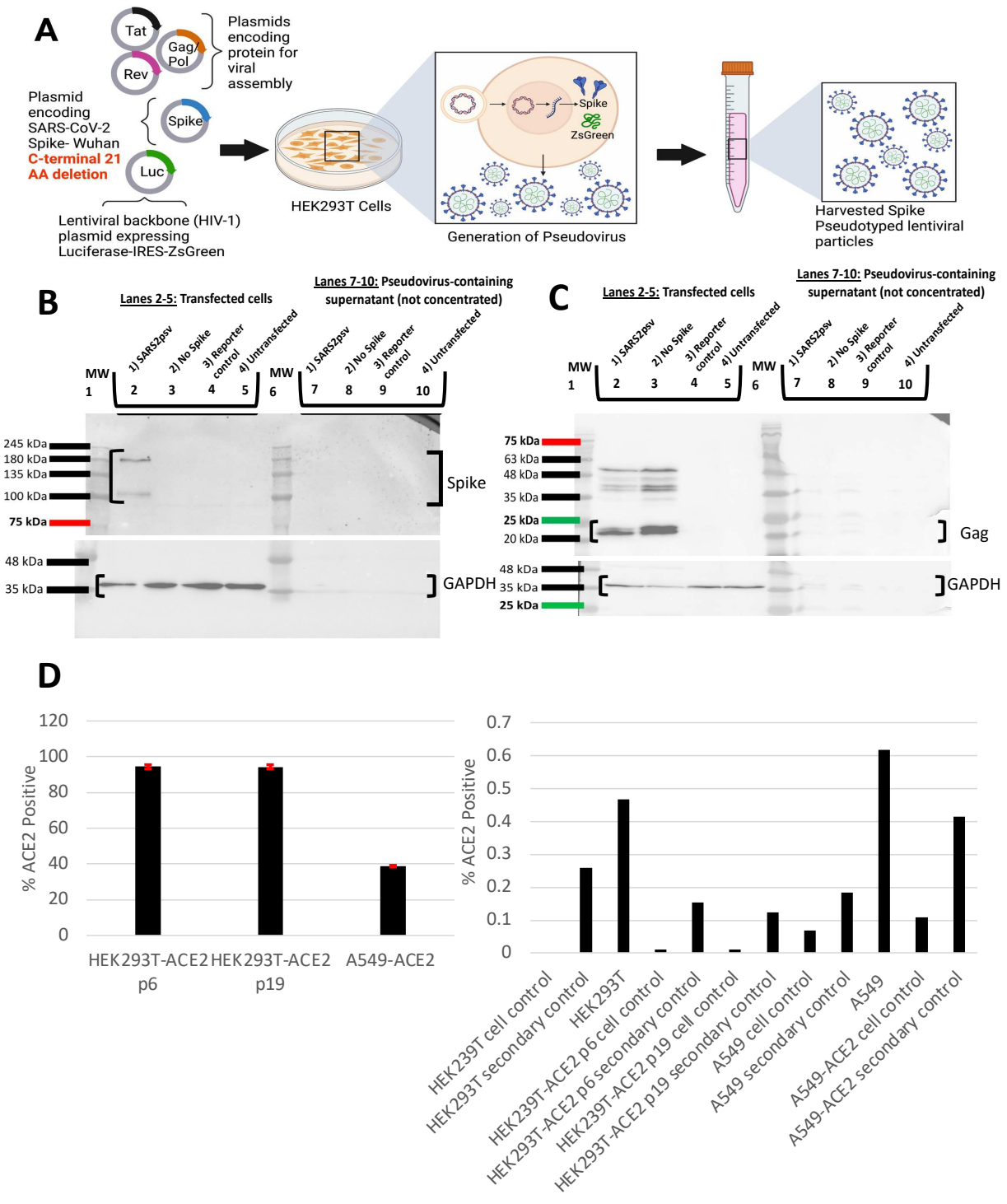

Figure 7: Generation, Verification, and Validation of the Pseudovirus Assay. (A) HEK293T cells were transfected with a plasmid containing the HIV-1 lentiviral backbone expressing the luciferase-IRES-ZsGreen reporter protein, a plasmid expressing spike (C-terminal Δ21), and the plasmids expressing the other HIV-1 proteins needed for virion formation (Gag/pol, Tat, Rev). Transfected cells produce the pseudovirus with spike on their surface and the fluorescent

marker as their genome. These particles were then harvested for use in experiments. (B) Verification of spike protein expression. An anti-SARS-CoV-2 spike S1 antibody was used. Bands were expected at 180 kDa and cleaved S1 at 90 kDa. (C) Verification of Gag protein expression. An anti-HIV-1-p24 Gag antibody was used, and a band was expected at 24 kDa. GAPDH was used as a loading control and was expected at 36 kDa (bottom panels). The Western blot results are representative images of 3 experiments. (D) Flow cytometry analysis of ACE2 expression. ACE2 positivity was determined by primary and secondary antibodies (denoted as just the cell line). A cell control (no antibodies) and secondary control (just the secondary antibody) was also used. Fluorescence was gated on the HEK293T-ACE2 cell control to set the threshold for ACE2 positivity. Each bar in the left graph of D shows the average triplicate values, with error bars indicating the standard error.

3.1.5 Determination of the Infection Capacity of the Δ21 Spike Pseudovirus.

A luciferase assay was utilized again to determine the generated Δ21 spike pseudovirus infection capacity. For these experiments, the HEK293T-ACE2 permissive cell line was used. The pseudovirus stock was generated using the Δ21 spike plasmid. The following experimental conditions were used: SARS2psv, No spike, reporter control, transfection control, cell control, cell medium control, and SARS2psv control. For a detailed description of experimental conditions, please refer to section 3.1.2. A schematic representation of the experimental workflow can be seen in Figure 8(A). The infection capacity of pseudoviruses produced using the new Δ21 spike sequence can be observed in Figure 8(B). The results presented in Figure 8(B) show more consistent pseudovirus infections with less variability. In addition, we also obtained a higher pseudovirus titer and had ≥100-fold between our infected "SARS2psv" and our background controls of SARS2psv only (SARS2psv control), complete medium only, and HEK293T cells (cell control). Based on these results, we concluded that our assay was ready to be used to measure the neutralization capacity in patient samples.

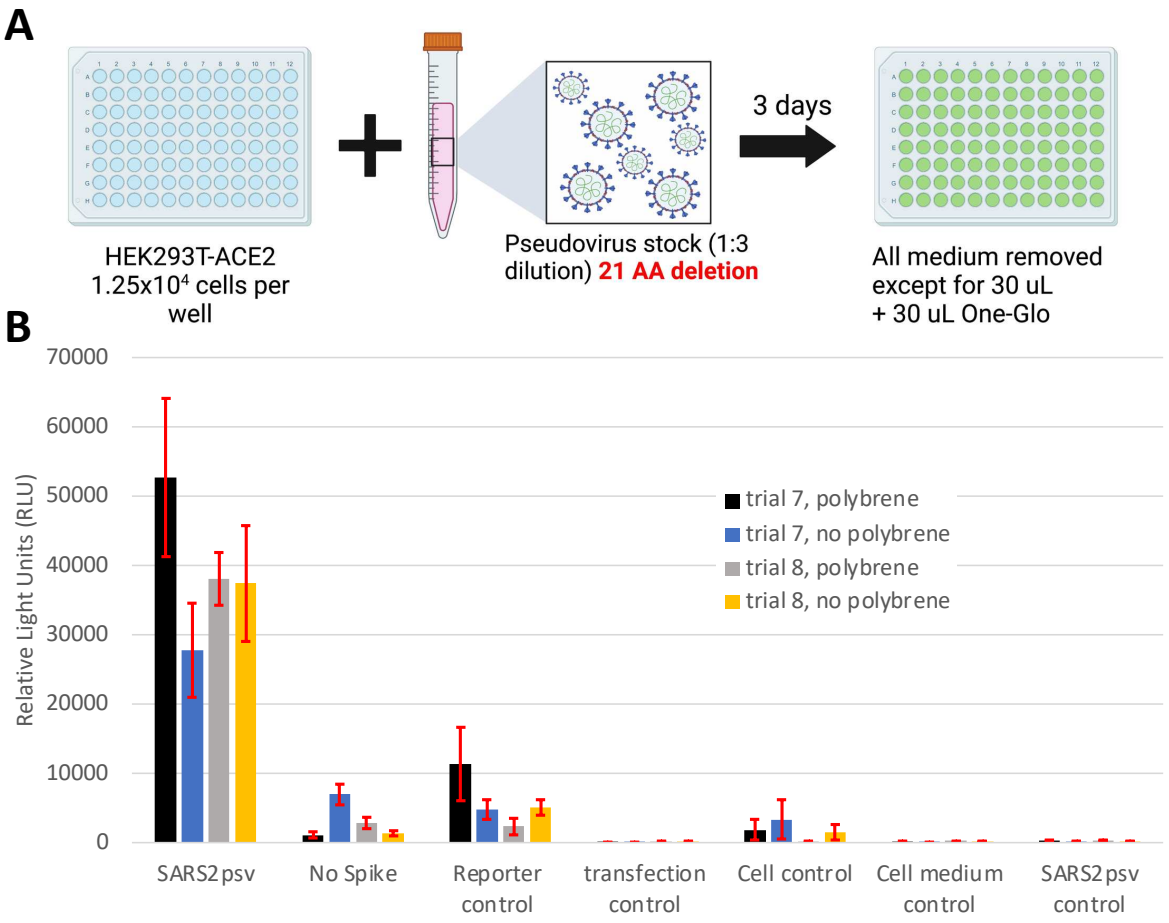

Figure 8: Infection Capacity of the Δ21 Spike Pseudovirus. (A) HEK293T-ACE2 cells were infected with a 1:3 pseudovirus dilution and left for 72 hours. The pseudovirus stock used in this experiment was prepared by transfection of HEK293T cells with the Δ21 spike plasmid. (B) HEK293T-ACE2 cells infected with pseudovirus stock from SARS2psv, No spike, reporter control, or transfection control. In addition, a cell control, cell medium control, and SARS2psv control were used. Depending on the experiment, some wells were also treated with 5 ug/mL polybrene. Each bar shows the average of triplicate values, with error bars indicating the standard error.

3.1.6 Quantification of Neutralizing Antibodies.

To study the immune response against COVID-19 vaccination, we used a neutralization assay to measure the neutralizing antibody titer capable of preventing 50% of the psv infection. The patient plasma samples were collected from vaccinated individuals roughly one month after receiving the second dose. These samples were confirmed to have an antibody response based on ELISAs performed in our collaborative laboratory. The negative sample was collected pre-pandemic and used upon gaining consent. In the early neutralization assay experiments, an initial 1:20 plasma dilution was made and then serially diluted 3-fold. The plasma was then incubated with a standardized volume of pseudovirus sufficient to achieve $2x10^5$ RLUs as recommended (Crawford et al., 2020). A schematic workflow of the neutralization assay can be found in Figure 9(A). In this experiment, a cell density of $1.25x10^4$ cells per well was used in Figure 9(B) per the recommendations of the Balazs and Bloom laboratories (Crawford et al., 2020). In Figure 9(C), we used a cell density of $4x10^3$ cells per well from the guidance of the Wang group (Nie et al., 2020). In this assay, the luciferase enzyme emits photons using ATP and molecular oxygen. Thus, there is a direct linear correlation between the luminescent signal and the number of infected cells. Therefore, in the neutralization assay, the inhibition of viral entry into cells by nAbs can be correlated to the decreased luciferase signals in the target cells (Crawford et al., 2020; Nie et al., 2020). The reduction observed in the total luminescent signal reflects the level of nAbs in the sample. Unfortunately, in Figure 9(B & C), such a result was not obtained. We would have expected to observe a sigmoidal curve in a dose-response manner. Our least dilute plasma sample should have a low fraction of infectivity as there would be a higher titer of nAbs. The more we dilute our plasma sample, the higher the fraction of

infectivity we should see. In addition, we would expect our negative control to have no neutralization capacity and therefore be a straight line. The result obtained made us think that there might be something interfering with our assay.

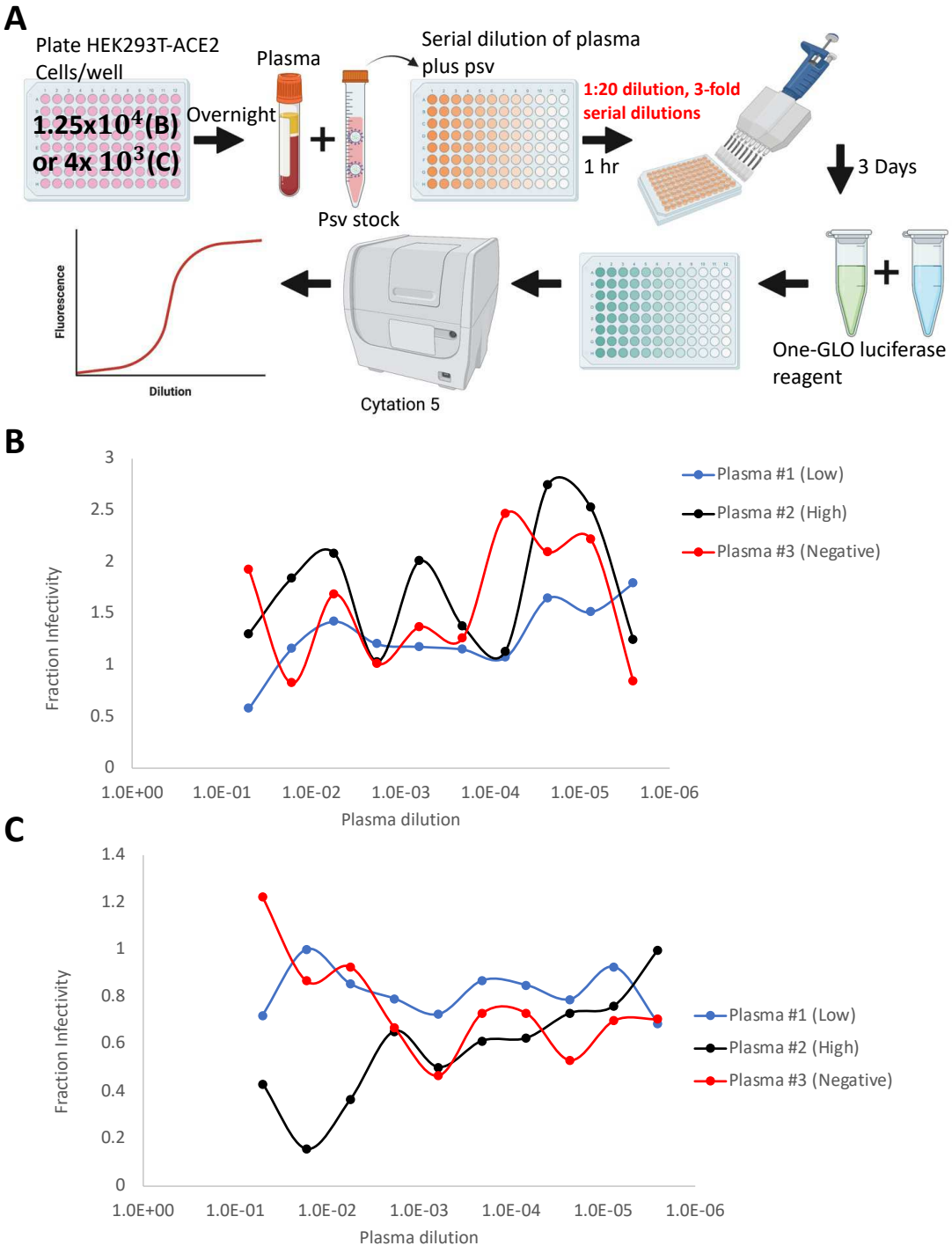

Figure 9: Quantification of the Neutralization Assay to Determine Immune Protection. (A) Schematic diagram of the neutralization assay set-up. Plasma samples (high, low, and negative antibody levels) were pre-incubated with a standardized amount of psv. A 1:20 plasma dilution was serially diluted 3-fold. (B) HEK293T-ACE2 were plated at $1.25x10^4$ cells per well. C) HEK239T-ACE2 were plated at $4x10^3$ cells per well. The fraction infectivity was calculated by taking the RLU from the infected wells (plasma and psv) divided by the SARS2psv control wells (virus only). Each point shows the average of duplicate replications.

3.1.7 Quantification of Neutralizing Antibodies in Plasma or Serum Samples.

After the previous experiment, it was clear that some aspect or component, unknown to us, was interfering with our assay. Upon further inspection of the One-Glo luciferase reagent manual, we realized that the medium and its components could reduce the signal. Therefore, the first experimental modification involved removing all mediums and adding PLB before the addition of One-Glo. Furthermore, through an updated literature search, we noticed that some groups used serum samples and others used plasma (Crawford et al., 2020, 2021; Garcia-Beltran, Lam, St. Denis, et al., 2021a; Nie et al., 2020). Thus, we wondered whether something in the whole blood collection tubes, such as organic solvents, divalent cations, and/or anticoagulant factors, might interfere with our assay (Lima-Oliveira et al., 2018; L. Liu et al., 2010; Vignoli et al., 2022). Therefore, we tried both serum and plasma samples as they were collected in serum-separating tubes (SST) or acid-citrate-dextrose (ACD) tubes, respectively. The serum and plasma samples were collected from two different vaccinated individuals ~four months after their second dose of a COVID-19 vaccine. The presence of serum anti-S antibodies was confirmed by ELISAs performed in the Grant laboratory. The experimental schematic can be seen in Figure 10(A). The result of these changes can be observed in Figure 10(B). Still, the results were not what we expected, but the plasma samples appeared to be trending in the right direction. The fraction infectivity started low where the most plasma was present (therefore the most nAbs) and generally trended upward as plasma was diluted. We decided to use plasma samples in the remaining neutralization experiments and kept adding PLB from these results.

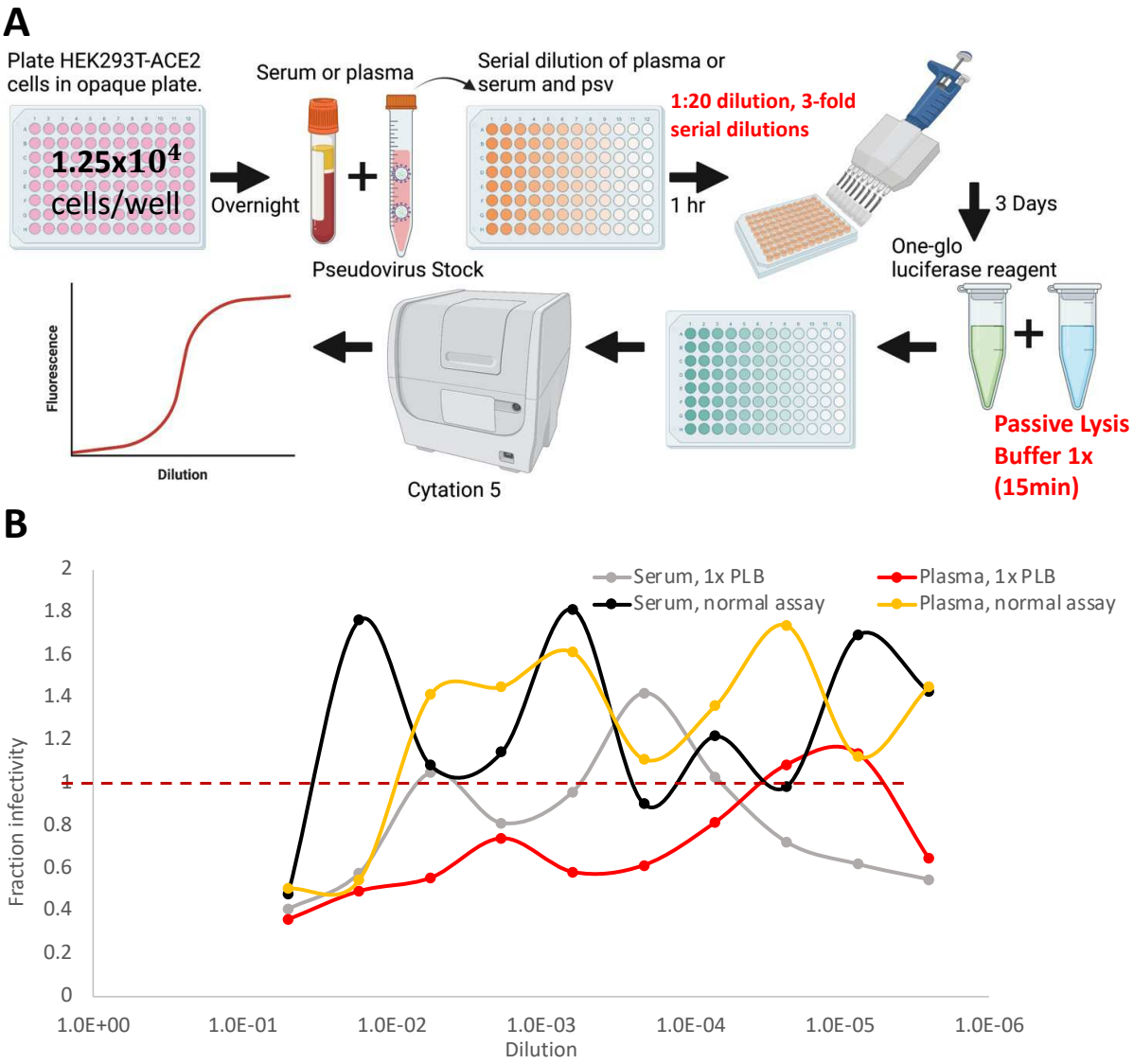

Figure 10: Quantification of Neutralizing Antibodies in Plasma or Serum Samples. (A) Schematic diagram of the neutralization assay set-up. Plasma or serum samples were pre-incubated with a standardized amount of psv. A 1:20 plasma dilution was serially diluted 3-fold. (B) Analysis of the serum or plasma sample with or without the addition of PLB. The fraction infectivity was calculated by taking the RLU from the infected wells (plasma and psv) divided by the SARS2psv control wells (virus only). The line is representative of infectivity threshold. Each point shows the average of duplicate replications.

3.1.8 Titering of Δ21 Spike Pseudovirus to Determine Infection Capacity.

For the next experiment, we quantified our infection capacity with the pseudovirus stock generated from the transfections of HEK293T cells with the spike plasmid containing the Δ21 deletion. To titer our pseudovirus, we used luciferase assays in conjunction with flow cytometry. A research group suggested that to obtain robust neutralization, a >1000-fold signal had to be maintained between our infected wells (SARS2psv) and virus-only and cell-only control wells (Crawford et al., 2020). The luciferase assay results can be seen in Figure 11(A), and the flow results can be seen in Figure 11(B). In all the previous experiments, we added a 1:3 psv dilution, but these results show that we were at the low end of reaching the infection capacity. A previous research report showed that flow cytometry infections would ideally be between 1-10% ZsGreen positive and our results agree (Crawford et al., 2020). To observe our infection capacity, we used various psv dilutions to obtain a linear correlation between the amount of psv and the resulting infection, as observed in Figure 11(C & D). In Figure 11(C) the psv infection medium was left on the cells for three days. In Figure 11(D) the infection medium was left on the cells for three hours. Thus, it should be noted that Figure 11(C & D) is not a direct comparison and the lower infection capacity in Figure 11(D) was the result of less infection potential. For the most part, we observed a linear correlation between the amount of psv (the highest psv amount having the highest infection) and the infection capacity. In addition, we were also obtaining titers >1000-fold above our background controls.

It should be noted that this assay was also done in the more physiologically relevant A549-ACE2 cell line. Since the ACE2 expression was only ~40%, the infection capacity was low; therefore, the results were not shown.

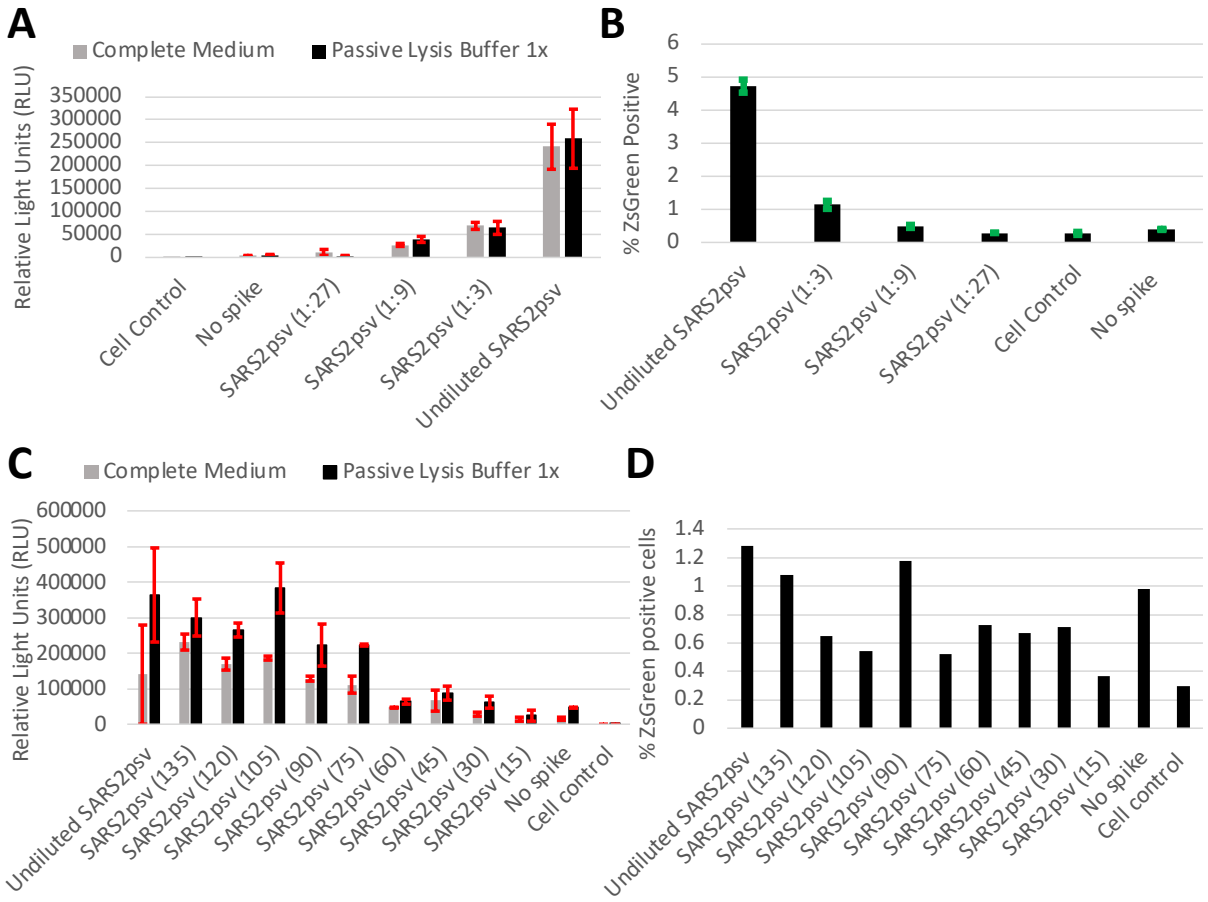

Figure 11: Titering of Spike Pseudotyped Particles to Determine Infection Capacity. HEK293T-ACE2 ($1.25x10^4$ cells per well for luciferase and $2.5x10^4$ cells per well for flow cytometry) were infected with various psv dilutions. RLUs and % ZsGreen positive cells were determined ~72 hours post-infection. (A) luciferase assay using SARS2psv at 1:27, 1:9, 1:3 and undiluted dilutions. (B) Flow cytometry using SARS2psv at 1:27, 1:9, 1:3 and undiluted dilutions. (C) Luciferase assay with various SARS2psv dilutions where the number corresponds to the volume of psv added (example 135 is equal of 135 μL of psv and 15 μL medium for a well total of 150 μL) to observe a linear correlation and (D) cytometry of the same dilutions. Titers of SARS2psv were determined by measuring RLUs or the % ZsGreen positive cells. Each bar in A, B, and C shows the average of duplicate replications with error bars indicating the standard error.

3.1.9 Quantification of Neutralizing Antibodies on Plasma Samples Using a New Pseudovirus Dilution.

The previous experiment showed that adding a 1:3 psv dilution was at the lower end of our assay's infection capacity. Therefore, we performed another neutralization assay to compare a different serial dilution. For this experiment, we used the same plasma samples as in section 3.1.7. A schematic diagram can be seen in Figure 12(A). In Figure 12(B), an initial plasma dilution of 1:20 was serially diluted 3-fold. In Figure 12(C), an initial plasma dilution of 1:20 was serially diluted 10-fold. Three different standardized amounts of pseudovirus were added (135 μL,105 μL, and 75 μL) as they obtained a $>$1000-fold signal above our background. The collective results from Figure 12 still showed unexpected results. When we added a higher titer of pseudovirus, we expected to observe a more robust infection. The greater the infection, the more potential for neutralizing antibodies to block infection. However, the sigmoidal curve was still not observed. Next, we examined a different plasma serial dilution. By changing the dilution factor, we thought there might be a more significant difference in the presence of neutralizing antibodies between the sample. However, even with a 10-fold dilution, the results still needed to improve potentially from an increased dilution as we still weren't observing a dose response.

It should be noted that this same experiment was repeated using a different plasma sample to rule out a specific sample hindrance. Those results will not be shown but were similar to those shown above and below.

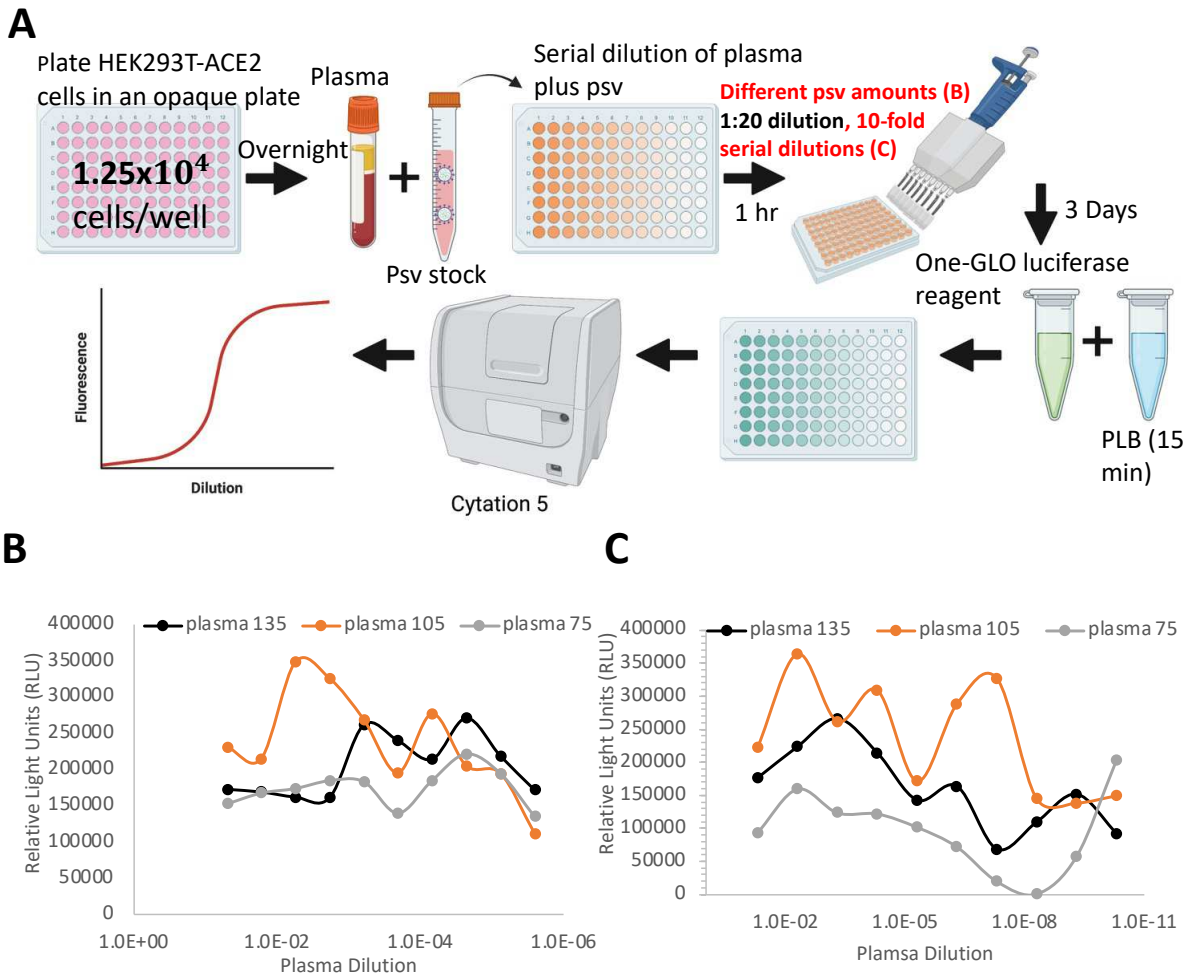

Figure 12: Quantification of Neutralizing Antibodies in Plasma Samples Using a New Pseudovirus Dilution. (A) Schematic diagram of the neutralization assay set-up. HEK293T-ACE2 plated at 1.25x10^4 cells per well were infected with various (135 μL, 105 μL, and 75 μL) standardized psv amounts. An initial plasma dilution of 1:20 was used. (B) Plasma is serially diluted by 3-fold. (C) serially diluted by 10-fold. Each point shows the average of duplicate replications.

3.1.10 Verification of Neutralization by a Monoclonal Antibody

To test whether the continuous unexpected results stemmed from an assay complication with the serum or plasma, we obtained an anti-SARS-CoV-2 spike RBD neutralizing human IgG antibody to quantify neutralization. When the monoclonal antibody is pre-incubated with psv, it is expected to bind to the SARS2psv spike and block subsequent infection. The neutralizing human IgG antibody was previously used for ELISAs and therefore did not include a protocol or recommendations about the required concentrations aside from the IC50 value. We used the IC50 value to guide the selection of the various antibody concentrations, which can be seen in Figure 13(A & B). Figures 13(A & B) are results from our luciferase assay and show no infection prevention by the monoclonal antibody compared to our SARS2psv infected control (SARS2psv and cells only). In Figure 13(A) we started with lower mAb concentrations and for Figure 13(B) we changed the antibody concentrations to hopefully observe a dose response. Flow cytometry was also utilized. In the right panel of Figure 13(C), there again was no real inhibition of infection when compared to the SARS2psv-infected control. The indistinguishable result might be due to a problem with our psv stocks. The previous experiments in Figure 11(B) showed that our average infection capacity was ~5%; here and in Figure 11(D), it was less than 2%. In Figure 11(D) the infection medium was incubated with the cells for three hours instead of three days like the other assays. In Figure 13(D), we used a different psv stock and observed some inhibition infection compared to our SARS2psv infected control. Thus, flow cytometry may be a better tool to examine neutralization.

3.1.11 Quantification of Neutralization Capacity in Patient Samples.

While troubleshooting the luciferase assay, we decided to try to quantify the neutralization capacity in patient samples by flow cytometry. The plasma samples used in this experiment were collected from vaccinated individuals roughly three months after receiving the third dose. The shift to a third dose sample was due a high antibody response generated from our collaborative laboratories ELISA. Various plasma dilutions were made with antibody-positive and antibody-negative samples and were pre-incubated with 300 μL SARS2psv. In the left panel of Figure 13(C), it can be observed that there was no significant inhibition. Figure 13(D) shows some inhibition of infection by nAbs compared to our SARS2psv-infected control. The inhibition of infection also seems to be trending in an expected dose-response pattern. The 1:50 lowest plasma dilution showed the highest level of neutralization.

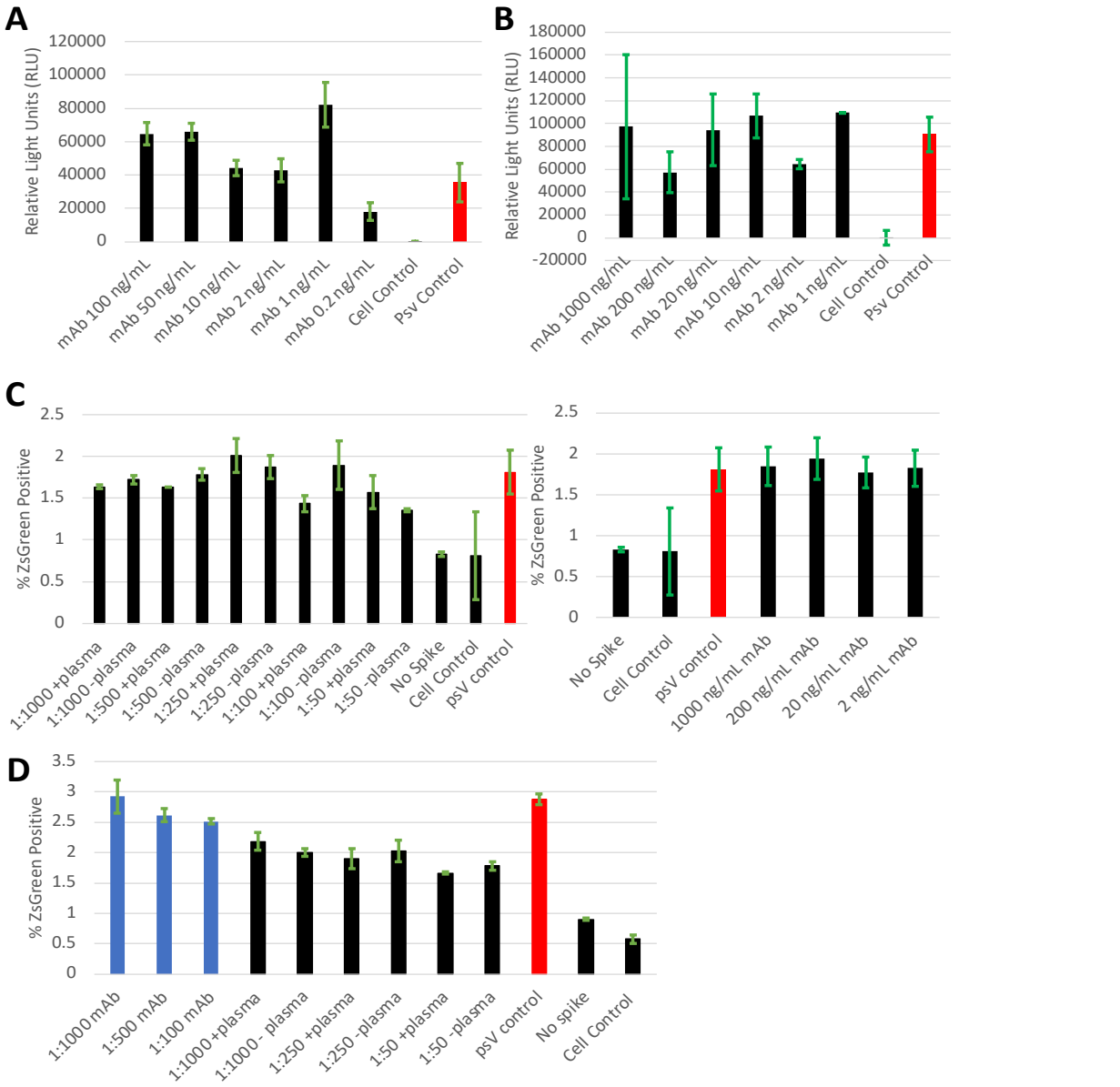

Figure 13: Quantification of Neutralization Capacity Through a Monoclonal Antibody and Patient Samples. For luciferase assays, $1.25x10^4$ cells per well were used. For flow cytometry, $7.5x10^4$ cells per well were used. Plasma or the anti-SARS-CoV-2 spike RBD neutralizing human IgG antibody were pre-incubated (1 hour) with psv sufficient to achieve >1000-fold signal over the virus-only/cell-only controls. (A) luciferase assay with the mAb at various dilutions. (B) luciferase assay with the mAb at different, more widespread dilutions to determine the inhibitory concentration. (C) Flow cytometry of plasma samples at various dilutions with antibody-positive and antibody-negative samples to observe the percent ZsGreen positive cells. (D) plasma and mAb samples at various dilutions to determine the percent ZsGreen positive cells. The cell control (just cells) samples were used to set the gate threshold of ZsGreen positivity. Each bar shows the average of duplicate replications, with error bars indicating the standard error.

3.2 Rationale for Project.

The introductory part of this thesis focused on the adaptive immune response in relation to the SARS2psv assay. Due to the unforeseen technical difficulties with the assay, we decided to continue troubleshooting while pivoting to a secondary project. The accompanying part of this thesis continued the focus on the immune response to SARS-CoV-2 infection by studying innate immunity.

3.2.1 Analysis of the Ability of SARS-CoV-2 ORF3a to Activate Pyroptotic Cell Death.

Previous research into SARS-CoV and SARS-CoV-2 ORF3a protein showed that it could induce or activate pyroptotic programmed cell death (I.-Y. Chen et al., 2019; Vora et al., 2021; Xu et al., 2022; Yap et al., 2020b). To verify their findings, we utilized flow cytometry and a caspase-1 probe. The caspase-1 probe binds to activated caspase-1, which is a marker for the induction of pyroptosis. The experimental conditions used were an un-transfected “negative” control, a MOCK control (all transfection components except for plasmids), SARS-CoV-2 E protein, SARS-CoV-2 ORF3a protein, and a positive control of LSP/Nigericin. As mentioned in the introduction, the ORF3a and E proteins act as viroporins and, therefore, could activate the NLRP3 inflammasome. In Figure 14(A), it can be observed that ~15% of the ORF3a-transfected cells showed caspase-1 activation. This result confirms the previous research and shows that caspase-1 was being activated in SARS-CoV-2 ORF3a transfected cells at some capacity (I.-Y. Chen et al., 2019; Vora et al., 2021; Xu et al., 2022; Yap et al., 2020b). However, since we confirmed that caspase-1 was activated, we wanted to utilize an inflammasome array kit to determine the critical regulatory and mediatory factors involved in the SARS-CoV-2 ORF3a-

mediated inflammatory response. Future work will confirm ORF3a expression and determine any toxicity with ORF3a overexpression.

3.2.2 Identification of Key Regulatory Factors in SARS-CoV-2 ORF3a-mediated Pathogenesis.

To identify the key regulatory factors that might be involved in SARS-CoV-2 ORF3a-mediated pathophysiology, we utilized an RT^2 inflammasome PCR array. This array contains 96 pathway-focused genes, including five housekeeping genes and a panel of proprietary controls. The controls monitor for genomic DNA contamination, the first strand synthesis, and the RT-PCR efficiency. We performed three biological replicates of HEK293T cells transfected with MOCK (all transfection components except for plasmids) and ORF3a (ORF3a plasmid). The Qiagen Geneglobe Web Portal was used to analyze the results after exporting files to excel. The results showed many genes were upregulated between the control (MOCK) and the test (ORF3a) samples. In the gene table (Figure 14(B)), some upregulated genes have an A or B comment following the fold-change values. The A comment means that the average threshold cycle between the control and test sample was high in one sample and low in the other. These results might be indicative of a significant upregulation but would require more biological replications to confirm. The B comment implies that the average threshold cycle was high and, therefore, its relative expression level is low. Thus, these results were not used. The genes that were upregulated without comments are shown in Figure 14(C). Statistically significant changes are denoted with * where $p<0.05$ by a student's paired t-test. The results show that *CCL5, MEFV, NLRC5, NLRP3, MOK,* and *TNF* were all significantly upregulated. These genes have multiple roles and have been implicated in apoptosis and/or pyroptosis. A detailed discussion of these genes can be found on pages 83-86.

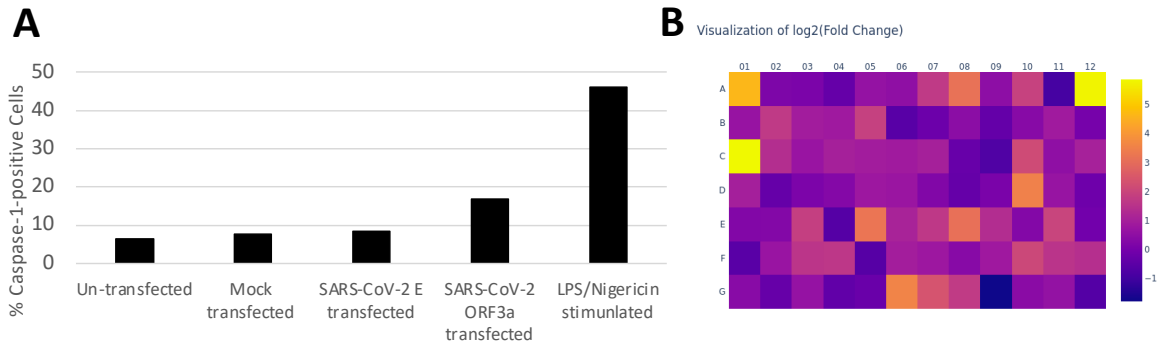

Layout	01	02	03	04	05	06	07	08	09	10	11	12
A	AIM2 / 24.92 / A	BCL2 / 1.09	BCL2L1 / 1.07	BIRC2 / -1.27	BIRC3 / 1.51	CARD18 / 1.42 / B	CARD6 / 3.21	CASP1 / 8.78 / B	CASP5 / 1.36 / B	CASP8 / 3.74	CCL2 / -1.91 / A	CCL5 / 55.24
B	CCL7 / 1.57 / B	CD40LG / 3.23 / B	CFLAR / 1.88	CHUK / 1.8	CIITA / 3.66 / B	CTSB / -1.51	CXCL1 / -1.15 / B	CXCL2 / 1.33	FADD / -1.28	HSP90AA1 / 1.27	HSP90AB1 / 1.82	HSP90B1 / -1.01
C	IFNB1 / 58.58 / A	IFNG / 2.57 / B	IKBKB / 1.61	IKBKG / 2.0	IL12A / 1.88	IL12B / 1.81 / B	IL18 / 1.99 / B	IL1B / -1.24 / A	IL33 / -1.69 / B	IL6 / 4.4 / B	IRAK1 / 1.42	IRF1 / 2.02
D	IRF2 / 1.95	MAP3K7 / -1.26	MAPK1 / 1.08	MAPK11 / 1.21	MAPK12 / 1.72	MAPK13 / 1.66	MAPK3 / 1.16	MAPK8 / -1.27	MAPK9 / 1.04	MEFV / 11.21	MYD88 / 1.59	NAIP / -1.12
E	NFKB1 / 1.18	NFKBIA / 1.19	NFKBIB / 3.53	NLRC4 / -1.57	NLRC5 / 9.34	NLRP1 / 2.12 / B	NLRP12 / 3.1 / B	NLRP3 / 8.58	NLRP4 / 2.52 / B	NLRP5 / 1.19 / B	NLRP6 / 3.93 / B	NLRP9 / -1.06
F	NLRX1 / -1.5	NOD1 / 1.62	NOD2 / 2.97 / B	P2RX7 / 3.08 / B	PANX1 / -1.55	PEA15 / 1.91	PSTPIP1 / 1.73	PTGS2 / 1.27	PYCARD / 1.77	PYDC1 / 4.18 / B	MOK / 2.89	RELA / 2.65
G	RIPK2 / 1.28	SUGT1 / -1.26	TAB1 / 1.53	TAB2 / -1.34	TIRAP / -1.2	TNF / 11.84	TNFSF11 / 5.22 / B	TNFSF14 / 3.28 / B	TNFSF4 / -3.47 / A	TRAF6 / 1.31	TXNIP / 1.5	XIAP / -1.6

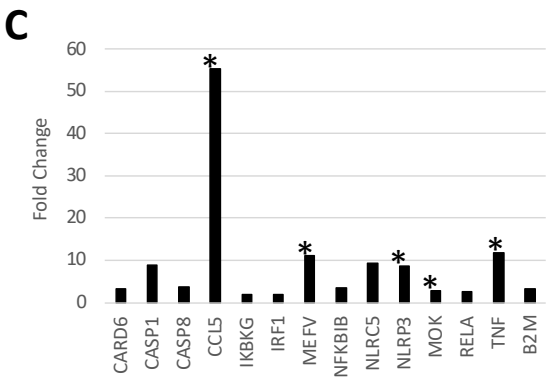

Figure 14: Identification of Key Regulatory Factors in SARS-CoV-2 ORF3a-mediated Pathogenesis. (A) Flow cytometry analysis of caspase-1 activation to observe if pyroptosis was occurring. HEK239T cells were transfected with SARS-CoV-2 ORF3a, E proteins, or MOCK (no plasmids). In addition, there was an un-transfected control and positive LPS/Nigericin control. (B) Analysis of the fold-change gene expression and the corresponding table shows the genes' location and actual fold-change values. (C) Plot showing the upregulated genes from the inflammasome array with significant difference denoted as * when $p<0.05$. C_t values were normalized based on a manual selection of reference genes. Fold-Change (2^(-Delta Delta C_t)) is the normalized gene expression (2^(- Delta C_t)) in the test sample divided by the normalized gene expression (2^(- Delta C_t)) in the control Sample. The p values were calculated based on a Student's t-test of the replicate 2^(- Delta C_t) values for each gene in the control and treatment groups. The data are representative of three biological replications.

Discussion

4. Discussion

4.1 Summary

In this research, we aimed to bridge innate and adaptive immune responses to uncover the pathophysiological factors that mediate immune pathogenicity. The introductory part of the project was focused on the adaptive immune response to measure how antibodies and sera affect spike-mediated viral infection. We successfully generated a SARS-CoV-2 spike pseudovirus, verified its function, and established a neutralization assay. The second part of this research concentrated on the innate immune responses to SARS-CoV-2 ORF3a viral infection. We found that the *CCL5, MEFV, NLRC5, NLRP3, MOK*, and *TNF* genes were all statistically significantly upregulated. These genes have implications in both apoptosis and pyroptosis, and both cell death pathways could be activated simultaneously in response to the SARS-CoV-2 ORF3a protein.

4.1.1 Generation of Pseudovirus

Throughout this research, we successfully pseudotyped the SARS-CoV-2 spike glycoprotein onto the safer non-replicative HIV-1-based viral particles in place of the envelope entry protein. Employing this methodology meant that the pseudovirus entry depended on spike, which is the only target of SARS-CoV-2 neutralizing antibodies. In addition, using the pseudovirus technique meant we were able to alleviate the biosafety limitations currently in place. At the beginning of the pandemic (and this research), we utilized a spike plasmid containing the original Wuhan-Hu-1 spike sequence. After a few months, we noticed that multiple research groups were substituting the previous plasmid with a spike plasmid containing the original Wuhan-Hu-1

spike sequence with the Δ21 deletion (Crawford et al., 2021; Garcia-Beltran, Lam, Astudillo, et al., 2021; Garcia-Beltran, Lam, St. Denis, et al., 2021b). The truncation removed the ER retention signal. The modification significantly and consistently increased our pseudovirus titers, thereby improving our infection capacity. By removing the ER retention signal, the products could leave the ER and Golgi to be translated and transcribed (Crawford et al., 2021). Thus, improving the plasma-membrane expression of spike. The increased incorporation of spike onto the pseudovirus meant we increased the infection efficiency without affecting neutralization sensitivity (Crawford et al., 2021).

4.1.2 Verification of Pseudovirus

We included various controls to verify the quality of our assay and the production of pseudovirus. These controls verified that spike was being expressed and mediating entry in our infections. The first control was the elimination of spike (No Spike). In this control, a pseudovirus stock was prepared by transfection of HEK293T cells with the HIV-1 lentiviral backbone with the luciferase-IRES-ZsGreen reporter and the other HIV-1 proteins needed for virion formation (Gag/pol, Tat, Rev). Thus, the pseudovirus produced would be able to form but would not have spike protein to mediate entry. Our results showed a slight background signal in these wells, but it was significantly lower than that of our SARS2psv wells. In addition, we included a reporter control. The reporter control was prepared by transfection of HEK293T cells with just the HIV-1 lentiviral backbone containing the luciferase-IRES-ZsGreen reporter plasmid. The reporter control was used to show background levels of luminescence. Again, in these wells, we obtained slight background, which was to be expected but was lower than our SARS2psv wells. We also included a cell control (HEK239T cells infected with SARS2psv),

pseudovirus control (SARS2psv only-no cells), cell medium control (only medium), and a transfection control (transfection of HEK293T cells exposed to transfection reagents supernatant used to infect HEK293T-ACE2 cells). The signal from these wells was extremely low. These results proved that we were producing pseudovirus and that the spike protein was mediating entry.

Furthermore, we also verified our pseudovirus production by examining protein expression through Western blot analysis. In this experiment, we used pseudovirus stock from SARS2psv, no spike, reporter, and un-transfected controls. We examined both the cell lysates and supernatant following a transfection. We observed spike protein expression at ~180 kDa and cleaved S1 at ~90 kDa in the cell lysates transfected with SARS2psv. In this experiment, we also verified Gag protein expression. To do this, we used a p24 HIV-1 Gag antibody, as p24 is the cleaved product essential for the viral capsid assembly (Anderson et al., 2018). Protein expression of Gag was seen in the cell lysates in SARS2psv, and no spike (still has all the HIV-1 machinery components) lanes. We also observed the full-length Gag and its processing intermediates in this Western blot. There was no protein expression detected in our supernatant samples. This result is most likely due to the supernatant not being concentrated. In the future, we could use ultracentrifugation techniques to concentrate the supernatant to overcome this hurdle. Nevertheless, our results showed that the transfection was working properly, and the proteins of interest were being expressed to generate our pseudovirus.

4.1.3 Quantification of Neutralization.

Most of the quantification experiments done in this research yielded unexpected results. Since we previously established and verified that we were producing pseudovirus in cell lysates,

which did express functional protein capable of infection, we thought the insufficient infection and neutralization might be due to an issue with the expression levels of the SARS-CoV-2 ACE2 receptor. We acquired our ACE2 overexpressing cell lines from an external company instead of producing them in the laboratory. Therefore, we postulated that perhaps the ACE2 receptor expression could be low, resulting in a lower infection capacity. Therefore, we carried out another experiment to verify the overexpression of the ACE2 receptor in our cell lines. For this experiment, we subjected the cells to primary and secondary antibodies. The primary and secondary antibody results showed that within our parental cell lines, HEK293T and A549, there was less than 1% of cells expressing ACE2. In the HEK293T-ACE2 and A549-ACE2 cell lines, our secondary- and cell controls also had less than 1% of cells positive for ACE2. In HEK293T-ACE2 cells, we saw that ~95% had ACE2 expression in both newer and older cell passages. In the A549-ACE2 cell line, we saw that ~40% of the cells had ACE2 expression. This result could explain why our A549 experiments did not show high levels of infection. We concluded that subsequent problems in our neutralization assays were not due to the level of ACE2 expression on target cells.

Aside from being cumbersome and expensive, one of the major hurdles of neutralization assays is the need for robust infections. Per the recommendations and guidance from the Balazs and Bloom laboratories' publications, we established our system and assay based on their protocols. Initially, we used their suggested 1:3 pseudovirus dilution. Upon obtaining unexpected results, we decided to titer our pseudovirus stocks to determine the infection capacity of our assay. To measure the titer, we used luciferase assays and flow cytometry. The results showed that the 1:3 pseudovirus dilutions used in our experiments were on the lower

end of our infection capacity- the flow cytometry analysis performed in conjunction confirmed this result. We utilized a linear assay with various pseudovirus dilutions to determine our infection capacity to observe a dose-response. Our results showed that the more pseudovirus inoculated onto the cells, the greater the extent of infection, and as the pseudovirus was diluted, we obtained lower levels of infection. We then chose a pseudovirus inoculum that resulted in a >1000-fold higher signal for SARS2psv versus psv-only/cell-only control wells. This amount was chosen as it was believed to translate into a sufficient breadth of serum neutralization to overcome the high levels of variation in antigens across viral populations (Rees-Spear et al., 2021). Since we met this requirement, we assumed we were producing enough pseudovirus to have a robust infection that would allow us to quantify neutralization by antibodies.

To study the immune response to COVID-19 vaccination, we utilized neutralization assays to assess how antibodies and sera/plasma affect spike-mediated pseudovirus infection. Our results showed that we tried various methods to establish and optimize our neutralization assay. The first method interchanged the original Wuhan-Hu-1 sequence spike with the Δ21 spike sequence. The results from this substitution showed a higher, more consistent pseudovirus titer and infection, but alone did not improve the functionality of our neutralization assay. Polybrene was added next to decrease the charge repulsion between the pseudovirus and cells. The polybrene aided in increasing our infection capacity but did not improve the neutralization results. Next, we examined our luciferase One-Glo reagent. The product manual stated that the medium and its components could lead to a reduction in signal. Therefore, we removed all mediums and added PLB to lyse the cells before adding the One-Glo

reagent. Upon still getting undesired results, we considered the possibility that components such as organic solvents, divalent cations, or anticoagulant factors from the whole blood collection process were interfering with the assay (Lima-Oliveira et al., 2018; L. Liu et al., 2010; Vignoli et al., 2022). Thus, we decided to test serum and plasma samples because they were collected using different chemical preservatives. A monoclonal antibody was also utilized as a positive control for neutralization. Upon the continuation of unexpected results, we used flow cytometry to determine if the problem was in our luciferase assay.

In addition to the previous modifications, we also tried different heat-inactivations of plasma samples by changing the temperature or duration. Heat treatment is used to inactivate complement components contained in the blood that could potentially destroy cells coated with antibodies. We also changed the plasma dilution factors, the plated cell amounts, the amount of pseudovirus we were adding based on the titer analysis, changed the serial fold dilution factors, tried using another physiologically relevant cell line (A549-ACE2), and tried an MLV-based pseudovirus system. By making these modifications, we hoped to capture the experimental conditions required to observe and quantify neutralizing antibodies successfully. Unfortunately, every change, whether methodical or technical, still gave the unexpected results we observed throughout our results.

When establishing the neutralization assay in our laboratory, we knew what results we should expect to see. Previous laboratories have shown that the relative light units observed are directly proportional to the number of infected cells (Crawford et al., 2020; Nie et al., 2020). However, this is relative, as the light could be refracted, and we did not have a way to measure refraction. Thus, we also used flow cytometry as the number of infected cells would be

indicated by the % of ZsGreen positive cells, which is a more quantifiable and absolute result. The results obtained throughout this thesis did not give us the expected results described above. However, a few of our results did trend in the right direction. In Figure 10(B), we saw that the plasma sample fraction infectivity started low since there is the most plasma present. Then there was a general trend upward as the plasma got diluted. In Figure 13(D), we observed some inhibition of infection in a dose-dependent manner in both the plasma and mAb neutralization experiments.

The unanticipated results obtained throughout this thesis could have been the result of various potential complications. The first could be the DNA quality. Our maxi preps could have contained a spillover of endotoxins and salts that could inhibit our transfection or cause cell death (Hawley-Nelson et al., 2008). This is unlikely, as we checked DNA purity and observed no substantial cell death. Furthermore, during all of our transfections, we added the same quantity of plasmid mix. It is possible that the amount of plasmid we were adding was not high enough. Another possibility was published by the Zheng laboratory, where they suggested that heat-inactivation of the serum interfered with the immunoanalysis of antibodies to SARS-CoV-2 (Hu et al., 2020). While this might be possible, numerous research groups have published neutralizing and total antibody data with the same general applications. Lastly, our laboratory did not quantify the amount of pseudovirus produced. We generated our pseudovirus stocks by doing large-scale transfections that were further pooled. By pooling our stocks, we controlled for a diminished transfection (cell confluency lower) and standardized the amount of pseudovirus in each aliquot. In our assays, we added a relative pseudovirus amount to achieve >1000-fold signal above the background controls, which might not have been enough. To

control for this, we could concentrate our pseudovirus transfections after harvest. After concentration, we could determine the 50% tissue culture infectious dose (TCID_{50}) using the Reed-Muench method or use a Gag ELISA to measure the protein concentration of psv in the supernatant. Both methods could quantify the transfection output to then standardize the input of psv (Hawley-Nelson et al., 2008).

4.1.4 Future Directions.

Future directions could examine the possibility of getting another negative control sample or at least test our sample for any cross-reactivity with other coronaviruses (Lv et al., 2020). Ideally, we should not have seen any neutralization within this sample. However, the result could be due to foreign material, cell damage, incomplete inactivation of complement, or improper blood sample storage and collection (Hu et al., 2020; Soltis et al., 1979). In addition, we could also acquire a different positive control, such as VSV, to test infection capacity. Another avenue would be to try Vero E6 cells (African green monkey cell line). These cells, like HEK293T, are known for their high transfection efficiency. Future experiments could also acquire another well-established neutralizing antibody. The last result in our neutralizing antibody experiments suggested some inhibition of infection. Due to time constraints, we were unable to obtain more data for this cohort of experiments or to receive another antibody. Thus, future work could continue to explore this avenue. The general lack of infection prevention in our neutralizing antibody experiments could be due to weak antibody binding affinity or the lack of a robust infection (due to our psv stock). Future applications could also try another spike plasmid, or a different stock of the same plasmid was working well for another laboratory. Since

this research occurred during the bulk of the pandemic, there were shipping delays and lockdowns, which made this avenue not feasible.

4.1.5 Conclusion.

Overall, we successfully pseudotyped the SARS-CoV-2 spike glycoprotein onto the safer non-replicative HIV-1-based viral particles in place of the envelope entry protein. Our verification and quantification experiments showed that pseudoviruses were being produced, we were obtaining a high infection capacity, the pseudovirus proteins were being expressed, that we had robust and sufficient ACE2 expression in our permissive cell line, and our neutralization assays by luciferase and flow cytometry were working and established. When the assays are optimized further, future investigations would be to obtain the neutralization data on how antibodies and sera affect spike-mediated viral infection in our study population cohort. The results obtained would be a valuable complement to our collaborative laboratory ELISA-based methods.

4.2 Rationale for Accompanying Experiments.

Previous research into SARS-CoV showed that the ORF3a protein acts as a viroporin and is implicated in viral pathogenesis and replication (Vora et al., 2021). Since there is ~72% sequence homology between SARS-CoV and SARS-CoV-2 ORF3a proteins, it was thought there would be a conservation of function (J. Zhang et al., 2022). Multiple groups have shown that ORF3a from both viruses can induce pyroptosis (Li et al., 2020; Vora et al., 2021; Xu et al., 2022; J. Zhang et al., 2022). To verify this finding in our system, we quantified caspase-1 activation in ORF3a-transfected cells. As previously mentioned, caspase-1 is recruited and activated in the inflammasome pathway, which processes pro-IL-1β and pro-IL-18 into their functional cytokine forms and cleaves the pyroptotic executor protein GSDMD. Thus, caspase-1 activation can be

used as a biomarker for the induction of pyroptosis. In our experiments, we observed that the SARS-CoV-2 ORF3a protein did induce some caspase-1 activation, and we deduced that pyroptosis was occurring in some capacity. With this confirmed, we then moved to the evaluation of inflammasome-related gene regulation studies using commercially available inflammasome arrays.

4.2.1 Inflammasome Array.

The inflammasome array has 96 key regulatory mediators or factors related to inflammasome activation. The inflammasome array results showed *CARD6, Caspase-1, Caspase-8, CCL5, IKBKG, IRF1, MEFV, NFKB1B, NLRC5, NLRP3, MOK, RELA, TNF,* and *B2M* were upregulated in the SARS-CoV-2 ORF3a protein-transfected cells compared to the MOCK-transfected cells. However, only *CCL5, MEFV, NLRP3, MOK,* and *TNF* proved statistically significantly upregulated. As observed in the results in Figure 14, some genes were observed to be upregulated but had an A comment next to them. The A comment means that the threshold C_t was high in one sample and low in the other, therefore flagging the result as potentially false. The assay manual suggested that doing more biological replicates could distinguish if this result was occurring. Thus, we decided to further validate our SARS-CoV-2 ORF3a-transfected inflammasome assay results by developing our own gene expression panel.

Using RT-qPCR, we developed an in-house gene expression panel to confirm the inflammasome array results. In the inflammasome array data, one of our MOCK triplicates was flagged for low expression levels of DNA contamination. Furthermore, when wells were marked as undetermined, the inflammasome array analysis software will arbitrarily assign a value so it can still calculate the fold change. Therefore, some of the results obtained might not be as

significant. Thus, a panel was developed and used SYBR green dye and a focused group of the genes of interest. The following gene targets were examined: *MOK, TNFα, Caspase-1, Caspase-8, CCL5, NLRC5, IRF1, NF-κB, IL-1β, IL-18, NLRP3, AIM2, IFN-β1 and GAPDH*. These genes were chosen as they were either upregulated in the inflammasome array or had an A comment next to them. Secondly, the proteins these genes encode are critical mediators in either apoptosis or pyroptosis cell death pathways. While the preliminary data obtained from these experiments were not shown, the gene expression panel was developed. Once further established, this gene expression panel could be used for similar projects on other viruses studied in our laboratory.

The inflammasome biomarkers listed above are involved in various aspects of the inflammatory response. MAPK/MAK/MRK-overlapping protein kinase (*MOK*) is a PRR on the surface of various cell types, such as endothelial, epithelial and fibroblast (Bongarzone et al., 2017; Fields et al., 2007; Ramya et al., 2021). *MOK* activates the inflammatory response by mediating various signalling pathways such as *MAPK* (mitogen-activated protein kinase) and *NF-κB* (Ramya et al., 2021). The facilitation through *MOK* leads to the production of pro-inflammatory cytokines, which activates *NF-kB*, which then overexpresses genes for cytokines, growth factors and adhesion molecules (Veloso et al., 2011; S. D. Yan et al., 1994). Tumour necrosis factor alpha (*TNFα)* is a cytokine used by the innate immune response for cell signalling and immune functions (Fitzgerald et al., 2001). *TNFα* signalling through *TNFR1* tends to lead to apoptosis (through caspase-8), whereas *TNFR2* has a more anti-inflammatory role in promoting cell proliferation (Gough & Myles, 2020). Cysteine aspartic acid protease (caspase) caspase-8 is an initiator protease in extrinsic apoptosis by death receptors (Salvesen & Walsh, 2014). When death receptors mediate death (*TNF* or *Fas*), the caspase-8 in the extrinsic

pathway and caspase-9 in the intrinsic pathway converge, and activation of executioner caspases-3 and -7 are recruited, leading to cleavage of proteins and the result of apoptosis (Salvesen & Walsh, 2014). Caspase-1 is an inactive zymogen in the cytosol of phagocytic cells (Cerretti et al., 1992; Franchi et al., 2009; Thornberry et al., 1992). It is postulated that the NLRs drive caspase-1 activation through the formation of oligomers. The inflammasome complex is formed through the recruitment and activation of procaspase-1 through CARD-CARD and PYD protein interactions that create a scaffold. Once caspase-1 is activated, as previously mentioned, it is essential for the cleavage of *pro-IL-1β* and *pro-IL-18* into their biologically active forms. For pyroptosis to be induced, active caspase-1 cleaves GSDMD into fragments that form pores in the plasma membrane. These pores promote the influx of ions and water through osmotic pressure, resulting in cell lysis and death (Franchi et al., 2009; Wang et al., 2002). CC chemokine ligand 5 (*CCL5*) induces apoptosis through Bcl2. For apoptosis, there is a release of cytochrome c in the cytoplasm and subsequent activation of caspase-9 and caspase-3 (Zeng et al., 2022). The NOD-like receptor family CARD domain containing 5 (*NLRC5*) is an intracellular protein that plays a role in both the innate and adaptive branches. *NLRC5* can induce the *NLRP3* or *NLRP1* inflammasome complex (through type-II interferons such as IFN-γ). Interferon regulatory factor 1 (*IRF1*) can be activated through various cytokines such as type I and II interferons (*IFNα, IFNβ, and IFNγ*), *TNFα, IL-6,* and viral infection (Feng et al., 2021; Tamura et al., 2008). Binding and activation can then regulate apoptosis. *NF-κB* is a significant transcription factor that links cellular danger and pathogenic signals to organize cellular resistance. *NF-κB* is sequestered in the cytoplasm in the quiescent state by its inhibitor of *NF-κB* (*IkB*) molecules (T. Liu et al., 2017). Upon activation, IkB kinase (*IKK*) complex

phosphorylates IkB leading to its degradation. *NF-κB* can then be transported to the nucleolus, and its proteins initiate the downstream transcription of target genes (T. Liu et al., 2017). Thus, it has roles in both apoptosis and pyroptosis. *IL-1β* is a cytokine implicated in the pro-inflammatory response. The caspase-1 protease cleaves *pro- IL-1β*. As previously mentioned, caspase-1 is activated via the recruitment of the inflammasome. Mature *IL-1β* is rapidly secreted from the cell, although this mechanism is unclear (Franchi et al., 2009). Thus, as previously mentioned, it has a major role in pyroptosis. *IL-18* is another cytokine synthesized as an inactive precursor. As previously mentioned, it requires processing by caspase-1 to go from *pro-IL-18* to its active form. Aside from activation through the *NLRP3* inflammasome and caspase-1, *IL-18* is also involved in Fas signalling. The Fas signalling pathway induces *IL-18* and activates caspase-8, which can trigger apoptosis—suggesting that the processing of *IL-1β* and *IL-18* might occur independently of *NLRP3* (Dinarello et al., 2013). Thus, *IL-18* can also have roles in both cell death pathways. The upregulated genes observed in our results are components of both apoptosis and pyroptosis. Therefore, both cell death pathways could be activated simultaneously in response to the SARS-CoV-2 ORF3a protein.

4.2.2 Future Directions.

Future experiments could investigate RNA sequencing to validate the results by quantifying the presence and quantity of RNA targets in the sample. Other experiments could confirm the sensor responsible by trying treatment with MCC950, a known *NLRP3* inhibitor, to see if ORF3a-mediated pyroptosis is prevented. Future experiments could also utilize siRNA knockdown or CRISPR knockouts of the various pathway components to gauge the effects. Lastly, since the inflammatory response is vital to the innate immune response, identifying genes or regulatory

factors to mitigate pyroptosis induced by ORF3a expression but leave the antiviral pathway intact could aid in the development of new therapeutics.

4.3 Conclusion.

The introductory part of this project was focused on the adaptive immune response to SARS-CoV-2 infection and/or vaccination. The SARS-CoV-2 endogenous entry glycoprotein of spike was successfully pseudotyped onto a non-replicative HIV-1-based viral particles. In addition, the assays utilized are established and can be used to measure how antibodies and sera affect spike-mediated viral infection. These results would highlight a valuable complement to ELISA-based methods. The accompanying part of this research concentrated on the innate immune responses to SARS-CoV-2 ORF3a viral infection. Overall, we concluded that the ORF3a protein works in a complex mosaic to activate and induce pyroptosis and apoptosis based on the observed upregulated genes. These results highlight a future application for therapeutic development for SARS-CoV-2 and other inflammatory diseases. Furthermore, the advancements of these research projects lay a foundation for other trainees to continue their professional development and expand on unexplored objectives.

References

Abdelrahman, Z., Li, M., & Wang, X. (2020). Comparative Review of SARS-CoV-2, SARS-CoV, MERS-CoV, and Influenza A Respiratory Viruses . In *Frontiers in Immunology* (Vol. 11). https://www.frontiersin.org/articles/10.3389/fimmu.2020.552909

Almahboub, S. A., Algaissi, A., Alfaleh, M. A., ElAssouli, M. Z., & Hashem, A. M. (2020). Evaluation of Neutralizing Antibodies Against Highly Pathogenic Coronaviruses: A Detailed Protocol for a Rapid Evaluation of Neutralizing Antibodies Using Vesicular Stomatitis Virus Pseudovirus-Based Assay. *Frontiers in Microbiology*, *11*(September), 1–12. https://doi.org/10.3389/fmicb.2020.02020

Amanat, F., Stadlbauer, D., Strohmeier, S., Nguyen, T. H. O., Chromikova, V., McMahon, M., Jiang, K., Arunkumar, G. A., Jurczyszak, D., Polanco, J., Bermudez-Gonzalez, M., Kleiner, G., Aydillo, T., Miorin, L., Fierer, D. S., Lugo, L. A., Kojic, E. M., Stoever, J., Liu, S. T. H., … Krammer, F. (2020). A serological assay to detect SARS-CoV-2 seroconversion in humans. *Nature Medicine*, *26*(7), 1033–1036. https://doi.org/10.1038/s41591-020-0913-5

Anderson, A. M., Tyor, W. R., Mulligan, M. J., Waldrop-Valverde, D., Lennox, J. L., & Letendre, S. L. (2018). Measurement of Human Immunodeficiency Virus p24 Antigen in Human Cerebrospinal Fluid With Digital Enzyme-Linked Immunosorbent Assay and Association With Decreased Neuropsychological Performance. *Clinical Infectious Diseases : An Official Publication of the Infectious Diseases Society of America*, *67*(1), 137–140. https://doi.org/10.1093/cid/ciy056

Barber, R. D., Harmer, D. W., Coleman, R. A., & Clark, B. J. (2005). GAPDH as a housekeeping gene: analysis of GAPDH mRNA expression in a panel of 72 human tissues. *Physiological Genomics*, *21*(3), 389–395. https://doi.org/10.1152/physiolgenomics.00025.2005

Blight, K. J., McKeating, J. A., & Rice, C. M. (2002). Highly permissive cell lines for subgenomic and genomic hepatitis C virus RNA replication. *Journal of Virology*, *76*(24), 13001–13014. https://doi.org/10.1128/jvi.76.24.13001-13014.2002

Bongarzone, S., Savickas, V., Luzi, F., & Gee, A. D. (2017). Targeting the Receptor for Advanced Glycation Endproducts (RAGE): A Medicinal Chemistry Perspective. *Journal of Medicinal Chemistry*, *60*(17), 7213–7232. https://doi.org/10.1021/acs.jmedchem.7b00058

Cerretti, D. P., Kozlosky, C. J., Mosley, B., Nelson, N., Van Ness, K., Greenstreet, T. A., March, C. J., Kronheim, S. R., Druck, T., & Cannizzaro, L. A. (1992). Molecular cloning of the interleukin-1 beta converting enzyme. *Science (New York, N.Y.)*, *256*(5053), 97–100. https://doi.org/10.1126/science.1373520

Chen, I.-Y., Moriyama, M., Chang, M.-F., & Ichinohe, T. (2019). Severe Acute Respiratory Syndrome Coronavirus Viroporin 3a Activates the NLRP3 Inflammasome . In *Frontiers in Microbiology* (Vol. 10). https://www.frontiersin.org/articles/10.3389/fmicb.2019.00050

Chen, M., & Zhang, X.-E. (2021). Construction and applications of SARS-CoV-2 pseudoviruses: a mini review. *International Journal of Biological Sciences*, *17*(6), 1574–1580. https://doi.org/10.7150/ijbs.59184

Crawford, K. H. D., Dingens, A. S., Eguia, R., Wolf, C. R., Wilcox, N., Logue, J. K., Shuey, K., Casto, A. M., Fiala, B., Wrenn, S., Pettie, D., King, N. P., Greninger, A. L., Chu, H. Y., & Bloom, J. D. (2021). Dynamics of Neutralizing Antibody Titers in the Months After Severe Acute Respiratory Syndrome Coronavirus 2 Infection. *The Journal of Infectious Diseases*, *223*(2), 197–205. https://doi.org/10.1093/infdis/jiaa618

Crawford, K. H. D., Eguia, R., Dingens, A. S., Loes, A. N., Malone, K. D., Wolf, C. R., Chu, H. Y., Tortorici, M. A., Veesler, D., Murphy, M., Pettie, D., King, N. P., Balazs, A. B., & Bloom, J. D. (2020). Protocol and reagents for pseudotyping lentiviral particles with SARS-CoV-2 spike protein for neutralization assays. *Viruses*, *12*(5), 13–15. https://doi.org/10.3390/v12050513

Dinarello, C., Novick, D., Kim, S., & Kaplanski, G. (2013). Interleukin-18 and IL-18 Binding Protein . In *Frontiers in Immunology* (Vol. 4). https://www.frontiersin.org/articles/10.3389/fimmu.2013.00289

Ding, J., Wang, K., Liu, W., She, Y., Sun, Q., Shi, J., Sun, H., Wang, D.-C., & Shao, F. (2016). Pore-forming activity and structural autoinhibition of the gasdermin family. *Nature*, *535*(7610), 111–116. https://doi.org/10.1038/nature18590

Feng, H., Zhang, Y.-B., Gui, J.-F., Lemon, S. M., & Yamane, D. (2021). Interferon regulatory factor 1 (IRF1) and anti-pathogen innate immune responses. *PLoS Pathogens*, *17*(1), e1009220. https://doi.org/10.1371/journal.ppat.1009220

Fields, B. N., Knipe, D. M. (David M., & Howley, P. M. (2007). Fields virology . In *Virology* (5th ed.). Wolters Kluwer Health/Lippincott Williams & Wilkins.

Fitzgerald, K. A., O'Neill, L. A. J., Gearing, A. J. H., & Callard, R. E. (2001). TNFα. In K. A. Fitzgerald, L. A. J. O'Neill, A. J. H. Gearing, & R. E. B. T.-T. C. F. and W. (Second E. Callard (Eds.), *Factsbook* (pp. 474–480). Academic Press. https://doi.org/https://doi.org/10.1016/B978-012155142-1/50103-2

Franchi, L., Eigenbrod, T., Muñoz-Planillo, R., & Nuñez, G. (2009). The inflammasome: a caspase-1-activation platform that regulates immune responses and disease pathogenesis. *Nature Immunology*, *10*(3), 241–247. https://doi.org/10.1038/ni.1703

Gallo, R. C. (1986). The First Human Retrovirus. *Scientific American*, *255*(6), 88–101. http://www.jstor.org/stable/24976105

Garcia-Beltran, W. F., Lam, E. C., Astudillo, M. G., Yang, D., Miller, T. E., Feldman, J., Hauser, B. M., Caradonna, T. M., Clayton, K. L., Nitido, A. D., Murali, M. R., Alter, G., Charles, R. C., Dighe, A., Branda, J. A., Lennerz, J. K., Lingwood, D., Schmidt, A. G., Iafrate, A. J., & Balazs, A. B. (2021). COVID-19-neutralizing antibodies predict disease severity and survival. *Cell*, *184*(2), 476-488.e11. https://doi.org/10.1016/j.cell.2020.12.015

Garcia-Beltran, W. F., Lam, E. C., St. Denis, K., Nitido, A. D., Garcia, Z. H., Hauser, B. M., Feldman, J., Pavlovic, M. N., Gregory, D. J., Poznansky, M. C., Sigal, A., Schmidt, A. G., Iafrate, A. J., Naranbhai, V., & Balazs, A. B. (2021a). Multiple SARS-CoV-2 variants escape neutralization by vaccine-induced humoral immunity. *Cell*. https://doi.org/https://doi.org/10.1016/j.cell.2021.03.013

Garcia-Beltran, W. F., Lam, E. C., St. Denis, K., Nitido, A. D., Garcia, Z. H., Hauser, B. M., Feldman, J., Pavlovic, M. N., Gregory, D. J., Poznansky, M. C., Sigal, A., Schmidt, A. G., Iafrate, A. J., Naranbhai, V., & Balazs, A. B. (2021b). Multiple SARS-CoV-2 variants escape neutralization by vaccine-induced humoral immunity. *Cell*, *184*(9), 2372-2383.e9. https://doi.org/10.1016/j.cell.2021.03.013

Gough, P., & Myles, I. A. (2020). Tumor Necrosis Factor Receptors: Pleiotropic Signaling Complexes and Their Differential Effects. *Frontiers in Immunology*, *11*, 585880. https://doi.org/10.3389/fimmu.2020.585880

Grifoni, A., Sidney, J., Zhang, Y., Scheuermann, R. H., Peters, B., & Sette, A. (2020). A Sequence Homology and Bioinformatic Approach Can Predict Candidate Targets for Immune Responses to SARS-CoV-2. *Cell Host & Microbe*, *27*(4), 671-680.e2. https://doi.org/https://doi.org/10.1016/j.chom.2020.03.002

Guo, H., Callaway, J. B., & Ting, J. P.-Y. (2015). Inflammasomes: mechanism of action, role in disease, and therapeutics. *Nature Medicine*, *21*(7), 677–687. https://doi.org/10.1038/nm.3893

Hartenian, E., Nandakumar, D., Lari, A., Ly, M., Tucker, J. M., & Glaunsinger, B. A. (2020). The molecular virology of coronaviruses. *The Journal of Biological Chemistry*, *295*(37), 12910–12934. https://doi.org/10.1074/jbc.REV120.013930

Hawley-Nelson, P., Ciccarone, V., & Moore, M. L. (2008). Transfection of cultured eukaryotic cells using cationic lipid reagents. *Current Protocols in Molecular Biology*, *Chapter 9*, Unit 9.4. https://doi.org/10.1002/0471142727.mb0904s81

Holder, K. A., Ings, D. P., Harnum, D. O. A., Russell, R. S., & Grant, M. D. (2022). Moderate to severe SARS-CoV-2 infection primes vaccine-induced immunity more effectively than asymptomatic or mild infection. *NPJ Vaccines*, *7*(1), 122. https://doi.org/10.1038/s41541-022-00546-1

Hsieh, C.-Y., Chen, C.-L., Yang, K.-C., Ma, C.-T., Choi, P.-C., & Lin, C.-F. (2015). Detection of reactive oxygen species during the cell cycle under normal culture conditions using a modified fixed-sample staining method. *Journal of Immunoassay & Immunochemistry*, *36*(2), 149–161. https://doi.org/10.1080/15321819.2014.910806

Hu, X., An, T., Situ, B., Hu, Y., Ou, Z., Li, Q., He, X., Zhang, Y., Tian, P., Sun, D., Rui, Y., Wang, Q., Ding, D., & Zheng, L. (2020). Heat inactivation of serum interferes with the immunoanalysis of antibodies to SARS-CoV-2. *Journal of Clinical Laboratory Analysis*, *34*(9), e23411. https://doi.org/10.1002/jcla.23411

Huang, Y., Yang, C., Xu, X., Xu, W., & Liu, S. (2020). Structural and functional properties of SARS-CoV-2 spike protein: potential antivirus drug development for COVID-19. *Acta Pharmacologica Sinica*, *41*(9), 1141–1149. https://doi.org/10.1038/s41401-020-0485-4

Inglis, J. E., Radziwon, K. A., & Maniero, G. D. (2008). The serum complement system: a

simplified laboratory exercise to measure the activity of an important component of the immune system. *Advances in Physiology Education*, *32*(4), 317–321. https://doi.org/10.1152/advan.00061.2007

Ings, D. P., Hatfield, K. M., Fifield, K. E., Harnum, D. O. A., Holder, K. A., Russell, R. S., & Grant, M. D. (2022). Few SARS-CoV-2 infections detected in Newfoundland and Labrador in the absence of Public Health Laboratory-based confirmation. *PloS One*, *17*(1), e0262957. https://doi.org/10.1371/journal.pone.0262957

Junqueira, C., Crespo, Â., Ranjbar, S., Ingber, J., Parry, B., Ravid, S., de Lacerda, L. B., Lewandrowski, M., Clark, S., Ho, F., Vora, S. M., Leger, V., Beakes, C., Margolin, J., Russell, N., Gehrke, L., Adhikari, U. Das, Henderson, L., Janssen, E., … Lieberman, J. (2021). SARS-CoV-2 infects blood monocytes to activate NLRP3 and AIM2 inflammasomes, pyroptosis and cytokine release. In *medRxiv : the preprint server for health sciences*. https://doi.org/10.1101/2021.03.06.21252796

Kahn, J. S., & McIntosh, K. (2005). History and Recent Advances in Coronavirus Discovery. *The Pediatric Infectious Disease Journal*, *24*(11). https://journals.lww.com/pidj/Fulltext/2005/11001/History_and_Recent_Advances_in_Coronavirus.12.aspx

Khan, M. I., Mohammad, A., Patil, G., Naqvi, S. A. H., Chauhan, L. K. S., & Ahmad, I. (2012). Induction of ROS, mitochondrial damage and autophagy in lung epithelial cancer cells by iron oxide nanoparticles. *Biomaterials*, *33*(5), 1477–1488. https://doi.org/https://doi.org/10.1016/j.biomaterials.2011.10.080

Khan, S., Nakajima, R., Jain, A., de Assis, R. R., Jasinskas, A., Obiero, J. M., Adenaiye, O., Tai, S., Hong, F., Milton, D. K., Davies, H., & Felgner, P. L. (2020). Analysis of Serologic Cross-Reactivity Between Common Human Coronaviruses and SARS-CoV-2 Using Coronavirus Antigen Microarray. *BioRxiv*, 2020.03.24.006544. https://doi.org/10.1101/2020.03.24.006544

Lebeau, G., Vagner, D., Frumence, É., Ah-Pine, F., Guillot, X., Nobécourt, E., Raffray, L., & Gasque, P. (2020). Deciphering SARS-CoV-2 Virologic and Immunologic Features. In *International Journal of Molecular Sciences* (Vol. 21, Issue 16).

https://doi.org/10.3390/ijms21165932

Legros, V., Denolly, S., Vogrig, M., Boson, B., Siret, E., Rigaill, J., Pillet, S., Grattard, F., Gonzalo, S., Verhoeven, P., Allatif, O., Berthelot, P., Pélissier, C., Thiery, G., Botelho-Nevers, E., Millet, G., Morel, J., Paul, S., Walzer, T., … Pozzetto, B. (2021). A longitudinal study of SARS-CoV-2-infected patients reveals a high correlation between neutralizing antibodies and COVID-19 severity. *Cellular & Molecular Immunology*, *18*(2), 318–327. https://doi.org/10.1038/s41423-020-00588-2

Li, S., Zhang, Y., Guan, Z., Li, H., Ye, M., Chen, X., Shen, J., Zhou, Y., Shi, Z.-L., Zhou, P., & Peng, K. (2020). SARS-CoV-2 triggers inflammatory responses and cell death through caspase-8 activation. *Signal Transduction and Targeted Therapy*, *5*(1), 235. https://doi.org/10.1038/s41392-020-00334-0

Lima-Oliveira, G., Monneret, D., Guerber, F., & Guidi, G. C. (2018). Sample management for clinical biochemistry assays: Are serum and plasma interchangeable specimens? *Critical Reviews in Clinical Laboratory Sciences*, *55*(7), 480–500. https://doi.org/10.1080/10408363.2018.1499708

Liu, L., Aa, J., Wang, G., Yan, B., Zhang, Y., Wang, X., Zhao, C., Cao, B., Shi, J., Li, M., Zheng, T., Zheng, Y., Hao, G., Zhou, F., Sun, J., & Wu, Z. (2010). Differences in metabolite profile between blood plasma and serum. *Analytical Biochemistry*, *406*(2), 105–112. https://doi.org/10.1016/j.ab.2010.07.015

Liu, T., Zhang, L., Joo, D., & Sun, S.-C. (2017). NF-κB signaling in inflammation. *Signal Transduction and Targeted Therapy*, *2*(1), 17023. https://doi.org/10.1038/sigtrans.2017.23

Liu, X., Zhang, Z., Ruan, J., Pan, Y., Magupalli, V. G., Wu, H., & Lieberman, J. (2016). Inflammasome-activated gasdermin D causes pyroptosis by forming membrane pores. *Nature*, *535*(7610), 153–158. https://doi.org/10.1038/nature18629

Lugrin, J., & Martinon, F. (2018). The AIM2 inflammasome: Sensor of pathogens and cellular perturbations. *Immunological Reviews*, *281*(1), 99–114. https://doi.org/10.1111/imr.12618

Lv, H., Wu, N. C., Tsang, O. T.-Y., Yuan, M., Perera, R. A. P. M., Leung, W. S., So, R. T. Y., Chan, J. M. C., Yip, G. K., Chik, T. S. H., Wang, Y., Choi, C. Y. C., Lin, Y., Ng, W. W., Zhao, J., Poon, L. L. M., Peiris, J. S. M., Wilson, I. A., & Mok, C. K. P. (2020). Cross-reactive antibody response

between SARS-CoV-2 and SARS-CoV infections. In *bioRxiv : the preprint server for biology*. https://doi.org/10.1101/2020.03.15.993097

Man, S. M., Hopkins, L. J., Nugent, E., Cox, S., Glück, I. M., Tourlomousis, P., Wright, J. A., Cicuta, P., Monie, T. P., & Bryant, C. E. (2014). Inflammasome activation causes dual recruitment of NLRC4 and NLRP3 to the same macromolecular complex. *Proceedings of the National Academy of Sciences*, *111*(20), 7403–7408. https://doi.org/10.1073/pnas.1402911111

Merten, O.-W., Hebben, M., & Bovolenta, C. (2016). Production of lentiviral vectors. *Molecular Therapy. Methods & Clinical Development*, *3*, 16017. https://doi.org/10.1038/mtm.2016.17

Miller, A. D. (1990). Retrovirus packaging cells. *Human Gene Therapy*, *1*(1), 5–14. https://doi.org/10.1089/hum.1990.1.1-5

Moore, M. J., Dorfman, T., Li, W., Wong, S. K., Li, Y., Kuhn, J. H., Coderre, J., Vasilieva, N., Han, Z., Greenough, T. C., Farzan, M., & Choe, H. (2004). Retroviruses pseudotyped with the severe acute respiratory syndrome coronavirus spike protein efficiently infect cells expressing angiotensin-converting enzyme 2. *Journal of Virology*, *78*(19), 10628–10635. https://doi.org/10.1128/JVI.78.19.10628-10635.2004

Ni, W., Yang, X., Yang, D., Bao, J., Li, R., Xiao, Y., Hou, C., Wang, H., Liu, J., Yang, D., Xu, Y., Cao, Z., & Gao, Z. (2020). Role of angiotensin-converting enzyme 2 (ACE2) in COVID-19. *Critical Care*, *24*(1), 1–10. https://doi.org/10.1186/s13054-020-03120-0

Nie, J., Li, Q., Wu, J., Zhao, C., Hao, H., Liu, H., Zhang, L., Nie, L., Qin, H., Wang, M., Lu, Q., Li, X., Sun, Q., Liu, J., Fan, C., Huang, W., Xu, M., & Wang, Y. (2020). Quantification of SARS-CoV-2 neutralizing antibody by a pseudotyped virus-based assay. *Nature Protocols*, *15*(11), 3699–3715. https://doi.org/10.1038/s41596-020-0394-5

Nova, Z., Skovierova, H., Strnadel, J., Halasova, E., & Calkovska, A. (2020). Short-Term versus Long-Term Culture of A549 Cells for Evaluating the Effects of Lipopolysaccharide on Oxidative Stress, Surfactant Proteins and Cathelicidin LL-37. *International Journal of Molecular Sciences*, *21*(3). https://doi.org/10.3390/ijms21031148

Okba, N. M. A., Müller, M. A., Li, W., Wang, C., GeurtsvanKessel, C. H., Corman, V. M., Lamers, M. M., Sikkema, R. S., de Bruin, E., Chandler, F. D., Yazdanpanah, Y., Le Hingrat, Q.,

Descamps, D., Houhou-Fidouh, N., Reusken, C. B. E. M., Bosch, B.-J., Drosten, C., Koopmans, M. P. G., & Haagmans, B. L. (2020). Severe Acute Respiratory Syndrome Coronavirus 2-Specific Antibody Responses in Coronavirus Disease Patients. *Emerging Infectious Diseases*, *26*(7), 1478–1488. https://doi.org/10.3201/eid2607.200841

Owen, J. A. (2013). Kuby immunology. In J. Punt, S. A. Stranford, P. P. Jones, & J. Kuby (Eds.), *Immunology* (Seventh Ed). New York : W.H. Freeman and Company.

Perlman, S. (2020). Another Decade, Another Coronavirus. *New England Journal of Medicine*, *382*(8), 760–762. https://doi.org/10.1056/NEJMe2001126

Pi-Estopiñan, F., Pérez, M. T., Fraga, A., Bergado, G., Díaz, G. D., Orosa, I., Díaz, M., Solozábal, J. A., Rodríguez, L. M., Garcia-Rivera, D., Macías, C., Jerez, Y., Casadesús, A. V, Fernández-Marrero, B., Bermúdez, E., Plasencia, C. A., Sánchez, B., & Hernández, T. (2022). A cell-based ELISA as surrogate of virus neutralization assay for RBD SARS-CoV-2 specific antibodies. *Vaccine*, *40*(13), 1958–1967. https://doi.org/https://doi.org/10.1016/j.vaccine.2022.02.044

Piret, J., & Boivin, G. (2020). Pandemics Throughout History. *Frontiers in Microbiology*, *11*, 631736. https://doi.org/10.3389/fmicb.2020.631736

Ramya, R., Coral, K., & Bharathidevi, S. R. (2021). RAGE silencing deters CML-AGE induced inflammation and TLR4 expression in endothelial cells. *Experimental Eye Research*, *206*, 108519. https://doi.org/https://doi.org/10.1016/j.exer.2021.108519

Redondo, N., Zaldívar-López, S., Garrido, J. J., & Montoya, M. (2021). SARS-CoV-2 Accessory Proteins in Viral Pathogenesis: Knowns and Unknowns . In *Frontiers in Immunology* (Vol. 12). https://www.frontiersin.org/articles/10.3389/fimmu.2021.708264

Rees-Spear, C., Muir, L., Griffith, S. A., Heaney, J., Aldon, Y., Snitselaar, J. L., Thomas, P., Graham, C., Seow, J., Lee, N., Rosa, A., Roustan, C., Houlihan, C. F., Sanders, R. W., Gupta, R. K., Cherepanov, P., Stauss, H. J., Nastouli, E., Doores, K. J., … McCoy, L. E. (2021). The effect of spike mutations on SARS-CoV-2 neutralization. *Cell Reports*, *34*(12). https://doi.org/10.1016/j.celrep.2021.108890

Ren, Y., Shu, T., Wu, D., Mu, J., Wang, C., Huang, M., Han, Y., Zhang, X.-Y., Zhou, W., Qiu, Y., & Zhou, X. (2020). The ORF3a protein of SARS-CoV-2 induces apoptosis in cells. *Cellular &*

Molecular Immunology, *17*(8), 881–883. https://doi.org/10.1038/s41423-020-0485-9

Riera Romo, M. (2021). Cell death as part of innate immunity: Cause or consequence? *Immunology*, *163*(4), 399–415. https://doi.org/10.1111/imm.13325

Saleemi, M. A., Ahmad, B., Benchoula, K., Vohra, M. S., Mea, H. J., Chong, P. P., Palanisamy, N. K., & Wong, E. H. (2020). Emergence and molecular mechanisms of SARS-CoV-2 and HIV to target host cells and potential therapeutics. *Infection, Genetics and Evolution : Journal of Molecular Epidemiology and Evolutionary Genetics in Infectious Diseases*, *85*, 104583. https://doi.org/10.1016/j.meegid.2020.104583

Salvesen, G. S., & Walsh, C. M. (2014). Functions of caspase 8: the identified and the mysterious. *Seminars in Immunology*, *26*(3), 246–252. https://doi.org/10.1016/j.smim.2014.03.005

Schultze, J. L., & Aschenbrenner, A. C. (2021). COVID-19 and the human innate immune system. *Cell*, *184*(7), 1671–1692. https://doi.org/10.1016/j.cell.2021.02.029

Shah, K., & Maghsoudlou, P. (2016). Enzyme-linked immunosorbent assay (ELISA): the basics. *British Journal of Hospital Medicine (London, England : 2005)*, *77*(7), C98–C101. https://doi.org/10.12968/hmed.2016.77.7.C98

Shen, X., Tang, H., McDanal, C., Wagh, K., Fischer, W., Theiler, J., Yoon, H., Li, D., Haynes, B. F., Sanders, K. O., Gnanakaran, S., Hengartner, N., Pajon, R., Smith, G., Glenn, G. M., Korber, B., & Montefiori, D. C. (2021). SARS-CoV-2 variant B.1.1.7 is susceptible to neutralizing antibodies elicited by ancestral spike vaccines. *Cell Host & Microbe*, *29*(4), 529-539.e3. https://doi.org/10.1016/j.chom.2021.03.002

Shi, J., Zhao, Y., Wang, K., Shi, X., Wang, Y., Huang, H., Zhuang, Y., Cai, T., Wang, F., & Shao, F. (2015). Cleavage of GSDMD by inflammatory caspases determines pyroptotic cell death. *Nature*, *526*(7575), 660–665. https://doi.org/10.1038/nature15514

Soltis, R. D., Hasz, D., Morris, M. J., & Wilson, I. D. (1979). The effect of heat inactivation of serum on aggregation of immunoglobulins. *Immunology*, *36*(1), 37–45.

Swanson, K. V, Deng, M., & Ting, J. P.-Y. (2019). The NLRP3 inflammasome: molecular activation and regulation to therapeutics. *Nature Reviews Immunology*, *19*(8), 477–489. https://doi.org/10.1038/s41577-019-0165-0

Tamura, T., Yanai, H., Savitsky, D., & Taniguchi, T. (2008). The IRF family transcription factors in immunity and oncogenesis. *Annual Review of Immunology*, *26*, 535–584. https://doi.org/10.1146/annurev.immunol.26.021607.090400

Tang, D., Kang, R., Berghe, T. Vanden, Vandenabeele, P., & Kroemer, G. (2019). The molecular machinery of regulated cell death. *Cell Research*, *29*(5), 347–364. https://doi.org/10.1038/s41422-019-0164-5

Thornberry, N. A., Bull, H. G., Calaycay, J. R., Chapman, K. T., Howard, A. D., Kostura, M. J., Miller, D. K., Molineaux, S. M., Weidner, J. R., & Aunins, J. (1992). A novel heterodimeric cysteine protease is required for interleukin-1 beta processing in monocytes. *Nature*, *356*(6372), 768–774. https://doi.org/10.1038/356768a0

Ting, J. P.-Y., Lovering, R. C., Alnemri, E. S., Bertin, J., Boss, J. M., Davis, B. K., Flavell, R. A., Girardin, S. E., Godzik, A., Harton, J. A., Hoffman, H. M., Hugot, J.-P., Inohara, N., Mackenzie, A., Maltais, L. J., Nunez, G., Ogura, Y., Otten, L. A., Philpott, D., … Ward, P. A. (2008). The NLR gene family: a standard nomenclature. *Immunity*, *28*(3), 285–287. https://doi.org/10.1016/j.immuni.2008.02.005

Veloso, C. A., Fernandes, J. S., Volpe, C. M. O., Fagundes-Netto, F. S., Reis, J. S., Chaves, M. M., & Nogueira-Machado, J. A. (2011). TLR4 and RAGE: Similar routes leading to inflammation in type 2 diabetic patients. *Diabetes & Metabolism*, *37*(4), 336–342. https://doi.org/https://doi.org/10.1016/j.diabet.2010.12.005

Vignoli, A., Tenori, L., Morsiani, C., Turano, P., Capri, M., & Luchinat, C. (2022). Serum or Plasma (and Which Plasma), That Is the Question. *Journal of Proteome Research*, *21*(4), 1061–1072. https://doi.org/10.1021/acs.jproteome.1c00935

Vora, S. M., Lieberman, J., & Wu, H. (2021). Inflammasome activation at the crux of severe COVID-19. *Nature Reviews Immunology*, *21*(11), 694–703. https://doi.org/10.1038/s41577-021-00588-x

Wallace, H. L., & Russell, R. S. (2022). Promiscuous Inflammasomes: The False Dichotomy of RNA/DNA Virus-Induced Inflammasome Activation and Pyroptosis. *Viruses*, *14*(10). https://doi.org/10.3390/v14102113

Wallace, H. L., Wang, L., Gardner, C. L., Corkum, C. P., Grant, M. D., Hirasawa, K., & Russell, R. S.

(2022). Crosstalk Between Pyroptosis and Apoptosis in Hepatitis C Virus-induced Cell Death. *Frontiers in Immunology*, *13*, 788138. https://doi.org/10.3389/fimmu.2022.788138

Wang, L., Manji, G. A., Grenier, J. M., Al-Garawi, A., Merriam, S., Lora, J. M., Geddes, B. J., Briskin, M., DiStefano, P. S., & Bertin, J. (2002). PYPAF7, a novel PYRIN-containing Apaf1-like protein that regulates activation of NF-kappa B and caspase-1-dependent cytokine processing. *The Journal of Biological Chemistry*, *277*(33), 29874–29880. https://doi.org/10.1074/jbc.M203915200

Ward, T. H., Cummings, J., Dean, E., Greystoke, A., Hou, J. M., Backen, A., Ranson, M., & Dive, C. (2008). Biomarkers of apoptosis. *British Journal of Cancer*, *99*(6), 841–846. https://doi.org/10.1038/sj.bjc.6604519

WHO. (n.d.). *e655dadbfcfab6fae8c4651c0d54a18a1e5161d8 @ covid19.who.int*. WHO, 2023. Retrieved December 5, 2022, from https://covid19.who.int

Xu, H., Akinyemi, I. A., Chitre, S. A., Loeb, J. C., Lednicky, J. A., McIntosh, M. T., & Bhaduri-McIntosh, S. (2022). SARS-CoV-2 viroporin encoded by ORF3a triggers the NLRP3 inflammatory pathway. *Virology*, *568*, 13–22. https://doi.org/10.1016/j.virol.2022.01.003

Yan, S. D., Schmidt, A. M., Anderson, G. M., Zhang, J., Brett, J., Zou, Y. S., Pinsky, D., & Stern, D. (1994). Enhanced cellular oxidant stress by the interaction of advanced glycation end products with their receptors/binding proteins. *Journal of Biological Chemistry*, *269*(13), 9889–9897. https://doi.org/https://doi.org/10.1016/S0021-9258(17)36966-1

Yan, W., Zheng, Y., Zeng, X., He, B., & Cheng, W. (2022). Structural biology of SARS-CoV-2: open the door for novel therapies. *Signal Transduction and Targeted Therapy*, *7*(1), 26. https://doi.org/10.1038/s41392-022-00884-5

Yap, J. K. Y., Moriyama, M., & Iwasaki, A. (2020a). Inflammasomes and Pyroptosis as Therapeutic Targets for COVID-19. *The Journal of Immunology*, *205*(2), 307–312. https://doi.org/10.4049/jimmunol.2000513

Yap, J. K. Y., Moriyama, M., & Iwasaki, A. (2020b). Inflammasomes and Pyroptosis as Therapeutic Targets for COVID-19. *Journal of Immunology (Baltimore, Md. : 1950)*, *205*(2), 307–312. https://doi.org/10.4049/jimmunol.2000513

Zeng, Z., Lan, T., Wei, Y., & Wei, X. (2022). CCL5/CCR5 axis in human diseases and related

treatments. *Genes & Diseases*, *9*(1), 12–27. https://doi.org/10.1016/j.gendis.2021.08.004

Zhang, H., Luo, J., Alcorn, J. F., Chen, K., Fan, S., Pilewski, J., Liu, A., Chen, W., Kolls, J. K., & Wang, J. (2017). AIM2 Inflammasome Is Critical for Influenza-Induced Lung Injury and Mortality. *Journal of Immunology (Baltimore, Md. : 1950)*, *198*(11), 4383–4393. https://doi.org/10.4049/jimmunol.1600714

Zhang, J., Ejikemeuwa, A., Gerzanich, V., Nasr, M., Tang, Q., Simard, J. M., & Zhao, R. Y. (2022). Understanding the Role of SARS-CoV-2 ORF3a in Viral Pathogenesis and COVID-19. *Frontiers in Microbiology*, *13*, 854567. https://doi.org/10.3389/fmicb.2022.854567

Appendix

5. Ethics Approval

Research Ethics Office
Suite 200, Eastern Trust Building
95 Bonaventure Avenue
St. John's, NL
A1B 2X5

July 16, 2020

Dear Dr. Grant:

Researcher Portal File # 20210347
Reference # 2020.085

RE: Characterization of Cellular and Humoral Immunity Against SARS-CoV-2

Your application was reviewed by Co-Chair under the direction of the HREB or subcommittee under the direction of the HREB and the following decision was rendered:

X	Approval
	Approval subject to changes
	Rejection

Ethics approval is granted for one year effective July 16, 2020. This ethics approval will be reported to the board at the next scheduled HREB meeting.

This is to confirm that the HREB reviewed and approved or acknowledged the following documents (as indicated):

- Revised intake questionnaire 2020/07/13 approved
- Poster advertisement for study 2020/07/15 approved
- Consent Form 2020/07/13 approved

- Budget 2020/05/12 acknowledged
- Proposal 2020/05/12 approved

Please note the following:

- This ethics approval will lapse on July 16, 2021. It is your responsibility to ensure that the Ethics Renewal form is submitted prior to the renewal date.
- This is your ethics approval only. Organizational approval may also be required. It is your responsibility to seek the necessary organizational approvals.
- Modifications of the study are not permitted without prior approval from the HREB. Request for modification to the study must be outlined on the relevant Event Form available on the Researcher Portal website.
- Though this research has received HREB approval, you are responsible for the ethical conduct of this research.
- If you have any questions please contact info@hrea.ca or 709 777 6974.

The HREB operates according to the Tri-Council Policy Statement: Ethical Conduct for Research Involving Humans (TCPS2), ICH Guidance E6: Good Clinical Practice Guidelines (GCP), the Health Research Ethics Authority Act (HREA Act) and applicable laws and regulations.

We wish you every success with your study.

You Have Received Ethics Approval, Now What?: HREB Reporting Requirements

Once a study has received ethics approval from the Health Research Ethics Board (HREB), there are still associated reporting requirements. In the conduct of approved research researchers are required to report to the HREB, in a timely manner, proposed changes from approved research that affect participants at any stage of the process. This includes, but is not limited to, changes to the consent form, changes to the tasks or interventions involved in the research, or changes to measures to protect privacy and confidentiality.

Any substantive change to the research should not be implemented prior to documented approval by the HREB, except when necessary to eliminate an immediate risk(s) to the participants. Below are examples of post approval documentation that must be submitted to the HREB:

Amendments

Any proposed change in the conduct of a study must be submitted to the HREB, and approved, before the change may be implemented. Such changes might include modification of recruitment procedures, inclusion or exclusion criteria, revised sample size, addition or deletion

of study sites, changes to an intervention, consent forms, questionnaires or scripts, etc. If there are changes in project team members or changes to funding source(s)/sponsor(s), there are specific forms to complete to report this to the HREB.

Adverse Events

Serious and unanticipated adverse events that occur within Newfoundland and Labrador are required to be reported to the HREB. Such events may occur in both clinical trials and in other types of research, e.g. collapse during a rehabilitation program, emotional breakdown requiring follow up care during an interview, or breach of privacy during correspondence. Serious adverse events that are fatal or life-threatening are required to be reported to the HREB as soon as the research team is aware of the event.

Protocol Deviations

Deviations from an approved study protocol must be reported to the HREB. Changes that eliminate immediate hazards to participants do not require prior approval, but must be reported soon as reasonably possible.

Safety Reports

Safety reports providing information on all serious adverse events (SAEs) occurring in a clinical trial must be provided by the sponsor to the HREB, normally on a three or six monthly basis (i.e. in accordance with the specified reporting timelines that were outlined in the approved ethics application).

Investigator Brochure (IB) and Product Monograph (PM)

Throughout the course of a clinical trial, changes may be implemented to study documents. All revisions to approved study documents must be submitted to the HREB to ensure the record is up to date. If the revisions include new risk or safety information there may be a requirement to notify research participants.

Ethics Renewal/Study Closure

Ethics approval lasts for one year. Ethics renewal is required annually, on the anniversary of the date of the HREB notification of approval. Once data collection is no longer ongoing, a study closure form is required to be submitted to the HREB for the study to remain active or to be closed in good standing.